

Diss. ETH No. 17377

Characterisation of volatile organic compounds emission from grassland systems

A dissertation submitted to the
SWISS FEDERAL INSTITUTE OF TECHNOLOGY ZURICH

for the degree of
Doctor of Sciences

presented by
Aurelia Nyfeler-Brunner
Dipl. Natw. ETH
born on 9 August 1973
citizen of Eischoll (VS) and Horw (LU)

accepted on the recommendation of
Prof. Dr. Thomas Peter, examiner
Prof. Dr. René Schwarzenbach, co-examiner
Prof. Dr. Johannes Stähelin, co-examiner
Dr. Albrecht Neftel, co-examiner
Dr. Jürgen Wildt, co-examiner

Seite Leer /
Blank leaf

Content

Summary	9
Zusammenfassung	11
1 Introduction	13
1.1 Overview of the thesis	15
2 Background	17
2.1 VOCs in the atmosphere	17
2.1.1 Concentration, origin and removal of VOCs	17
2.1.2 Role of VOCs in the atmosphere	18
Ozone production	18
Secondary aerosol production	20
Radiative forcing	21
2.2 Biogenic VOCs	22
2.2.1 BVOCs production and emission	22
2.2.2 BVOCs in the context of global change	24
References (Chapter 1 and 2)	26
3 Technical note: Water vapour concentration and flux measurements with PTR-MS	29
Abstract	29
3.1 Introduction	30
3.2 Methods	31
3.2.1 The PTR-MS instrument	31
3.2.2 Field site	32
3.2.3 Eddy covariance flux measurements	32
3.2.4 Flux calculation and correction of high frequency losses	33
3.3 Results	37

Content

3.4	Discussion	41
3.4.1	Water vapour concentration and flux measurements	41
3.4.2	Analysis of high frequency damping	42
3.4.3	Implication for BVOC measurements.....	44
3.5	Conclusions	45
	Acknowledgements	46
	References	46
4	Cut induced VOC emissions from agricultural grasslands	51
	Abstract	51
4.1	Introduction	51
4.2	Materials and Methods	53
4.2.1	Site descriptions	53
4.2.2	VOC analysis.....	54
	PTR-MS	54
	GC-MS	56
	GC-FID-PTR-MS.....	57
4.2.3	Flux calculation	58
4.3	Results	60
4.3.1	Flux measurements.....	60
4.3.2	Compound identification.....	63
4.4	Discussion	65
	Acknowledgements	70
	References	70
5	Methanol exchange between grassland and the atmosphere.....	75
	Abstract	75

Content

5.1	Introduction	75
5.2	Materials and methods	77
5.2.1	Site and measurement description.....	77
5.2.2	PTR-MS measurements.....	80
5.2.3	Eddy covariance method	81
5.3	Results	82
5.3.1	Measurements above the intensively managed field.....	82
	Weather conditions and vegetation development.....	82
	Concentrations.....	83
	Fluxes	84
5.3.2	Measurements above the extensively managed field	87
	Weather conditions and vegetation development.....	87
	Concentrations.....	88
	Fluxes	89
5.3.3	Comparison of both fields	89
5.4	Discussion	92
5.4.1	Concentrations.....	92
5.4.2	Fluxes during growth	93
5.4.3	Empirical flux parameterisation	95
5.4.4	Time integrated methanol fluxes.....	98
5.5	Conclusions	100
	Acknowledgements	101
	References	101
6	Ozone triggered VOC emissions of grassland species	107
	Abstract	107

Content

6.1	Introduction	107
6.2	Materials and methods	111
6.2.1	Plant material.....	111
	Trifolium repens	111
	Lolium perenne	111
6.2.2	Experimental set-up.....	112
	Climate chambers (CC)	112
	Ozone exposures	113
	Dynamic chamber (DC)	115
6.2.3	Gas exchange measurements.....	117
	Volatile organic compounds (VOC)	117
	Other trace gases (H ₂ O, CO ₂ , O ₃)	119
6.3	Results	119
6.3.1	Time integrated VOC emissions	119
	VOC emissions under ozone fumigation	120
6.3.2	Methanol time series under ozone fumigation	125
	Methanol time series of <i>T. repens</i>	125
	Methanol time series of <i>L. perenne</i>	126
6.3.3	Ozone deposition fluxes	128
6.4	Discussion	131
6.4.1	Composition of VOC emission of <i>T. repens</i> and <i>L. perenne</i>	131
6.4.2	Temporal variations of methanol fluxes.....	131
6.4.3	Ozone triggered VOC emission dependencies.....	132
	Genotype	132
	Ozone exposure	134

Content

Plant age	134
6.5 Conclusions	135
Acknowledgements	135
References	136
7 Overall conclusions	141
Acknowledgements	145
Curriculum vitae.....	147

Seite Leer /
Blank leaf

Summary

Volatile organic compounds (VOCs) are trace gases in the atmosphere. They have biogenic and anthropogenic sources. On the one hand, they are by-products of any combustion process - on the other hand they are produced and emitted by vegetation because of many different reasons. The biogenic part of total emitted VOCs is approximately 90%. In the atmosphere, VOCs play an active role in the production of tropospheric ozone and particulate matter (aerosols). Enhanced ozone and aerosol concentration have harmful effect on human health as well as on vegetation. Also, ozone and aerosols influence the radiation budget of the earth and therefore the temperature on the earth surface. Reactions with radicals and dry and wet deposition lead to reduction of VOCs in the atmosphere. The reduction processes have characteristic time scales between minutes and months depending on the compound.

Due to the high importance of biogenic VOC emissions they were subject of many investigations. Until now, a lot of information about VOC emissions by of trees has been assembled.

Focal point of this work are VOC emissions of grassland. Grassland ecosystems cover one quarter of the earth's land surface. The actual VOC inventory of grassland mainly focuses on cut related emissions. Only a few field measurements showed emission time series during spring and summer month.

In this project four measuring campaigns were conducted: two field campaigns (2004 and 2005) and two laboratory campaigns (2006 and 2007). VOC emissions were measured by a proton-transfer-reaction mass-spectrometer (PTR-MS) which provides a high temporal resolution of data. The field measurements were conducted on the "Kyoto-Wiese" (originally established for the study of greenhouse gas exchange) in Oensingen. It consists of an intensively and an extensively managed grassland field.

The first measurement year provided high temporal resolution time series of methanol emission of the two fields, including growing periods and cut events (Chapter 5). We could show that the amount and the temporal course of the emissions of methanol strongly depend on the plant composition of the field. The accumulated methanol emissions related to the growing period are significantly higher, than those emitted during and after a cut event. In the second measurement year detailed information on the composition of emissions depending on the cut plant species were obtained (Chapter 4). The number (diversity) of emitted VOC

Summary

decreases for the investigated species in the following sequence: legumes, forbs and graminoids.

Ozone fumigation experiments were conducted in climate chambers in the laboratory (Chapter 6). Aim of these experiments was to characterise the VOC emission depending on ozone stress, plant species and plant age. For this purpose two grassland species commonly used in Switzerland (and in Central Europe) were selected: white clover (*Trifolium repens*) and English ryegrass (*Lolium perenne*). Two different genotypes of white clover were investigated in two experiments with different ozone exposure. English ryegrass of different age was fumigated in two other experiments. The results of these measurements show that ozone triggers the emissions of various VOCs and that the enhancement is related to plant species, genotype, plant age and the intensity of ozone exposure. White clover was found to be significantly more sensible to enhanced ozone concentrations than the English ryegrass. In each experiment, methanol emissions showed the largest absolute increase in VOC emissions in reaction to the ozone related stress.

Zusammenfassung

Flüchtige organische Verbindungen (engl.: volatile organic compounds; VOCs) sind Spurengase in der Erdatmosphäre. Sie haben biogene und anthropogene Quellen. Einerseits gelangen sie in die Atmosphäre als Folge von Verbrennungsprozessen und Verdampfung von Lösemitteln. Andererseits werden sie von der Vegetation für verschiedenste Verwendungszwecke produziert und schliesslich in die Atmosphäre emittiert. Der biogene Anteil der VOCs beträgt etwa 90% der global emittierten Menge. In der Atmosphäre spielen VOCs eine Rolle bei der Bildung von troposphärischem Ozon und Aerosolen (Feinstaub). Erhöhte Ozon- und Aerosol-Konzentrationen haben schädigende Wirkungen auf die menschliche Gesundheit und die Vegetation. Schliesslich beeinflussen Ozon und Aerosole auch den Strahlungshaushalt der Erde und damit die Temperatur auf der Erdoberfläche. Durch Reaktionen mit Radikalen und trockene und nasse Deposition werden VOCs aus der Atmosphäre entfernt. Die Abbaurate liegt je nach Verbindung zwischen Minuten und Monaten.

Biogene VOCs machen den grössten Teil der totalen VOC Menge aus. Sie sind dementsprechend oft Thema von Forschungsarbeiten. Bisher wurden hauptsächlich Emissionen von Laub- und Nadelbäumen untersucht.

Schwerpunkt dieser Arbeit sind die VOC Emissionen von Grasland. Graslandsysteme bedecken einen Viertel der Landoberfläche auf der Erde. Das bisherige VOC-Inventar von Grasland beschränkt sich hauptsächlich auf Emissionen während und nach dem Mähen. Nur einige Feldmessungen zeigen niedrig aufgelöste Zeitreihen von Emissionen während Frühlings- und Sommermonaten.

Im Rahmen dieser Arbeit wurden vier Messkampagnen durchgeführt: zwei Feldmessungen (2004 und 2005), sowie zwei Labormessungskampagnen (2006 und 2007). Die VOC Emissionen wurden mit einem Proton-Transfer-Reaktions Massenspektrometer gemessen (PTR-MS), welches eine hohe zeitliche Datenauflösung erzeugen kann. Die Feldmessungen wurden auf der „Kyoto-Wiese“ des ART Versuchsgelände in Oensingen durchgeführt. Das Messfeld besteht aus einem intensiv und einem extensiv bewirtschafteten Teil. Die Resultate des ersten Messjahres (Kapitel 5) zeigen hoch aufgelöste Methanolemissionszeitreihen der beiden Felder während dem Wachstum und verschiedenen Schnittereignissen. Dabei konnte gezeigt werden, dass die Menge und der zeitliche Verlauf der Methanolemissionen stark von der Pflanzenzusammensetzung des jeweiligen Feldes abhängt. Die aufsummierten

Zusammenfassung

Wachstumsemissionen sind deutlich grösser als die beim Mähen freigesetzten Mengen. Das zweite Messjahr lieferte vor allem die Komponentenzusammensetzung der Schnittermissionen abhängig von der geschnittenen Graslandspezies (Kapitel 4). Die Anzahl der flüchtigen organischen Komponenten nimmt für die untersuchten Spezies in der Reihenfolge ihrer funktionellen Gruppe ab: Leguminosen, Kräuter und Gräser.

Bei den Labormessungen handelt es sich um Ozonbegasungsexperimente in Klimakammern (Kapitel 6). Ziel dieser Versuche war es, die Emissionen abhängig von Ozonstress, Spezies und Pflanzenalter zu charakterisieren. Dabei wurden zwei hierzulande (und auch in Zentraleuropa) häufige Graslandspezies, Weissklee (*Trifolium repens*) und Englisches Raigras (*Lolium perenne*) verwendet. Zwei verschiedene Weissklee Genotypen wurden in zwei Versuchen unterschiedlichen Ozonepisoden ausgesetzt. Unterschiedlich altes Englisches Raigras wurde für zwei weitere Begasungsversuche verwendet. Die Resultate dieser Versuche zeigen, dass die Ozonexposition zu erhöhten VOC Emissionen führt. Dabei ist die Zunahme der Emissionen abhängig von der Pflanzenspezies, dem Genotyp, dem Alter der Pflanzen und der Ozonbegasungsintensität. Weissklee reagierte wesentlich empfindlicher auf erhöhte Ozonkonzentrationen als Raigras. Bei allen Versuchen zeigten die Methanolemissionen die absolut grösste Zunahme als Reaktion auf den Ozonstress.

1 Introduction

Summer smog and episodes of enhanced fine particulate matter in the winter, global warming and increasing CO₂ concentrations – these topics occur in headlines in the daily newspapers throughout the year. All of these four catchwords concern the atmosphere. And they concern human beings and nature. Local and global scales are involved. Short and long time scales, past, present and future play a role.

These catchwords also embrace a large field of chemistry, physics and biology and they hint at how complex the atmosphere and the reactions between its constituents must be.

The atmosphere consists mainly of nitrogen (N₂ 78%), oxygen (O₂ 21%) and argon (Ar 0.9%) and variable amounts of water. Thousands of chemical species make up the remaining 0.1%, the so-called trace gases. Even though their concentrations are small, they play an active role in the atmosphere. The production of tropospheric ozone (O₃), for example, depends on the concentrations of volatile organic compounds (VOCs) and nitrogen oxides (NO_x = NO + NO₂). NO_x are mostly of anthropogenic origin (Galloway et al., 2004). They are formed during combustion processes and released by solvent evaporation and emitted to the atmosphere. However, approximately 90% of total global VOCs are of biogenic origin (Seinfeld and Pandis, 1998; Guether et al., 1995). The main producer and emitter of biogenic VOCs are plants. These biogenic VOCs (BVOCs) are part of the plant metabolism, they are emitted during growth and as floral scents and some of them act as attractor of pollinators (Fall, 1999 and references therein). The family of VOCs consists of several hundred compounds. The emission of isoprene and monoterpenes, both BVOCs, form about 50% of the total global annual VOC emission. Many investigations considered isoprene and monoterpenes (e.g. Fehsenfeld et al., 1992; Schade and Goldstein, 2001; Spirig et al., 2005; Karl et al., 2005; Schade and Goldstein, 2006). They are formed in the chloroplast of woody plant species as a thermal protectant for the photosynthetic apparatus (isoprene) or as defense against herbivores and pathogens (monoterpenes). Their emission to the atmosphere depends on light and temperature (Fall, 1999). Concerning the other 50% of BVOCs much less is known and quantitative description of their emissions as function of environmental parameters are not well established. E.g., for grasslands which cover one quarter of the earth's surface (Graedel and Crutzen, 1993) only few studies have been published so far.

1 Introduction

In this work, we focus on BVOCs emitted by grassland. The project “Characterisation of volatile organic compounds emission from grassland systems” funded by the Swiss National Foundation aims to improve the knowledge about the biosphere-atmosphere exchange of VOCs from grassland systems. The project focuses on the following two parts:

(I) Assessment of VOC loss of grassland systems under different management practises. In the framework of the long-term experiment “Kyoto-Wiese” of the Agroscope Reckenholz-Tänikon, ART, Research Station, a research site on Central Swiss Plateau near Oensingen had been established. The site consists of two parallel fields, one managed as intensive and the other as extensive grassland. VOC emissions were measured using the proton-transfer-reaction mass-spectrometry (PTR-MS) device in conjunction with Eddy Covariance (EC) and dynamic chamber (DC) flux measurement techniques (Chapter 3, 4 and 5).

(II) Fingerprints of VOC emissions from grassland species exposed to air pollution stress. Two grassland species commonly grown in Switzerland, white clover and English ryegrass, were exposed to elevated levels of ozone. These fumigation experiments were conducted in climate chambers which provide full control of environmental parameters such as photosynthetically active radiation (PAR), air temperature and relative air humidity (Chapter 6).

The investigations focused on grassland in a temperate climate as typical for Switzerland. Grassland systems are the dominant agricultural production system in Switzerland and cover about 69% of the agricultural land. On the European scale this fraction amounts to 49%, representing 30% of the total land area. In the wake of the Kyoto-Protocol, interest in grassland systems has been increasing because the conversion of cropland to permanent grassland is considered an important option to reduce net emissions of greenhouse gases. Emissions of VOCs constitute a small, but important fraction of the C-budget. Also for upscaling purposes and comparison to other studies, it is useful to relate VOC emissions to common carbon exchange terms like the net assimilation.

1.1 Overview of the thesis

Chapter 2 gives some scientific background information about the role of VOCs in the troposphere and biogenic VOCs.

Chapter 3 comprises the paper “Technical note: Water vapour concentration and flux measurements with PTR-MS” published in *Atmospheric Chemistry and Physics*, 2006 (*Atmos. Chem. Phys.*, 6, 4643-4651, 2006). The measurement technique described here is used for the following field and laboratory experiments.

Chapter 4 presents a publication about the characterisation of VOCs emitted by grassland species: “Cut induced VOC emissions from agricultural grasslands”, published in *Plant Biology*, 2007 (*Plant Biol.*, doi:10.1055/s-2007-965043, 2007). These results base on the field campaign during Summer 2005 in Oensingen. The collected air samples of cut induced VOC emissions were analysed by two different gas chromatography devices (GC-FID-PTR-MS and GC-MS).

Chapter 5 includes the paper “Methanol exchange of grasslands and the atmosphere”, published in *Biogeoscience*, 2007 (*Biogeosciences*, 4, 395-410, 2007). The discussed data were measured during summer 2004 above two differently managed grassland fields in Oensingen.

Chapter 6 is a draft of the paper “Ozone triggered VOC emissions of grassland species” that will be submitted to *Biogeosciences* in 2007. The influence of ozone on white clover and English ryegrass was investigated with fumigation experiments conducted in climate chambers.

Chapter 7 summarises the overall conclusions. It gives answers to the following questions: What additional information about BVOCs do we have thanks to this work? What is still a challenge? What deserves further investigations?

2 Background

2.1 VOCs in the atmosphere

Volatile organic compounds (VOCs) are gaseous organic species in the atmosphere which belong to the trace gases. They make a percentage of less than 1% of the total atmosphere (Seinfeld and Pandis, 1998). The family of volatile organic compounds comprises all gaseous organics (including various functional groups; e.g. alcohols, aldehydes, ketones, monoterpenes), excluding CO and CO₂. Actually methane (CH₄) is the most abundant VOC in the atmosphere (average mixing ratio 1.7 ppmv; Seinfeld and Pandis, 1998). Due to its low reactivity (atmospheric lifetime of ~8 years) and its importance as a greenhouse gas (IPCC, 2007), it is frequently treated separately from other VOCs, the so-called non-methane VOCs (NMVOCs).

2.1.1 Concentration, origin and removal of VOCs

VOCs are found in concentrations of a few pptv up to ppbv in the troposphere originating from biogenic and anthropogenic sources (Fehsenfeld et al., 1992; Fall, 1999). The anthropogenic part is mainly produced by combustion, as any sort of combustion (fossil fuel and biomass burning) leads to the formation of VOCs. Other anthropogenic sources are the fossil fuel storage and transport, solvent use, industrial production, and biological processes (Friedrich and Obermeier, 1999). Next to the oceans, out gassing from soil, sediments and geological hydrocarbon reservoirs, vegetation is the main natural source of VOCs. The latter biogenic VOCs are formed during plants growth (Galbally and Kirstine, 2002) and as by-products of their metabolism (Fall, 1999). Plants also produce and emit VOCs to defend themselves against herbivore attacks (Dicke et al., 2001) and in case of several other mechanical stresses such as cutting (De Gouw et al., 1999), senescing (Karl et al., 2005), and ozone fumigation (Wildt et al., 2003). Section 2.2.2 gives more details on BVOCs. The biogenic portion makes approximately 90% of the total globally emitted VOCs (Günther et al., 1995). The atmospheric lifetime of VOCs varies within the range of a few seconds to several days and months depending on their reactivity (Atkinson and Arey, 1998). The reaction with radicals (OH, O₃, HO₂ and others) is the major loss process of VOCs, next to the dry and wet deposition (Atkinson, 2000; Fuentes et al., 2000, Lee et al., 2003).

2 Background

2.1.2 Role of VOCs in the atmosphere

Once emitted into the atmosphere, VOCs play an active role in the atmospheric chemistry on a local and a global scale (Seinfeld and Pandis, 1998). They influence the oxidation capacity of the troposphere by reacting with the radicals (OH, NO₃, HO₂ and O₃). The tropospheric ozone concentration depends on the concentration of VOC and nitrous oxides (NO_x = NO + NO₂). The oxidation of certain VOCs (e.g. monoterpenes and isoprene) can lead to the formation of secondary aerosols (Hoffmann et al., 1997; Claves et al., 2004). Enhanced ozone concentrations are harmful to human beings (e.g. lung disease; Brook et al., 2005) and nature (e.g. crop yield loss; Fuhrer et al. 1997). High concentrations of aerosols as they are observed during winter smog episodes lead to the increased appearance of heart disease (Zanobetti et al., 2000)

Tropospheric oxidation and ozone production

Tropospheric ozone production during day time depends on the concentration of VOCs and NO_x. In this context two radical chain reaction cycles, which are closely related, are first looked at separately:

(I) Photostationary state: it describes the connection between nitrogen oxides and ozone. Nitrogen dioxide (NO₂) is photolysed by sunlight (hν, with wavelength 290 < ν < 430 nm), resulting in nitrogen oxides and an oxygen atom in the ground state (O(³P)). This oxygen atom reacts with molecular oxygen (O₂) and the help of air compounds (M) to ozone (O₃). O₃ and nitrogen oxides lead again to the educts (NO₂ and O₂).

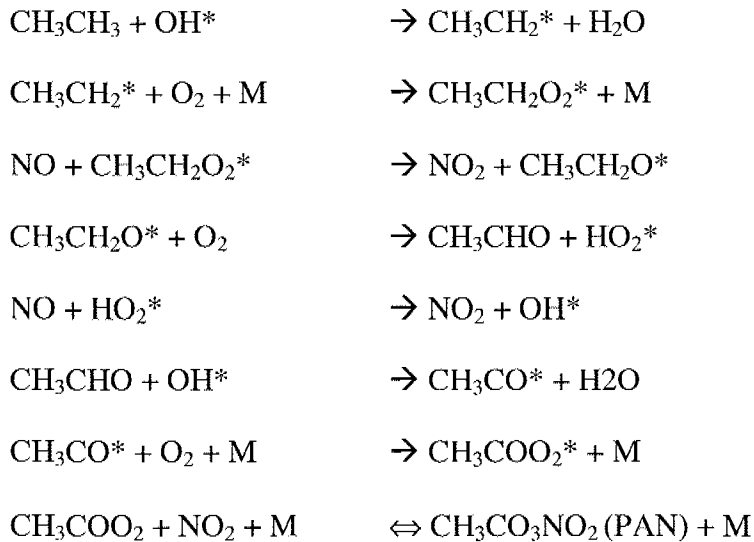


The equilibrium between these three fast reactions, also called photostationary state is reached within minutes. There is no net-production of any compound in this cycle.

(II) RO_x radical chain: it describes the involvement of peroxy radicals (RO₂*; in the following (*) stands for radical). The reaction of VOCs with OH radical leads to the

2.1 VOCs in the atmosphere

formation of organic peroxy radicals. They are important oxygen donors that react with NO to produce NO₂. As an example, the reaction chain for ethane (CH₃CH₃) is shown here:



The first part of this reaction chain leads to the net production of NO₂. The second part (in square brackets) ends in the production of peroxy acetyl nitrate (PAN).

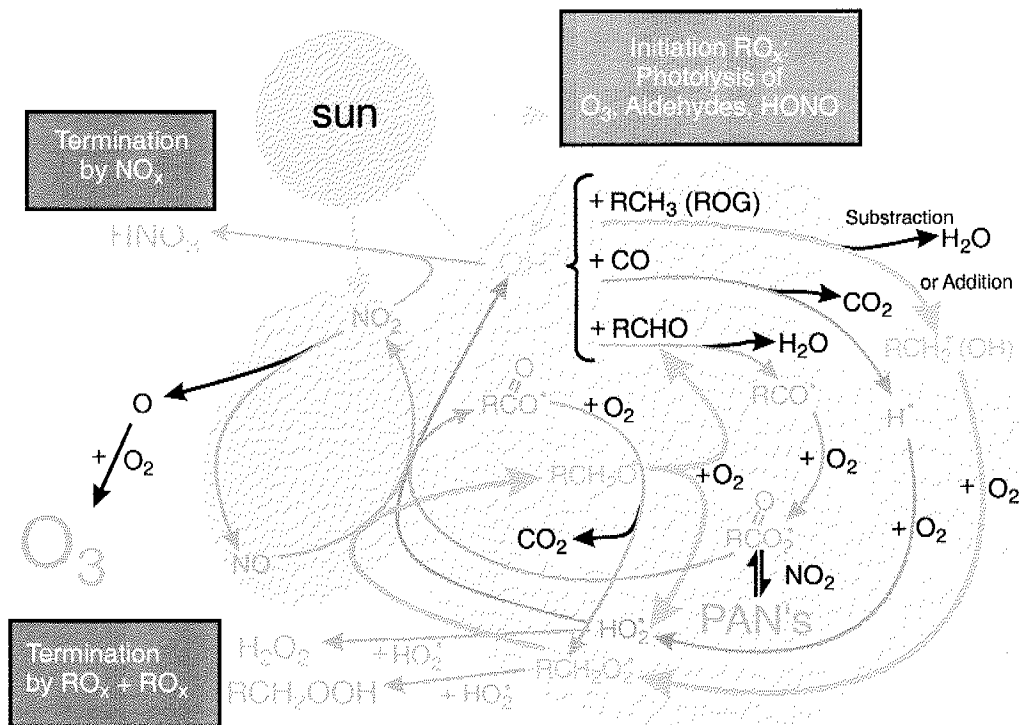
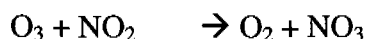


Figure 1: Schematic diagram of the tropospheric ozone formation during day (Staehelin et al., 2000).

2 Background

Figure 1 shows the combination of the two cycles (I) and (II) and reveals their full complexity (Staehelin et al., 2000). The production of ozone is a nonlinear process depending on the ratio $[\text{VOCs}]/[\text{NO}_x]$. NO concentration above than 10 ppt leads to the production of O_3 , whereas NO concentration below than 10 ppt leads to the destruction of O_3 .

At night, the photochemical reactions are stopped. Ozone is reduced by the reaction with NO_2 . NO_2 , NO_3 and N_2O_5 reach an equilibrium within minutes.



OH radicals are the most important oxidants for VOC degradation in the troposphere (see Figure 1). They are produced by the photolysis of ozone and aldehydes. During night, NO_3 is the most important oxidant.

Secondary aerosol production

Aerosols are suspended particles in the air and are characterised by their aerodynamic diameter (PM₁₀: particle matter with aerodynamic diameter < 10 μm). Sources of aerosols are manifold: ash particles, soot, organic materials (pollen, spores, bacteria), sulphate, nitrate and inorganic salt. Directly emitted particles are called primary aerosols, whereas particles formed in the atmosphere are called secondary aerosols. The oxidation of VOCs (e.g. monoterpenes, sesquiterpenes and isoprene) can lead to the formation of secondary organic aerosols (SOA) (Hoffmann et al., 1997; Clayes et al., 2004). The volatility of the oxidation products is one of the most important parameters influencing aerosol formation. Oxidation products with low vapour pressure will predominately be in the condensed phase, either forming new particles or condense onto pre-existing particles (Finlayson-Pitts and Pitts, 2000). Aerosols are necessary in the formation of clouds as condensation nuclei.

Aerosols have an important influence on the radiation balance of the earth surface. On one hand, they reflect and scatter the incoming short wave radiation, leading to a reduction of radiation on the earth surface (IPCC, 2007). On the other hand, aerosols lead to cloud formation. Clouds reflect the incoming short wave radiation back to space, but they also reflect the long wave radiation back to the earth surface, increasing the temperature at the surface.

2.1 VOCs in the atmosphere

Radiative forcing

Changes in the atmospheric abundance of greenhouse gases and aerosols, in solar radiation and in land surface properties alter the energy balance of the climate system. These changes are expressed in terms of radiative forcing, which are used to compare how a range of human and natural factors drive warming or cooling influences on global climate. Radiative forcing (in Wm^{-2}) is a measure of the influence that a factor has in altering the balance of incoming and outgoing energy in the earth-atmosphere system. It is an index of the importance of the factor as a potential climate change mechanism. Positive forcing tends to warm the surface while negative forcing tends to cool it (IPCC, 2007). Following the forth assessment report of the intergovernmental panel on climate change (AR4, IPCC, 2007) there is a direct positive effect on radiative forcing caused by VOC, principally due to the increase of methane. Further VOC are involved in two indirect effects on the radiative forcing: the increase of tropospheric ozone due to emissions of ozone-forming chemicals (among others VOCs) contribute to a positive radiative forcing, whereas aerosols produce a cooling effect. Figure 2 shows the globally averaged radiative forcing estimates and ranges in 2005 for anthropogenic dioxide, methane, nitrous oxide and other important agents.

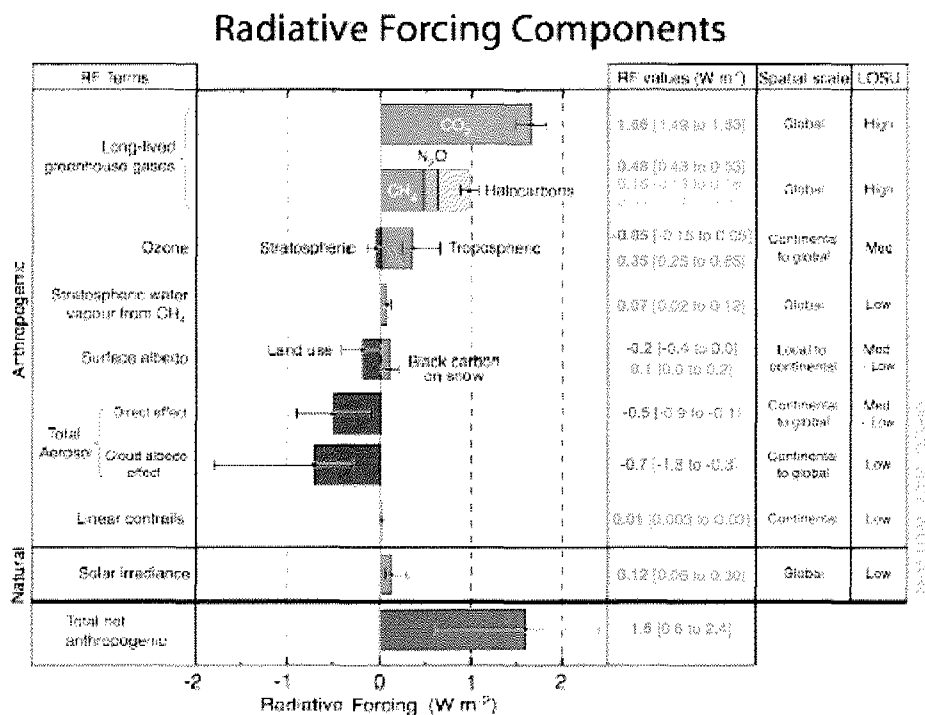


Figure 2: Global-averaging radiative forcing estimates and ranges in 2005 for anthropogenic dioxide, methane, nitrous oxide and other important agents and mechanisms, together with the typical

2 Background

geographical extent (special scale) of the forcing and the assessed level of scientific understanding (LOSU). The net anthropogenic radiative forcing and its range are also shown. These require summing asymmetric uncertainty estimates from the component terms, and cannot be obtained by simple addition. Additional forcing factors not included here are considered to have a very low LOSU. Volcanic aerosols contribute an additional natural forcing but are not included in this figure due to their episodic nature. Range for linear contrails does not include other possible effects of aviation on cloudiness (IPCC, 2007).

2.2 Biogenic VOCs

2.2.1 BVOCs production and emission

Biogenic volatile organic compounds (BVOCs) constitute approximately 90% of total VOCs emitted into the atmosphere (Guenther et al., 1995). Today several thousands different BVOC are known. Floral scents are mixtures of different BVOCs (Knudsen et al., 1993). Just the family of monoterpenes alone includes some 1000 structures. In addition, there are potentially thousands of volatile or semi-volatile isoprenoids known to exist in plants, but which are not yet reported in atmospheric samples or floral scents. The major “families” of BVOCs are summarized in Table 1. It gives seven VOC classes, their primary natural sources, the estimated annual global emissions and their atmospheric lifetime. Methane is the listed compound with the longest atmospheric lifetime. Omitting methane in the following calculation, isoprene and the monoterpene family together make 65% of the total NMVOCs annually emitted into the atmosphere. The two other important classes are the “other reactive VOCs” and the “other less reactive VOCs”, containing mostly oxygenated compounds. They form 35% of the total annually emitted NMVOCs. Except for dimethylsulfide and ethylene, these NMVOCs are primarily emitted by terrestrial plants.

The BVOCs are produced in many different plant tissues and compartments and they are the products of diverse physiological processes. The VOC species characterised in the following paragraphs are described in detail in Fall (1999), an excellent review.

2.2 Biogenic VOCs

Table 1: the major biogenic VOC or families of biogenic VOCs (from: Fall, 1999; and references therein)

species	primary natural sources	estimated annual global emissions [Tg C / y]	reactivity (averaged atmospheric lifetime in days)
methane	wetlands, rice paddies	319-412	4000
isoprene	plants	175-503	0.2
monoterpene family	plants	127-480	0.1-0.2
dimethylsulfide	marine phytoplankton	15-30	< 0.9
ethylene	plants, soils, oceans	8-25	1.9
other reactive VOCs (e.g. acetaldehyde, 2-methyl-3-buten-2-ol, hexenal family)	plants	~260	< 1
other less reactive VOCs (e.g. methanol, ethanol, formic acid, acetic acid, acetone)	plants, soils	~260	> 1

One of the most investigated BVOC is isoprene (2-methyl-1,3-butadiene). Nowadays, it has been established that isoprene is produced in chloroplasts. The production strongly depends on the instantaneous light and temperature, but also the growth environment of plants and the leaf development play an active role. Isoprene emissions occur without a leaf reservoir, it is directly released via the stomata. The emission strength correlates well with light. Most isoprene emitters are wood plant species. The role of isoprene in plant physiology is not yet fully established. One hypothesis was presented by Sharkey and Singaas (1995): isoprene as

2 Background

a thermal protectant for the photosynthetic apparatus. However, conflicting observations by Logan and Monson (1999) indicate that this hypothesis may not be the final explanation.

The monoterpene family contains more than thousand different C_{10} compounds. The monoterpene-producing plants, such as conifers, mint and the citrus family, synthesise always a mixture of monoterpenes which includes an array of cyclic and acyclic structures. They are stored in the leaf and its release depends on temperature. Monoterpenes have multiple functions: direct defense against herbivores and pathogens, indirect defense by attraction of enemies of herbivores, attraction of pollinators and allelopathic effects on competing plants.

The other reactive and less reactive BVOCs are oxygenated VOCs. Methanol (C_1 compound) is produced during plant growth which leads to the demethylation of the pectin matrix of the cell walls. Methanol is water soluble and stored in the liquid of the apoplasts. It is released to the atmosphere mostly via the stomata. Depending on the rate and time of production, the emission of methanol shows a sigmoidal diurnal cycle. If there is a nocturnal methanol production, the diurnal emission cycle shows a distinct morning peak. Methanol emissions are also triggered by stresses such as cutting and ozone fumigation. Grassland species as well as trees are known to emit methanol.

Not much is known about the mechanism and regulation of formation of C_2 (acetaldehyde), C_3 (acetone) and C_4 (e.g. methyl ethyl ketone) compounds although several field measurements showed distinct emissions of these compounds.

The family of C_6 aldehydes and C_6 alcohols (referred to as hexenal family or wound compounds) characterise the smell of fresh mown grasses. Their production is linked to physical wounding of leaves or to signals produced by herbivores and plant pathogens as they attack plants. Their formation is a result of the breakdown of C_{18} fatty acids (octadecanoid pathway). A potential regulator of this production pathway in plants may be ultraviolet radiation. Various C_6 alcohols and aldehydes have antibiotic properties. The production of hexenals in leaves is to inhibit invasion and infection by opportunistic bacteria residing on the leaf surface.

2.2.2 BVOCs in the context of global change

Based on an interactive global biogenic emission and dynamic vegetation model, Lathière et al. (2005) investigated the evolution of volatile organic compound emissions by the terrestrial

2.2 Biogenic VOCs

biosphere for the year 2100 (among others), considering a CO₂ concentration of 560 ppmv. The combined effects of foliar expansion, climate change, and ecosystems redistribution impact strongly on biogenic emissions. Lathière et al. (2005) simulated the emission change of eight different BVOC and found a future increase for all of them (Table 2). This increase is mostly due to the change in ecosystem distribution. Tropical regions remain a strong VOC source but a significant decrease in emissions is simulated in 2100 for the Amazon region, owing to a decrease in both the coverage of tropical trees and leaf area index (LAI). A large expansion of temperate and boreal forests is simulated over northern mid- and high latitudes, leading to a strong increase of biogenic emission.

Table 2: Biogenic VOC emission for the present-day and for the future (2100, [CO₂]: 560 ppmv) with dynamic vegetation (Lathière et al., 2005)

VOC species	present	future ^{a)}
	[Tg C / yr]	[Tg C / yr]
isoprene	502	638 (+27)
monoterpenes	175	265 (+51)
methanol	132	192 (+45)
acetone	63	96 (+52)
acetaldehyde	22	33 (+50)
formaldehyde	15	23 (+53)
formic acid	2.2	3.3 (+50)
acetic acid	0.4	0.7 (+75)
total	912	1251 (+37)

^{a)} Percentage change in emissions relative to present-day is shown in parentheses.

2 Background

References (Chapter 1 and 2)

Atkinson, R. and Arey, J.: Atmospheric chemistry of biogenic organic compounds, *Acc. chem. res.*, 31, 9, 574-583, 1998.

Atkinson, R.: Atmospheric chemistry of VOCs and NO_x, *Atmos. Environ.*, 34, 2063-2101, 2000.

Brook, R. D., Brook, J. R., Urch, B., Vincent, R., Rajagopalan, S. and Silverman, F.: Inhalation of fine particulate air pollution and ozone cause acute arterial vasoconstriction in healthy adults, *Circulation*, 105, 13, 1534-1536, 2002.

Clayes, M., Graham, B., Vas, G., Wang, W., Vermeulen, R., Pashynska, V., Cafmeyer, J., Guyon, P., Andreae, M. O., Artaxo, P. and Maenhaut, W.: Formation of secondary organic aerosols through photooxidation of isoprene, *Science*, 303, 1173-1176, 2004.

De Gouw, J. A., Howard, C. J., Custer, T. G., Baker, B. M. and Fall, R.: Emissions of volatile organic compounds from cut grass and clover are enhanced during the drying process, *Geophys. Res. Lett.*, 26(7), 811-814, 1999.

Dicke, M. and Bruin, J.: Chemical information transfer between plants: back to the future, *Biochemical Systematics and Ecology*, 29, 981-994, 2001.

Fall, R.: Biogenic emissions of volatile organic compounds from higher plants. In C. N. Hewitt (Editor), *Reactive hydrocarbons in the atmosphere*. Academic Press, New York, pp. 41-96, 1999.

Fehsenfeld, F., Calvert, J., Fall, R., Goldan, P., Guenther, A. B., Hewitt, C. N., Lamb, B., Liu, S., Trainer, M., Westberg, H. and Zimmerman, P.: Emissions of volatile organic compounds from vegetation and the implications for atmospheric chemistry, *Global Biogeochem. Cycles*, 6(4), 389-430, 1992.

Finlayson-Pitts, B. J. and Pitts, J. N.: *Chemistry of the Upper and Lower Atmosphere: Theory, Experiments, and Applications*, 969 pp., Academic Press, San Diego, 2000.

Fuentes, J. D., Lerdau, M., Atkinson, R., Baldocchi, D., Bottenheim, J. W., Ciccioli, P., Lamb, B., Geron, C., Gu, L., Guenther, A., Sharkey, T. D. and Stockwell, W.: Biogenic hydrocarbons in the atmospheric boundary layer: A review, *Bulletin of the American Meteorological Society*, 81, 7, 1537-1575, 2000.

2. References

- Fuhrer, J. and Achermann, B.: Critical levels for ozone; a UN-ECE workshop report, FAC Report No16, Swiss Federal Research Station for Agricultural Chemistry and Environmental Hygiene, Liebefeld-Bern, Switzerland, 1994.
- Friedrich, R. and Obermeier A.: Anthropogenic Emissions of Volatile Organic Compounds, In: Reactive Hydrocarbons in the aTmosphere, Ed. C. N. Hewitt, Academic Press, San Diego, USA, pp1-39, 1999.
- Galbally, I. E. and Kirstine, W.: The Production of Methanol by Flowering Plants and the Global Cycle of Methanol, *J. Atmos. Chem.*, 43, 195-229, 2002.
- Galloway, J. N., F. J. Dentener, D. G. Capone, E. W. Boyer, R. W. Howarth, S. P. Seitzinger, G. P. Asner, C. C. Cleveland, P. A. Green, E. A. Holland, D. M. Karl, A. F. Michaels, J. H. Porter, A. R. Townsend and C. J. Vorosmarty.: Nitrogen Cycles: Past, Present, and Future, *Biogeochemistry*, 70, 2, 153-226, doi:10.1007/s10533-004-0370-0, 2004.
- Graedel, T. E. and Crutzen P. J.: Atmospheric change: An Earth System Perspective, W. H. Freeman, New York, 1993.
- Hoffmann, T., Odum, J. R., Bowman, F., Collins, D., Klockow, D., Flagan, R. C. and Seinfeld, J. H.: Formation of organic aerosols from the oxidation of biogenic hydrocarbons, *J. Atmos. Chem.*, 26, 198-222, 1997.
- IPCC (Intergovernmental Panel on Climate Change), Climate Change, 2007, The Physical Science Basis, Summary for Policymakers, 2007
- Karl, T., Harren, F., Warneke, C., de Gouw, J., Grayless, C. and Fall, R.: Senescing grass crops as regional sources of reactive volatile organic compounds, *J. Geophys. Res.*, 110, D15302, doi:10.1029/2005JD005777, 2005.
- Lathière, J., Hauglusaine, D. A. and De Nobelt-Ducoudré, N.: Past and future changes in volatile organic compound emissions simulated with a global dynamic vegetation model, *Geophys. Res. Let.*, 32, L20818, doi:10.1029/2005GL024164, 2005.
- Lee, A.; Goldstein, A. H.; Keywood, M.; Varutbangkul, V.; Bahreini, R.; Gao, S.; Flagan, R.; Seinfeld, J.: Ozone Oxidation of Monoterpenes, Sesquiterpenes, and Oxygenated Terpenes: Product Yields and Relevance to Field Observations and Atmospheric Chemistry, American Geophysical Union, Fall Meeting 2003, abstract #A21F-02, 2003.

2 Background

Logan, B. A. and Monson, R. K.: Thermotolerance of leaf discs from four isoprene-emitting species is not enhanced by exposure to exogenous isoprene, *Plant Physiol.*, 120, 821-825, 1999.

Schade, G. W. and Goldstein, A. H.: Fluxes of oxygenated volatile organic compounds from a ponderosa pine plantation, *J. Geophys. Res.*, 106(D3), 3111-3123, 2001.

Schade, G. W. and Goldstein, A. H.: Seasonal measurements of acetone and methanol: Abundances and implications for atmospheric budgets, *Global Biogeochemical cycles*, 20, GB1011, doi:10.1029/2005GB002566, 2006.

Seinfeld, J. H. and Pandis, S. N.: Atmospheric chemistry and physics: from air pollution to climate change, Wiley-Interscience publication, New York, 1326 pp, 1998.

Sharkey, T. D. and Singsaas, E. L.: Why plan emit isoprene, *Nature*, 374, 769, 1995.

Spirig, C., Nefel, A., Ammann, C., Dommen, J., Grabmer, W., Thielmann, A., Schaub, A., Beauchamp, J., Wisthaler, A. and Hansel, A.: Eddy covariance flux measurements of biogenic VOCs during ECHO 2003 using proton transfer reaction mass spectrometry, *Atmos. Chem. Phys.*, 5, 465-481, 2005.

Staehelin, J., Prévôt, A. S. H. and Barnes, I.: Photochemie der Troposphäre, in Guderian, R. (Ed.), *Handbuch der Umweltveränderungen und Ökotoxikologie – Atmosphäre*, Springer Verlag, Berlin, 2000.

Wildt, J., Kobel, K., Schuh-Thomas, G. and Heiden, A. C.: Emissions of oxygenated Volatile Organic Compounds from Plants Part II, *J. of Atmospheric Chemistry*, 45, 173-196, 2003.

Zanobetti, A., Schwartz, J. and Dockery, D. W.: Airborne particles are a risk factor for hospital admissions for heart and lung disease, *Environ Health Perspect.*, 108, 1071-1077, 2000.

3 Technical note: Water vapour concentration and flux measurements with PTR-MS

C. Ammann, A. Brunner, C. Spirig, A. Neftel

Agroscope ART, Federal Research Institute, Zurich, Switzerland

Published in Atmospheric Chemistry and Physics, 6, 4643-4651, 2006.

Abstract

The most direct approach for measuring the exchange of biogenic volatile organic compounds between terrestrial ecosystems and the atmosphere is the eddy covariance technique. It has been applied several times in the last few years using fast response proton-transfer-reaction mass spectrometry (PTR-MS). We present an independent validation of this technique by applying it to measure the water vapour flux in comparison to a common reference system comprising an infra-red gas analyser (IRGA). Water vapour was detected in the PTR-MS at mass 37 (atomic mass units) corresponding to the cluster ion $\text{H}_3\text{O}^+\bullet\text{H}_2\text{O}$. During a five-week field campaign at a grassland site, we obtained a non-linear but stable calibration function between the mass 37 signal and the reference water vapour concentration. With a correction of the high-frequency damping loss based on empirical ogive analysis, the eddy covariance water vapour flux obtained with the PTR-MS showed a very good agreement with the flux of the reference system. The application of the empirical ogive method for high-frequency correction led to significantly better results than using a correction based on theoretical spectral transfer functions. This finding is attributed to adsorption effects on the tube walls that are presently not included in the theoretical correction approach. The proposed high-frequency correction method can also be used for other trace gases with different adsorption characteristics.

3.1 Introduction

Proton transfer reaction mass spectrometry (PTR-MS) has become widely used for the detection of biogenic volatile organic compounds (BVOC), and in the last five years it has been applied several times for respective flux measurements by the eddy covariance (EC) technique (e.g. Karl et al., 2001, 2002, 2004; Schade and Custer, 2004; Lee et al., 2005; Spirig et al., 2005; Holzinger et al., 2006). Before, the EC technique had been applied only for few single organic trace gases like isoprene (Guenther and Hills, 1998). PTR-MS systems used so far for EC measurements included quadrupole mass filtering and detection of a few selected ions with an integration time between 0.2 and 1 s. Thus, for multi-component EC measurements with sequential detection, the effective sampling frequency for each compound becomes about 1 Hz or less. In addition, the sampled time series of the individual compounds are – in the strict sense – disjunct, because of the gaps during the sampling of the other compounds. As a consequence, special evaluation schemes have been used for the flux calculation, mainly the 'virtual disjunct' approach (Karl et al., 2002) and a low-pass filter approach with an averaging over the unresolved high frequencies (Spirig et al., 2005). Especially for flux measurements over low vegetation, limitations in the temporal resolution of the sampling (also due to the design of the air inlet) can lead to considerable damping of the high-frequency fluctuations and an underestimation of the flux that has to be corrected for. Therefore, a validation of the measured fluxes with independent and reliable methods would be useful. However, flux measurement techniques that could serve as a reference for eddy covariance are not available, and presently there are no alternative analytical systems for BVOC with similar or better capabilities than PTR-MS.

We present here a validation of EC measurements with PTR-MS based on the water vapour flux, for which well established reference systems exist. EC flux measurements for water vapour combining a sonic anemometer and an infra-red absorption gas analyser (IRGA) are most widely used nowadays also as part of large operational measuring flux programs such as EUROFLUX (Aubinet et al., 2000). During the vegetation period 2004 we measured water vapour fluxes over an intensively managed grassland field at the Swiss CarboEurope grassland site using the PTR-MS and the IRGA methodology in parallel. We present an empirical correction method for the high-frequency damping effect based on ogive analysis and compare the resulting fluxes of the two methods.

3.2 Methods

3.2 Methods

3.2.1 The PTR-MS instrument

Proton-Transfer Reaction Mass Spectrometry (PTR-MS) utilizes the ionisation of air constituents by reaction with hydronium ions (H_3O^+) in a drift tube and subsequent detection of the protonated compounds by a mass selective quadrupole detector. For details of this analytical technique, the reader is referred to Lindinger et al. (1998), de Gouw et al. (2000), or Ammann et al. (2004). The instrument used in this study was the commercially available instrument manufactured by IONICON (GmbH, Innsbruck, Austria). It features a drift tube with a small reaction volume allowing a short residence time of the sample air of only 0.1 s. However, the effective time resolution of PTR-MS measurements is additionally limited by the integration time necessary to obtain sufficient counts of the respective ion mass.

For the instrument setup used in the present study, the signal of the primary ions H_3O^+ at mass 19 amu (m19) was in the order of $5 \cdot 10^6$ cps (counts per second). For practical reasons, the H_3O^+ signal was detected at mass 21 (as $\text{H}_3^{18}\text{O}^+$ with a constant isotope ratio of 1:500 relative to m19). Observed sensitivities for BVOCs were typically in the order of 10^2 cps/ppb. The signals of product ions are proportional to the concentration of primary ions and therefore given in normalised counts per second (ncps), i.e. the counts at a specific mass per 10^6 counts of the primary ions H_3O^+ .

The primary hydronium ions can form clusters with water molecules present in the drift tube. The resulting cluster ions $\text{H}_3\text{O}^+ \cdot \text{H}_2\text{O}$ are detected at mass 37. The water molecules in the drift tube originate to one part from the neighbouring ion source volume and to another part from the water vapour in the sample air. For a given setup of the instrument it is assumed that the first H_2O source is relatively constant while the second is related to the absolute humidity of the ambient air. The formation and stability of water clusters strongly depend on the conditions in the drift tube, especially on the ratio of the electric field strength (E) and the gas density (N). E/N has to be chosen high enough to avoid excessive clustering (de Gouw et al., 2003), but on the other hand as low as possible to minimize fragmentation. During the whole measuring period we ran the PTR-MS with a ratio of E/N 130 Td (10^{-17} V cm² molec⁻¹) and also the other operation parameters were held constant. For this setup of the PTR-MS, the

3 Technical note: Water vapour concentration and flux measurements with PTR-MS

$\text{H}_3\text{O}^+\bullet\text{H}_2\text{O}$ ion signal m37 is only a few percent of the un-clustered hydronium ion signal m19. It is expected that m37 has a stable quantitative relationship to the water vapour concentration of the sample air and thus can be used, with an adequate calibration, to measure the water vapour flux.

3.2.2 Field site

The experimental site is located at Oensingen in Central Switzerland (47° 17' N / 07° 44' E; 450 m a.s.l.). The prevailing climate is temperate continental, with an average annual rainfall of about 1100 mm and a mean annual air temperature of 9°C. The experimental plot (size 52x146 m) is part of a carbon and greenhouse gas budget experiment (for details see Flechard et al., 2005; Ammann et al., 2006) and was converted from an arable rotation into permanent grassland (newly sown grass-clover mixture) in 2001. The measurements reported here were performed during the third growth period in 2004, between 25 June and 2 August. During the experiment, the grass canopy height increased from 0.08 m to 0.20 m.

3.2.3 Eddy covariance flux measurements

CO_2 and H_2O fluxes are routinely measured at the Oensingen site by the eddy covariance (EC) technique using a combination of a sonic anemometer (HS research anemometer, Gill Instruments, Lymington, UK) and an open-path infra-red gas analyser (IRGA, Li-7500, Li-Cor, Lincoln NE, USA) installed at 1.2 m above ground. Data of both instruments were sampled at a frequency of 20 Hz. Details of the instrumental setup and the flux calculation procedure are given by Ammann et al. (2004; 2006).

The EC flux measurement with the PTR-MS was done with the same sonic anemometer as for the IRGA system. Ambient air close to the sonic sensor head (distance c. 15 cm) was continuously sampled through a 30 m long inlet line (PFA O.D. ¼", I.D. 3.5 mm) leading to the PTR-MS instrument. The inlet line was purged with a flow rate of 4 L/min, resulting in a likely laminar flow regime with a Reynolds number of 1620 and an average tube residence time (delay time between sonic wind and PTR-MS measurements) of about 4.3 s.

3.2 Methods

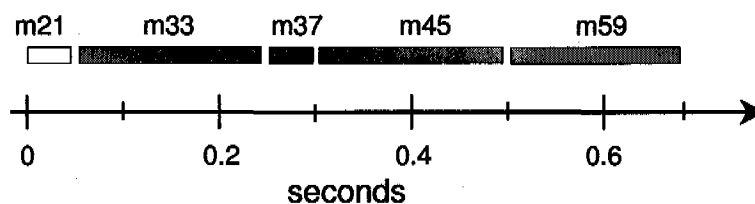


Figure 1. Typical eddy covariance measurement cycle with dwell times of 0.2 s for VOC related masses and 50 ms for primary ions (hydronium ion isotope m21 and hydronium cluster ion m37).

The effective measurement interval of the PTR-MS of 0.7 s was about 14 times longer compared to the sonic/IRGA system. As the quadrupole filter only allows subsequent detection of different ion masses, the achievable time resolution decreases with the number of scanned masses. In the present study we scanned five different ion masses, allowing to measure the fluxes of three different BVOC species and of m37 (as water vapour signal). Beside m37 and the primary ion isotope m21, the ion masses m33 (methanol), m45 (acetaldehyde) and m59 (acetone) were detected. To determine the m21 and the m37 signal (both in the order of 10^4 cps) an integration interval of 50 ms was sufficient while for typical BVOC ambient concentrations of 1 ppb or less, an integration time of at least 0.2 s was necessary to avoid significant noise attributions due to counting statistics. The resulting measurement cycle with a total interval of 0.7 s is illustrated in Fig. 1. Usually the PTR-MS instrument was operated in the EC mode for half an hour within each full hour.

3.2.4 Flux calculation and correction of high frequency losses

To calculate the fluxes we used the EC calculation method described by Spirig et al. (2005). In a nutshell: The PTR-MS measurement for an individual ion mass is regarded to be representative for the whole time period of the measuring cycle of 0.7 s (see Fig. 1). Technically, this is implemented by simply repeating the PTR-MS mass concentrations of a particular cycle until the next PTR-MS data point is available. After this procedure similar equidistant time series (time resolution $\Delta t = 0.05$ s) of sonic wind data and PTR-MS data are available for the flux calculations. Following the eddy covariance method the vertical flux of a trace gas F_c (or of another scalar quantity) is calculated as the covariance of the discrete time series of the vertical wind $w(t)$ and the concentration $c(t)$ over an averaging period T_a of typically 30 min.:

3 Technical note: Water vapour concentration and flux measurements with PTR-MS

$$F_c = \text{cov}_{wc}(\tau_{del}) = \left(\frac{\Delta t}{T_a} \right) \cdot \sum_{t=0}^{T_a} w(t) \cdot c(t + \tau_{del}) \quad (1)$$

The two time series are adjusted to each other by a delay time τ_{del} that accounts for the residence time in the air sampling tube and possible time difference between the data acquisition systems. In the present evaluation, τ_{del} was determined empirically by searching the maximum of the covariance function (within a physically plausible range). Beside the delay time, the inlet tube also led to a damping of high-frequency turbulent fluctuations of the trace gas concentrations before the detection by the PTR-MS. Additional high-frequency damping effects of the PTR-MS signals stem from the limited time resolution and the corresponding data treatment, as well as from the separation distance between the sampling tube inlet and the anemometer sensor. These damping effects can have a considerable impact on the calculated flux, especially at low measurement heights, and have to be corrected for.

Several approaches to determine the high-frequency damping effect have been proposed in the literature (for a review, see Massman and Clement, 2004), among which the 'transfer function method' initiated by Moore (1986) is most widely used nowadays and is recommended in the operational procedure of large EC flux networks such as EUROFLUX (Aubinet et al., 2000). In this theoretical mechanistic approach, the frequency damping is calculated using known spectral transfer functions for each damping effect, i.e. sensor/inlet separation, radially differential flow speed in the sampling tube, and limited response or sampling frequency of the trace gas analyser. The transfer functions of the individual damping effects are subsequently applied to the ideal turbulent flux co-spectra after Kaimal (Kaimal et al., 1972; Kaimal and Finnigan, 1994) in order to quantify the integral flux damping factor. Beside instrument specific (quasi-constant) parameters, the transfer functions and the Kaimal spectra depend only on wind speed and for stable conditions also on stability. The problems of this theoretical approach are the ideal assumptions that are made on one hand about the shape of the co-spectra and on the other hand about the relevant damping mechanisms that have to be known a priori.

As an alternative, we developed an empirical correction approach using the spectral information of the measured time series, i.e. the flux 'ogives'. The ogive Og_{wc} is defined as the cumulative sum of the finite co-spectrum Co_{wc} (Desjardins et al., 1989; Oncley et al., 1996).

3.2 Methods

The co-spectrum is the real part of the discrete Fourier transform of the full covariance function $\text{cov}_{wc}(t)$ with $0 \leq t \leq T_a$. The ogive describes the cumulative contribution to the turbulent flux of the different fluctuation frequencies in the range limited by the averaging interval T_a and the time resolution Δt :

$$Og_{wc}(f_m) = \sum_{i=1}^m Co_{wc}(f_i) \quad f_i = \frac{i}{T_a} ; \quad m = 1, 2, \dots, \left[\frac{T_a}{2 \cdot \Delta t} \right] \quad (2)$$

The ogive over all frequencies is equal to the eddy covariance flux F_c (eq. 1) of the corresponding time series. For practical purposes the ogives are normalised by F_c to have a maximum value of 1 and they are reduced to 40–50 data points regularly distributed over the logarithmic frequency scale. Figure 2a shows two exemplary ogives derived from sonic and PTR-MS measurements. The heat flux ogive is calculated from the sonic temperature that experienced almost no damping. This ogive shape represents the true cumulative contribution of the various frequencies to the turbulent flux. In contrast, the ogive of the m37 signal reaches the maximum value of 1 already at lower frequencies because some higher frequency contributions were damped out by the measurement process.

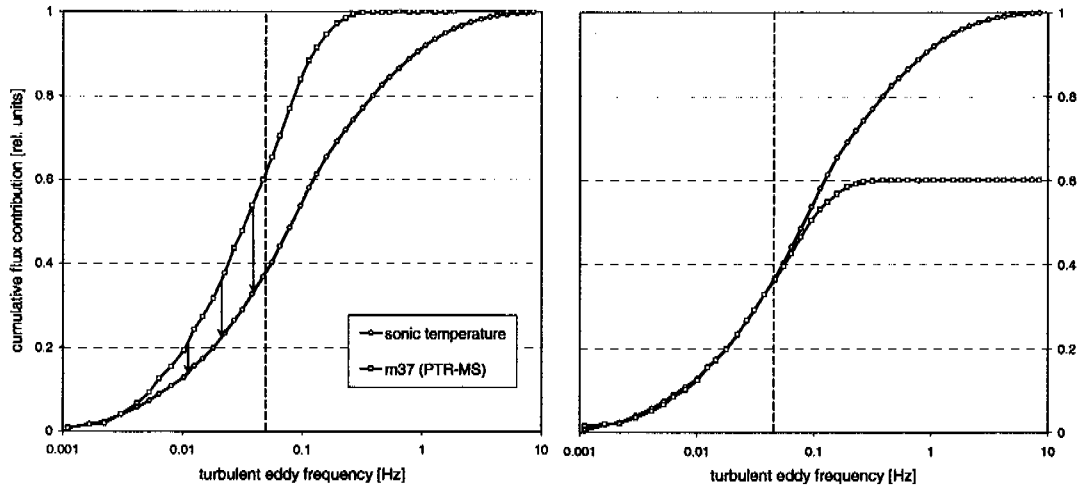


Figure 2. Illustration of the empirical approach to determine high frequency loss based on relative flux ogives. The ogive of the damped quantity (here PTR-MS m37) is adjusted to the ogive of the almost un-damped sonic temperature in the lower frequency range (up to 0.065 Hz), where almost no damping occurs. The displayed ogives represent averages over 5 half-hourly measurements at the field site on 16 July 2004 between 11:00 and 15:00.

3 Technical note: Water vapour concentration and flux measurements with PTR-MS

The total damping effect is determined empirically by scaling the damped ogive at the low frequencies (up to 0.065 Hz representing a time period of 15 s) to the respective un-damped ogive of the sensible heat flux as illustrated in Fig. 2b. The damping factor is then indicated by the right-end of the adjusted ogive. In the example case it is 0.60 for the PTR-MS m37 flux.

The damping factors, empirically determined in this way for each individual half-hour flux, are relatively noisy and sometimes unusable if e.g. the reference heat flux is close to zero. Thus a correction of the fluxes with individual damping factors would increase the noise of the flux data. To overcome this problem, we made a quality selection of the damping factors and parameterised their dependence on the main influencing parameters, in particular wind speed and stability. We excluded cases with either raw m37 flux or sensible heat flux close to zero ($|F_{m37}| < 0.2 \text{ mmol m}^{-2} \text{ s}^{-1}$, $|F_H| < 5 \text{ W m}^{-2}$), or with an obvious disturbance in the low-frequency part of the normalised ogives (value > 0.3 at 0.002 Hz). Finally all measured fluxes were corrected for the parameterised damping factor. Beside the empirically determined damping factor, also the theoretically estimated damping factor after Moore (1986) was calculated for comparison purposes. For the PTR-MS m37 flux, it included spectral damping functions for (a) sensor separation, (b) sonic path averaging, (c) the 0.7 s averaging interval of the PTR-MS signal, and (d) laminar flow in the sampling tube. The latter effect was described by the transfer function given by Lenschow and Raupach (1991).

Table 1. Effect of applied selection criteria on the number of half-hourly data available for the analysis/validation of PTR-MS derived water vapour concentration, flux, and ogive/damping factor within the observation period 25.6.2004 – 2.8.2004.

selection criterion	no. of data	percentage
correct operation of PTR-MS	644	100%
undisturbed IRGA conc. measurements (no disturbance by rain or dew on the open-path sensor)	543	84%
usable IRGA EC flux measurements (acceptable stationarity of fluxes, Aubinet et al., 2000)	442	69%
good conditions for ogive ratio calculation (acceptable ogive shape, fluxes not close to zero)	266	41%

3.3 Results

3.3 Results

Figure 3 shows the time series of the normalised m37 counts together with the ambient water concentration measured the by IRGA, as well as global radiation and wind speed for the study period that covered about five weeks (third growing period of the intensively cut grass field). A range of values between 8 and 26 mmol mol⁻¹ was recorded for the water vapour. Within the measuring period we had in total 644 half hourly measurement intervals with a correct operation of the PTR-MS instrument in the EC mode.

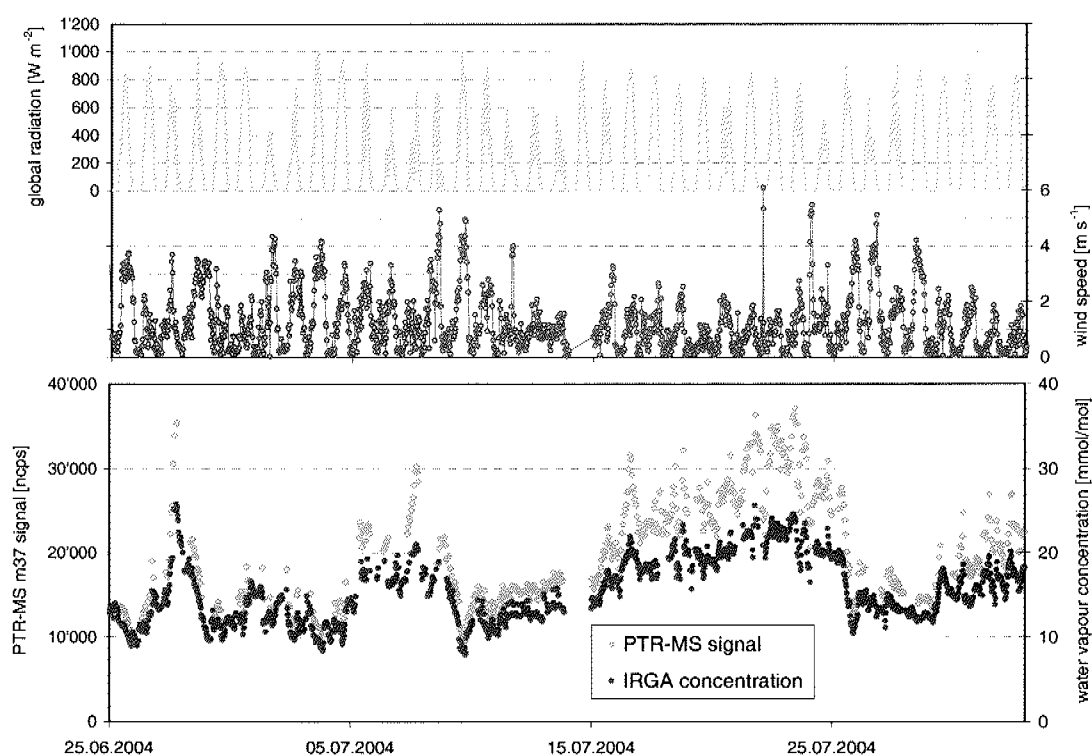


Figure 3. (a) Time series of global radiation and wind speed for the study period; (b) time series of water vapour concentration as measured by the open-path IRGA and the normalised m37 signal detected by PTR-MS.

First we investigated the relationship between the normalised m37 signal of the PTR-MS and the water vapour concentration in the sampled air as detected by the open-path IRGA near the sampling inlet. The m37 data are plotted against the reference IRGA concentrations in Fig. 4. Because of some gaps in the IRGA data due to disturbance by rain or due formation on the open-path sensor, the number of data points for this comparison was reduced by 16% (see Table 1). The m37 signal shows a non-linear but very stable relationship to the water vapour

3 Technical note: Water vapour concentration and flux measurements with PTR-MS

concentration that could be well described by a 2nd order polynomial fitted to the data by least squares regression. The resulting numerical function is also indicated in Fig. 4. The inverse of the polynomial has the form

$$[\text{H}_2\text{O}]_{(\text{mmol/mol})} = 0.160 \cdot \sqrt{[\text{m37}]_{(\text{ncps})} - 3764} - 4.39 \quad (3)$$

and was used for the calibration of the m37 based water vapour concentration for the entire measurement period.

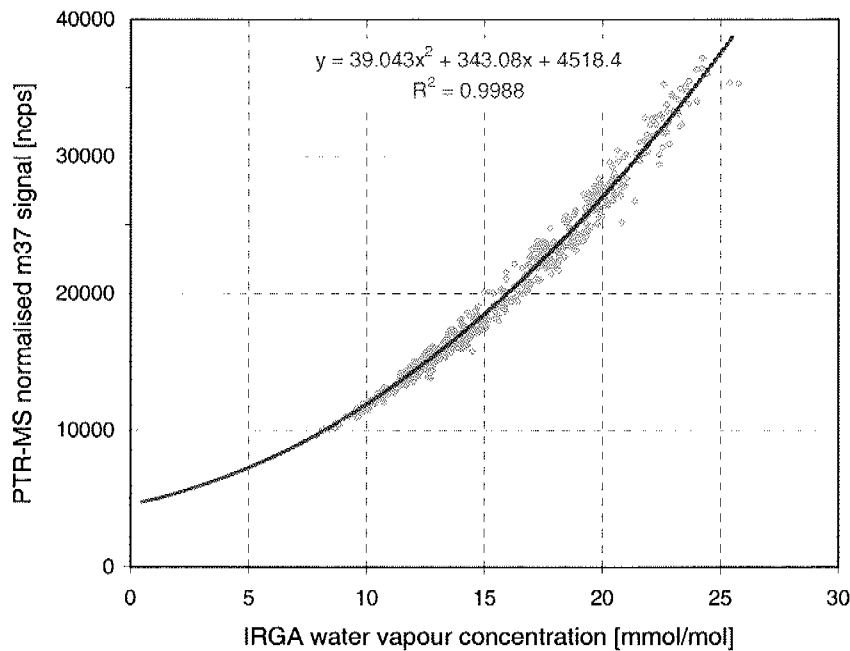


Figure 4. Relationship between the PTR-MS m37 signal and the water vapour concentration in the sampled air as measured by the open-path IRGA. A second order polynomial fitted to the data by least square regression is indicated by the solid curve.

For the flux calculation and validation a more restrictive data selection was applied than for the water vapour concentration. We selected only those conditions favourable for EC flux measurements. The IRGA water vapour flux had to pass a stationarity test as described by Aubinet et al. (2000) that compares the flux values obtained with different averaging intervals. Lacking stationarity of the turbulent transport was mainly a result of breakdown of turbulence during night-time conditions with very low wind speeds that were frequently observed at our site. This selection reduced the available flux data to 69% of the original dataset (see Table 1). As described in Sect. 2.4, an additional quality selection criterion for the

3.3 Results

empirical ogives was used. With this selection, the available data points for the damping factor analysis was reduced to 41% of the raw dataset (see Table 1). The selected flux and ogive data are strongly concentrated on daytime conditions, for which more measurements were originally performed and the described rejection criteria did not apply very often.

The empirically determined damping factors for the m37 flux ogive (as illustrated in Fig. 2) are plotted in Fig. 5 against wind speed, which was found to be the only relevant controlling parameter in the present evaluation. The influence of stability was not significant for the mostly unstable daytime conditions. Because of the relatively large scatter of the individual data, they were grouped into wind speed classes of 0.25 m s^{-1} width (up to 3 m s^{-1}) and of 1 m s^{-1} width (above 3 m s^{-1}), for which the median and upper and lower quartiles were determined. A 2nd order polynomial was fitted to the median values describing the overall dependence of the empirical damping factor on wind speed. For comparison, also the theoretical damping factor resulting from the parameterisation after Moore is displayed. The theoretical damping factors are clearly higher than the empirical ones for all wind speeds.

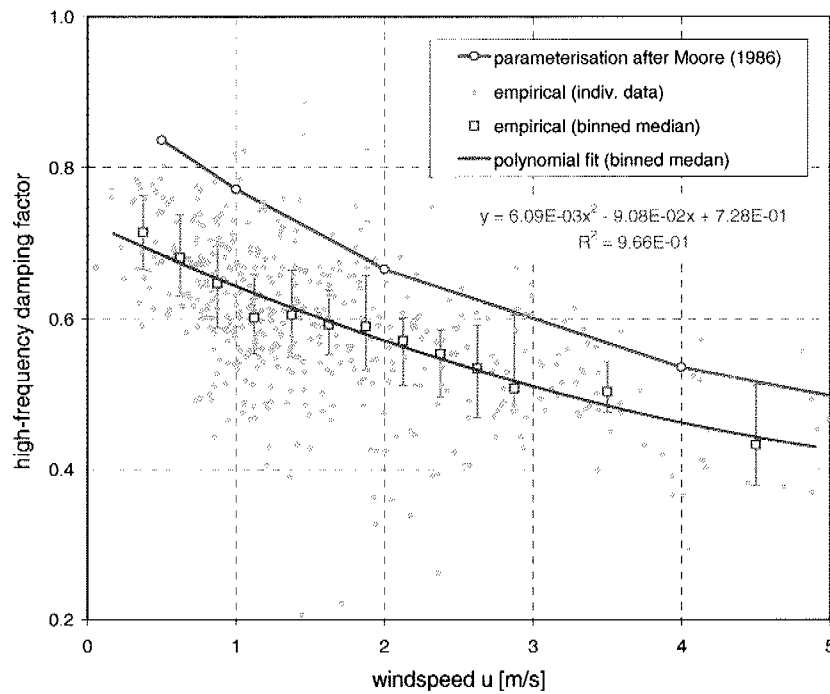


Figure 5. Empirically determined high-frequency damping factors plotted against wind-speed. The 2nd order polynomial fit to the median values of wind speed classes are displayed as solid curve. For comparison, the damping factor by the spectral transfer parameterisation after Moore (1986) is also shown.

3 Technical note: Water vapour concentration and flux measurements with PTR-MS

Finally, the raw m37 fluxes in units of ncps m s^{-1} were calibrated with the derivative of the nonlinear sensitivity function (Eq. 3) and the high frequency damping was corrected in two alternative ways with either the empirical ogive based polynomial function or the theoretical parameterisation displayed in Fig. 5. The resulting calibrated and corrected PTR-MS based water vapour fluxes are plotted against the respective IRGA fluxes in Fig. 6. The correspondence between the PTR-MS results with the theoretical (Fig. 6a) and the empirical (Fig. 6b) high-frequency correction is analyzed by means of simple linear regression. For the latter case a very good agreement is found with a slope of 0.97 ± 0.03 , an offset of 0.15 ± 0.12 $\text{mmol m}^{-2} \text{s}^{-1}$, and a correlation r^2 of 0.92. If, on the other hand, the Moore algorithm with a priori assumed transfer functions and Kaimal spectra is used for the damping correction, the slope drops to 0.80 ± 0.02 pointing to a systematic underestimation of the damping factor.

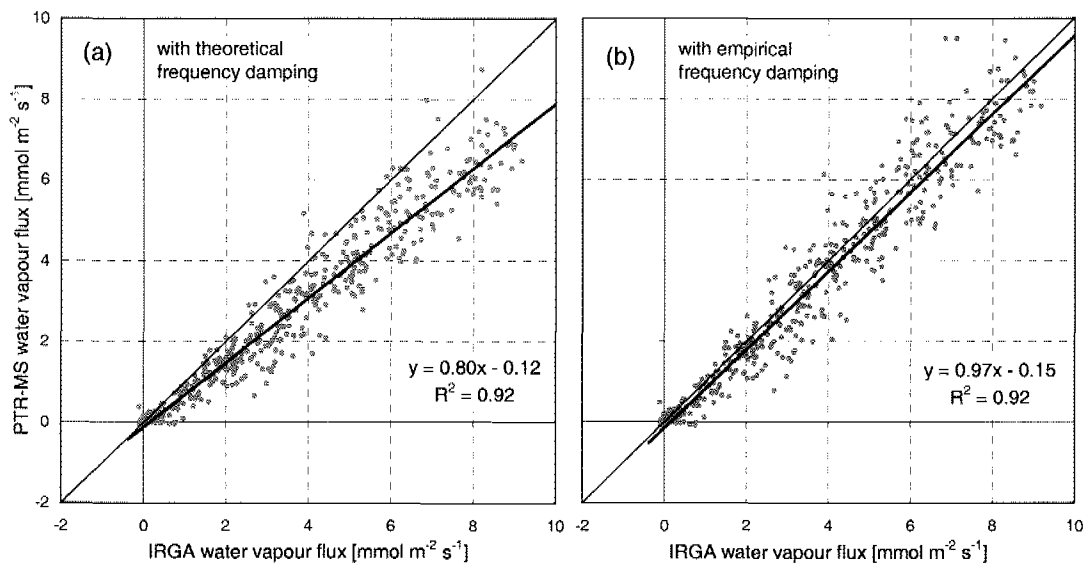


Figure 6. Comparison of water vapour fluxes obtained with PTR-MS and open-path IRGA. Only quality checked IRGA data ($n = 450$). (a) PTR-MS flux with theoretical high-frequency correction after Moore (1986); (b) PTR-MS flux with empirical high-frequency correction.

3.4 Discussion

3.4.1 Water vapour concentration and flux measurements

The relationship between the PTR-MS m37 cluster ion signal and the water vapour concentration during the present field experiment could be well described by a 2nd order polynomial fit function (Fig. 4). During the reported observation period, it did not show any drift with time, but it is valid only for the constant setup of the PTR-MS instrument used here. The choice of a second-order polynomial as fitting function was somewhat arbitrary and in the strict sense it is only valid within the range of the observed concentrations. Yet, calibration tests in the laboratory with similar E/N setting showed the same shape of the m37 signal as displayed in Fig. 4 (including the extrapolated parts of the fitted polynomial) with dry air offset signals of 3000-5000 ncps and an increase of the curve slope with increasing water vapour concentration. The latter effect was interpreted by Steinbacher et al. (2004) as a result of the collision induced cluster dissociation between drift-tube and quadrupole unit. However, for E/N values significantly lower than the 130 Td used here, the dependence of m37 on the water vapour concentration was found to change its shape considerably (see also de Gouw et al., 2003). It is therefore important to perform an individual calibration for each instrumental setup and/or measurement campaign and to keep the setup constant as far as possible.

In combination with the empirical high-frequency correction (discussed below), the calibrated m37 signal yielded water vapour fluxes that were highly comparable to the results of the reference system. The slope and offset in Fig. 6b showed only very minor deviations from the ideal 1:1 line and thus no indication for a systematic difference to the reference fluxes. In particular, the small offset results from few data points with zero m37 flux and non-zero but small IRGA flux. The scatter of individual half-hourly data points around the regression line shows a random-like distribution with a standard deviation of the residuals of $0.7 \text{ mmol m}^{-2} \text{ s}^{-1}$. For the upper flux range ($5\text{-}10 \text{ mmol m}^{-2} \text{ s}^{-1}$) the scatter of the residuals corresponds to a relative 2σ -precision of about 20%. In contrast to the empirical high-frequency correction, the theoretical Moore algorithm, taking into account only the known physical damping effects, yields a slope of only 0.80 that indicates a considerable systematic underestimation of the water vapour flux. This finding supports the usefulness of our empirical correction approach

based on ogive analysis for an adequate correction for high-frequency loss and for identifying potentially unknown but relevant damping effects.

3.4.2 Analysis of high frequency damping

The effect of high frequency damping on the PTR-MS measurements was empirically evaluated using the comparison of the ogives (cumulative co-spectra) of the sensible heat flux and the PTR-MS water vapour flux. Since only relative ogive values are used, they may be calculated from the raw data without full calibration. The empirical ogive approach assumes an originally equal spectral distribution of the water vapour and sensible heat flux, negligible damping for the heat flux measurement, and that damping of the water vapour flux measurement only starts at frequencies exceeding $f_{\text{limit}} = 0.065$ Hz corresponding to a period of 15 s. The frequencies below this limit contributed typically around 40% to the undisturbed heat flux and 60% to the damped water vapour flux (see Fig. 2). Since the turbulence spectra as well as the transfer functions depend on the measurement height and the wind speed (Moore, 1986; Kaimal and Finnigan, 1994), it may be necessary and useful to adapt the frequency range used for the ogive scaling when the method is applied to other sites and damping conditions. Our recommendation is to choose f_{limit} equal or lower than the frequency at which the damped ogive reaches a value of 0.6-0.7 in order to ensure that it is still in the undisturbed range. In cases where non-stationarity is a problem it might also be suitable to subtract the very low frequent contributions (e.g. below 0.002 Hz) from the ogives before the scaling is performed.

The damping correction as calculated by the theoretical Moore approach is weaker than the empirically determined one (Fig. 5) and leads to a corresponding underestimation of the water vapour flux (Fig. 6). Since no systematic difference between the empirical and theoretical co-spectra was found (not shown here), the reason for the discrepancy must be an important damping process that has not been considered in the theoretical approach. In order to characterize this effect, the average empirical spectral transfer function (ratio between damped and undamped ogive) is displayed in Fig. 7 for an exemplary day together with the total transfer function of all known damping effects. The observed empirical transfer function can be well described by a first order response function of the following form (Horst, 1997; Su et al., 2004):

3.4 Discussion

$$H_{wc}(f) \equiv \frac{Co_{wc}(f)_{damped}}{Co_{wT}(f)_{undamped}} = \frac{1}{1 + (2\pi \cdot \tau_d \cdot f)^2} \quad (4)$$

The characteristic response time τ_d resulting from the fit in Fig. 7 is 1.2 s. The transfer function found for our system is very similar to empirical transfer functions reported by Goulden et al. (1996), Laubach and Teichmann (1996), Leuning and Judd (1996), and Su et al. (2004) for water vapour flux measurements with closed path systems using a long inlet tube (materials: polyethylene or Teflon). They all applied a combined CO₂/H₂O IRGA instrument for the water vapour detection and observed the strong damping effect only for the H₂O and not for the CO₂ flux. Thus we follow their conclusions and also attribute the strong damping effect in our system to adsorption and desorption processes of water molecules on the inner walls of the sampling tube.

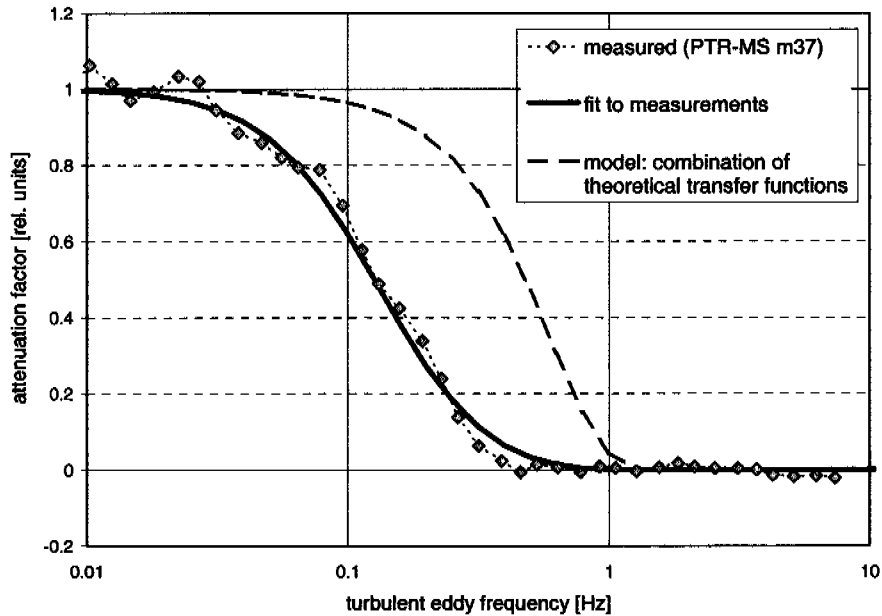


Figure 7. Comparison of theoretical and empirical total transfer function describing the high-frequency damping effect on the PTR-MS m37 flux. The empirical curve was derived from average ogives of 5 half-hourly measurements at the field site on 16 July 2004 between 11:00 and 15:00 (same as in Fig. 2). The modelled curve is the product of known theoretical transfer functions for laminar tube flow, sensor separation, and block averaging over the PTR-MS sampling interval of 0.7 s according to Moore (1986).

Some of the authors also reported that the strength of the damping effect depended on the length of operation of the inlet tube and that it could be reduced by cleaning of the inner

surfaces. Su et al. (2004) obtained τ_d values for the H₂O flux between about 0.5 s and 4.6 s for new/cleaned and aged sampling tubes, respectively. These values were always higher than for the simultaneously measured CO₂ flux with a relatively constant τ_d of only about 0.3 s. Thus water vapour obviously experiences always an additional tube related damping compared to inert trace gases but the magnitude of this effect depends on the age and cleanness of the tube walls. Leuning and Judd (1996) explain this behaviour with the gradual deposition of salt crystals and other small hydrophilic particles, which are able to pass the inlet filter, onto the inner tube wall during operation. A heating of the inlet line could probably reduce the sorption effects. In the present study it was not used because it had been found to cause contamination with VOCs, possibly as a consequence of volatiles from the insulation diffusing through the PFA walls.

3.4.3 Implication for BVOC measurements

The main application purpose of the PTR-MS is the measurement of BVOC concentrations and fluxes. Therefore it is of special interest whether the damping effects quantified for water vapour also apply to the measured BVOC components. In the present study methanol (ion mass m33) was the only component with fluxes large enough to allow the determination of empirical damping factors from ogive analysis in a similar quality as for m37. Figure 8 shows the results of the empirical damping factors in comparison with the results for m37 and of the theoretical approach already discussed above. On average the empirical ogive analysis shows weaker high-frequency damping for methanol than for water vapour, but still stronger than predicted by the theoretical transfer functions. This indicates a smaller but still relevant wall sorption effect for methanol. For other BVOCs the effect presumably varies depending on the volatility, polarity, and water solubility properties of the individual compound. Since the 'stickiness' of methanol is considered to be high, the effect for other light-weight compounds of interest, like acetaldehyde or acetone, is supposed to be of similar magnitude or even lower. However, for eddy covariance flux measurements, an empirical ogive analysis is recommended for each individual component whenever possible.

3.4 Discussion

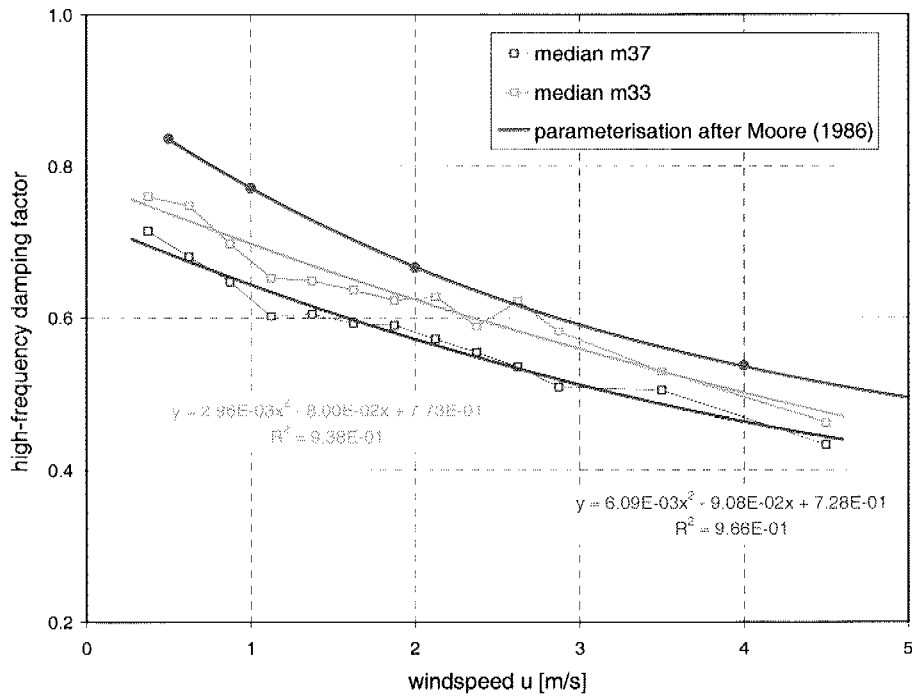


Figure 8. Same as Fig. 5 with individual data points omitted. In addition the empirically determined median damping factors for m33 (methanol) and the corresponding polynomial fit are displayed.

3.5 Conclusions

During a five week field measurement campaign at a grassland site we measured water vapour concentrations and eddy covariance fluxes using the PTR-MS instrument and a standard reference system based on an IR gas analyser. We obtained a non-linear but stable calibration function between the m37 signal of the PTR-MS and the water vapour concentration. With a correction of the high-frequency damping loss based on empirical ogive analysis, the water vapour flux obtained with the PTR-MS showed a very good agreement with the IRGA system. This positive validation for the H_2O flux also supports the ability of the PTR-MS for adequate eddy flux measurements of various volatile organic compounds (e.g. Karl et al, 2001; 2004; Spirig et al., 2005), for which no independent validation is possible.

The application of the empirical ogive method for high-frequency correction led to significantly better results than using the correction based on theoretical spectral transfer

models (e.g. Moore, 1986). This finding is attributed to adsorption effects on the tube walls that are presently not included in the models, since they are difficult to describe mechanistically and they may depend on the characteristics of the trace gas and the tube material and state (Su et al., 2004). Therefore the empirical determination and correction of high-frequency damping effects is particularly advantageous for closed-path systems with longer intake tubes and for trace gases with a high wall adsorption capacity like water vapour.

Acknowledgements

This work was financially supported by the Swiss National Science Foundation (Project COGAS, Nr. 200020-101636).

References

- Ammann, C., Spirig, C., Neftel, A., Steinbacher, M., Komenda, M., and Schaub, A.: Application of PTR-MS for Measurements of Biogenic VOC in a Deciduous Forest, *Int. J. Mass Spectrom.*, 239, 87-101, 2004.
- Ammann, C., Flechard, C.R., Fuhrer, J., and Neftel, A.: Greenhouse gas budget of intensively and extensively managed grassland, in A. Lüscher et al. (Eds.): *Land Use Systems in Grassland Dominated Regions*, 130-132, vdf Hochschulverlag, Zürich, 2004.
- Aubinet, M., Grelle, A., Ibrom, A., et al.: Estimates of the annual net carbon and water exchange of forests: the EUROFLUX methodology. *Adv. Ecol. Res.*, 30, 113-171, 2000.
- de Gouw, J. A., Howard, C. J., Custer, T. G., Baker, B. M., and Fall, R.: Proton-transfer chemical ionization mass spectrometry allows real-time analysis of volatile organic compounds released from cutting and drying of crops, *Environ. Sci. Technol.*, 34, 2640-2648, 2000.
- de Gouw, J., Warneke, C., Karl, T., Eerdekens, G., van der Veen, C., and Fall, R.: Sensitivity and specificity of atmospheric trace gas detection by proton-transfer-reaction mass spectrometry, *Int. J. Mass Spectrom.*, 223/224, 365-382, 2003.

3. References

- Desjardins, R. L., MacPherson, J. I., Schuepp, P. H., and Karanja, F.: An evaluation of aircraft flux measurements of CO₂, water vapor and sensible heat, *Boundary-Layer Met.*, 47, 55-69, 1989.
- Flechard, C. R., Neftel, A., Jocher, M., Ammann, C., and Fuhrer, J.: Bi-directional soil/atmosphere N₂O exchange over two mown grassland systems with contrasting management practices, *Global Change Biol.*, 11 (12), 2114-2127, 2005.
- Goulden, M. L., Munger, J. W., Fan, S.-M., Daube, B. C., and Wofsy, S. C.: Measurements of carbon sequestration by long-term eddy covariance: methods and a critical evaluation of accuracy, *Global Change Biol.*, 2, 169-182, 1996.
- Guenther, A. B. and Hills, A. J.: Eddy covariance measurement of isoprene fluxes, *J. Geophys. Res.*, 103, 13 145–13 152, 1998.
- Holzinger, R., Lee, A., McKay, M., and Goldstein, A. H.: Seasonal variability of monoterpene emission factors for a Ponderosa pine plantation in California, *Atmos. Chem. Phys.*, 6, 1267–1274, 2006.
- Horst, T. W.: A simple formula for attenuation of eddy fluxes measured with first-order-response scalar sensors, *Boundary-Layer Met.*, 82, 219-233, 1997.
- Kaimal, J., and Finnigan, J.: *Atmospheric boundary layer flows: Their structure and measurement*, Oxford University Press, Oxford, 1994.
- Kaimal, J. C., Wyngaard, J. C., Izumi, Y., and Coté, O. R.: Spectral characteristics of surface-layer turbulence, *Q. J. R. Meteorol. Soc.*, 98, 563-589, 1972.
- Karl, T., Guenther, A., Lindinger, C., Jordan, A., Fall, R., and Lindinger, W.: Eddy covariance measurements of oxygenated volatile organic compound fluxes from crop harvesting using a redesigned proton-transfer-reaction mass spectrometer, *J. Geophys. Res.*, 106, 24157-24167, 2001.
- Karl, T. G., Spirig, C., Rinne, J., Stroud, C., Prevost, P., Greenberg, J., Fall, R., and Guenther, A.: Virtual disjunct eddy covariance measurements of organic compound fluxes from a subalpine forest using proton transfer reaction mass spectrometry, *Atmos. Chem. Phys.*, 2, 279-291, 2002.

Karl, T., Potosnak, M., Guenther, A., Clark, D., Walker, J., Herrik, J. D., and Geron, C.: Exchange processes of volatile organic compounds above a tropical rain forest: Implications for modeling tropospheric chemistry above dense vegetation, *J. Geophys. Res.*, 109, D18306, doi:10.1029/2004JD004738, 2004.

Laubach, J. and Teichmann, U.: Measuring energy budget components by eddy correlation: Data corrections and application over low vegetation, *Beitr. Phys. Atmosph.*, 69, 307-320, 1996.

Lee, A., Schade, G. W., Holzinger, R., and Goldstein, A. H.: A comparison of new measurements of total monoterpene flux with improved measurements of speciated monoterpene flux, *Atmos. Chem. Phys.*, 5, 505–513, 2005.

Lenschow, D. H. and Raupach, M. R.: The attenuation of fluctuations in scalar concentrations through sampling tubes, *J. Geophys. Res.*, 96, 15 259–15 268, 1991.

Leuning, R. and Judd, M. J.: The relative merits of open- and closed-path analysers for measurement of eddy fluxes, *Global Change Biol.*, 2, 241-253, 1996.

Lindinger, W., Hansel, A., and Jordan, A.: Online monitoring of volatile organic compounds at pptv levels by means of Proton-Transfer-Reaction Mass Spectrometry (PTR-MS), Medical applications, food control and environmental research, *Int. Journal of Mass Spect. and Ion Processes*, 173, 191-241, 1998

Massman, W. and Clement, R.: Uncertainty in eddy covariance flux estimates resulting from spectral attenuation, in X. Lee et al. (Eds.): *Handbook of Micrometeorology*, 67-99, Kluwer Academic Publishers, Dordrecht, 2004.

Moore, C. J.: Frequency response correction for eddy correlation systems, *Boundary-Layer Met.*, 37, 17-35, 1986.

Oncley, S. P., Friehe, C. A., Larue, J. C., Businger, J. A., Itsweire, E. C., and Chang, S. S.: Surface-layer fluxes, profiles, and turbulence measurements over uniform terrain under near-neutral conditions, *J. Atmos. Sci.*, 53, 1029-1044, 1996.

Schade, G. W and Custer, T. G.: OVOC emissions from agricultural soil in northern Germany during the 2003 European heat wave, *Atmos. Environ.*, 38, 6105–6114, 2004.

3. References

Spirig, Ch., Neftel, A., Ammann, C., Dommen, J., Grabmer, W., Thielmann, A., Schaub, A., Beauchamp, J., Wisthaler, A., and Hansel, A.: Eddy covariance flux measurements of biogenic VOCs during ECHO 2003 using proton transfer reaction mass spectrometry, *Atmos. Chem. Phys.*, 5, 465–481, 2005.

Steinbacher, M., Dommen, J., Ammann, C., Spirig, Ch., Neftel, A., and Prévôt, A. S. H.: Performance Characteristics of a Proton-Transfer-Reaction Mass Spectrometer (PTR-MS) derived from laboratory and field measurements. *Int. J. Mass Spectrom.*, 239, 117–128, 2004.

Su, H.-B., Schmid, H. P., Grimmond, C. S. B., Vogel, C. S., and Oliphant, A. J.: Spectral characteristics and correction of long-term eddy covariance measurements over two mixed hardwood forests in non-flat terrain, *Boundary-Layer Met.*, 110, 213-253, 2004.

4 Cut induced VOC emissions from agricultural grasslands

B. Davison ¹, A. Brunner ², C. Ammann ², C. Spirig ², M. Jocher ², A. Neftel ²

¹ Department of Environmental Sciences, Lancaster University, LA1 4YQ UK

² Agroscope ART, Federal Research Institute, Zurich, Switzerland

Published in Plant Biology, doi 10.1055/s-2007-965043, 2007.

Abstract

The introduction of proton transfer reaction mass spectrometry (PTR-MS) for fast response measurements of volatile organic compounds (VOC) has enabled the use of eddy covariance methods to investigate VOC fluxes on the ecosystem scale. In this study PTR-MS flux measurements of VOC were performed over agricultural grassland during and after a cut event. Selected masses detected by the PTR-MS showed fluxes of methanol, acetaldehyde and acetone. They were highest directly after cutting and during the hay drying phase. Simultaneously, significant fluxes of protonated ion masses 73, 81 and 83 were observed. Due to the limited identification of compounds with the PTR-MS technique, GC-MS and GC-FID-PTR-MS techniques were additionally applied. In this way, ion mass 73 could be identified as 2-butanone, mass 81 mainly as (Z)-3-hexenal, and mass 83 mainly as the sum of (Z)-3-hexenol and hexenyl acetates. Hexenal, hexenols and the hexenyl acetates are mostly related to plant wounding during cutting. It was found that legume plants and forbs emit a higher number of different VOC species than graminoids.

4.1 Introduction

Plants are known to produce a number of volatile organic compounds (VOC) (Kesselmeier and Staudt, 1999). Their release into the atmosphere constitutes a significant source of

4 Cut induced VOC emissions of agricultural grasslands

reactive non-methane hydrocarbons (Cojocariu et al., 2005) which has an effect on ozone and aerosols formation and the oxidising capacity of the atmosphere (Arey et al., 1991; Bermejo et al., 2003).

Much of the past work has focused on isoprene and monoterpene emissions from green plants which represent a global source in the region of 175-500 Tg C yr⁻¹ (Ehhalt et al., 2001). However, many oxygenated compounds are also known to be emitted by plants (for a review see Fall, 1999; 2003 and references therein). Low molecular weight C₁ to C₃ compounds such as methanol, acetaldehyde and acetone are some of the most abundant of the oxygenated VOCs. Pectin demethylation is the most likely source of methanol production from plants (Galbally and Kirstine, 2002) though emissions from soils and leaf litter has been measured (Schade and Goldstein, 2001). Acetaldehyde is released from plant leaves as a result of fermentation reactions in roots and as such is very important in plants which experience periodic flooding and have their roots submerged in water (Kozlowski and Pallardy, 2002; Kreuzwieser et al., 2001). Emission of acetaldehyde from plants has also been observed to occur due to several stress factors such as wounding, high light and temperature exposure (Loreto et al., 2006) or light-dark transitions (e.g. Graus et al., 2004). Acetone may be produced under several pathways: as a product of the cyanohydrin lyase reaction in cyanogenic plants, while in non-cyanogenic plants such as pines acetone production is thought to be due to decarboxylation of acetoacetate in soil micro-organisms (Fall, 2003). While methanol, acetaldehyde, and acetone are known to have additional anthropogenic as well as biogenic sources their total global source has been estimated at ≈200 Tg yr⁻¹, double that of anthropogenic non-methane hydrocarbon emissions, and so their effect on the oxidising capacity of the atmospheric may be significant (Singh et al., 2001).

The total biogenic emission of oxygenated VOCs has been estimated to approximately 260 Tg C yr⁻¹ (Guenther et al., 1995). Beside methanol, acetaldehyde, and acetone, a range of other aldehydes, ketones, alcohols and carboxylic acids are known to contribute to the biogenic source. Many of these VOCs are C₆ aldehydes and alcohols often associated with plant wounding or damage. In a forest ecosystem they represent about 24% of the VOC budget (Guenther et al., 1994, 1995).

Little is known of the exact mechanism to signal wounding in plants though wounding is known to activate the release of lipases which may contain phospholipases or neutral lipid

4.1 Introduction

lipases. Fatty acids are released of which C₁₈ α -linolenic acid and linoleic acid are important in C₆ aldehyde and alcohol production. The lipoxygenase pathway (LOX) has been shown to be responsible for C₆ formation under aerobic conditions (Fall, 1999; Feussner and Wasternack, 2002). Oxygen is inserted at the C₁₃ of the α -linolenic acid, the process being catalysed by the enzyme lipoxygenase. The 13-(S)-hydroperoxylinolenic acid produced from this is cleaved by the enzyme hydroperoxide lyase from chloroplast membranes to produce (Z)-3-hexenal and C₁₂ oxoacid. The latter undergoes isomerisation to produce a wound hormone which assists in wound healing (Hatanaka, 1993) while the former is the precursor for the rest of the C₆ hexenal family (Fall, 1999). (Z)-3-hexenal can be converted into (Z)-3-hexenol, known as leaf alcohol which can undergo acetylation to (Z)-3-hexenyl acetate. (Z)-3-hexenal can also undergo enzyme induced isomerisation to (E)-2-hexenal, known as leaf aldehyde (Hatanaka, 1993; Fall, 1999; Noordermeer et al., 1999).

Online measurements of VOC concentrations and fluxes in the field are nowadays feasible using fast response instruments such as the PTR-MS (e. g. Karl et al., 2001a, b; Ammann et al., 2004b; Ammann et al., 2006). With the purely mass related measurements provided by PTR-MS isobaric compounds are not distinguishable. A further difficulty with PTR-MS is fragmentation during the ionisation process. Detected fragment ions may originate from several different parent ions and therefore can not always be simply related to specific compounds, and so additional analysis methods may be needed to identify the compounds. In this study we complemented the PTR-MS with GC-MS and GC-FID-PTR-MS analysis. The measurements were performed above agricultural grassland near Oensingen, Switzerland. They are focussed on cut related VOC emissions.

4.2 Materials and Methods

4.2.1 Site descriptions

During June and July 2005 a series of VOC emissions were monitored above a meadow near Oensingen on the Swiss Central Plateau (47°17' N, 7°44' E; 450 m a.s.l.). The prevailing climate there is temperate continental, with an average annual rainfall of about 1100 mm and a mean annual air temperature of 9°C. The experimental field had been converted from arable

4 Cut induced VOC emissions of agricultural grasslands

rotation to permanent grassland in 2001 and is part of the projects on carbon and greenhouse gas budgets CarboEurope and Greengrass (for details see Ammann et al., 2004a; 2007; Flechard et al., 2005). It has a size of 52 m x 146 m and is aligned in a northeast-southwest axis that also represents the two main wind directions at the site. The extensively managed field is cut three times a year and is not treated with any fertilizer. It is largely composed of twelve species: six graminoids (*Alopecurus pratensis*, *Arrhenatherum elatius*, *Dactylis glomerata*, *Lolium perenne*, *Poa pratensis*, and *Poa trivialis*), four forbs (*Chrysanthemum leucanthemum*, *Stellaria media*, *Taraxacum officinale*, and *Tragopogon orientalis*), and two legumes (*Lotus corniculatus*, and *Trifolium repens*). Legumes and graminoids, in nearly equal portions, account for more than 80% of the vegetation cover. On 1 June 2005 at 11:00 local time (LT) the field was cut for the first time of the year. Just before cutting, the canopy had an LAI of $5.2 \text{ m}^2 \text{ m}^{-2}$ and the cut biomass was 510 g-dw m^{-2} . Once cut the hay was left to dry. That day (15:00 LT) and the following day (06:30 and 13:30 LT) it was turned three times to facilitate the drying process. On 3 June at 15:00 LT the hay was removed from the field.

4.2.2 VOC analysis

PTR-MS

VOC concentrations were continuously measured by means of a proton-transfer-reaction mass-spectrometer (PTR-MS, Ionicon Analytik GmbH, Austria; Lindinger et al., 1998). The PTR-MS used here corresponds to the PTR-MS-HS type, featuring three turbo pumps for increased sensitivity and a drift tube (equipped with Teflon rings) optimized for fast time response and minimal interactions with polar compounds (Spirig et al., 2005).

The air was sampled in the middle of the field, close to the sonic anemometer which was placed at a height of 1.2 m. A pump pulled the air through a 30 m long Teflon tube to the inlet of the PTR-MS. In the PTR-MS instrument, the sample air first enters the drift tube where the VOCs are ionised: the reaction between H_3O^+ -ions (generated by electrical discharge of pure water vapour) and VOC molecules produces VOCH^+ ions. In principle, any VOC with a higher proton affinity than water can be ionised in this way. These charged compounds are then analysed with a quadrupole mass filter in conjunction with an ion multiplier (secondary electron multiplier, Mascom, MC-217, R-217).

4.2 Materials and Methods

In general the ionisation with H^+ is a soft or non-destructive ionisation. Nevertheless the larger a molecule the greater the possibility of its break up caused by the H^+ transition. This break up leads to a certain pattern of fragments, which remains constant under constant instrument settings. Molecules with mass higher than about 70 amu tend to fragment. The protonated mass 101 for example fragments in more than 90% of cases producing the two protonated masses 83 and 55. For different molecules with protonated mass 101, different percentage of mass 83 and 55 are detected.

During these field measurements the instrument was running under the following conditions: pressure drift tube: 2.1 mbar, pressure detection: 2.4×10^{-5} mbar, E/N: 122Td, drift tube temperature: 45°C.

The PTR-MS was calibrated with a gas standard (Apel-Riemer Environmental, Inc., Denver CO, US), containing methanol (m33), acetaldehyde (m45), acetone (m59), and (Z)-3-hexenol (m83). It was dynamically diluted with air generated by a zero air generator (ChromGas Zero Air Generator, model 1000, Parker Hannifin Co., Haverhill MA, US). The absolute accuracy of these concentration measurements is estimated to be $\pm 20\%$ due to mass flow controller and gas standard uncertainties. The sensitivity factor determined for m83 was also applied to the neighbouring ion mass m81, for which no standard was available. Concentrations of mass 73 were calculated using a semi-theoretical approach (Ammann et al., 2004b) which was approved at the ACCENT OVOC Intercomparison in January 2005. The accuracy of this semi-theoretical approach is estimated to be $\pm 25\%$.

The VOC fluxes were calculated using the eddy covariance method (EC) as described below (section 2.3). For the flux calculation with the EC method high temporal resolution data are necessary (< 2 seconds, 0.5 Hz). To fulfil this criterion the number of masses measured with PTR-MS had to be restricted. A mass scan before and during a test cut indicated the relative abundance of the ion masses. Table 1 shows the six masses that were found to be most abundant at our site and thus were selected for the continuous high-resolution measurements. The possible corresponding VOC species found in individual calibration measurements are also indicated.

4 Cut induced VOC emissions of agricultural grasslands

Table 1: Ion masses measured by PTR-MS, possible compounds related to these masses and the molecular weight (mw) of the compounds.

measured ion masses	possible VOC	mw
m33	methanol	32
m45	acetaldehyde	44
m59	acetone	58
	propanal	58
m73	2-butanone	72
	butanal	72
m81	fragment of (E)-2-hexenal	98
	fragment of (Z)-3-hexenal	98
	fragment of pinenes	136
m83	fragment of (Z)-3-hexenol	100
	fragment of (E)-3-hexenol	100
	fragment of (E)-2-hexenol	100
	fragment of hexanal	100
	fragment of (E,Z)-2-hexenyl acetate	142

GC-MS

To assist identification of the masses detected by PTR-MS, occasional measurements with gas-chromatographic methods were performed. The first GC method applied here was a GC-MS. Air samples were collected using stainless steel sampling tubes packed with 200mg Tenax and 100mg Carbopak B to pre-concentrate VOC. These samples were analysed by thermal desorption (Perkin Elmer Turbomatrix thermal desorption system) and GC-MS (Perkin Elmer Turbomass Gold GC-MS). The compounds were separated on an Ultra 2 column (50 m x 0.2 mm, I.D., 0.11 μ m P/N 19091-005 Agilent Technologies). Compound identification was by standards whenever possible and Wiley and NIST spectral libraries. Low molecular weight hydrocarbons, usually below C4 are readily lost in the pre-concentration step on the Tenax tubes and so are not reliably detected by this system.

4.2 Materials and Methods

A first series of samples were taken in the afternoon (14:00-16:00 LT) of 2 June 2005 during the turning of the cut hay in the field. Further samples were collected from 3 to 8 June 2005 from a 40 L static chamber containing cut grass. The chamber walls consisted of Teflon foil to minimise VOC deposition on its inner surfaces. Periodically performed blank chamber tests showed no indication of chamber artefacts that could be misleadingly interpreted as emissions. Samples were collected at intervals throughout the day. A flow rate of 200 ml min^{-1} was used for sampling a total air volume of 4 L.

GC-FID-PTR-MS

The second GC method applied here was a combination of GC-FID and PTR-MS, where the GC was responsible for the separation of compounds, and the PTR-MS and a parallel switched flame ionisation detector (FID) for the detection. A Hewlett-Packard gas chromatograph (HP 5890, Series II plus) was upgraded with an online thermal desorption system (TDS G, Gerstel, Germany) and a cooled injection system (CIS 3, Gerstel, Germany) equipped with a liquid CO_2 cooling device. The compounds were separated on a DB-624 column (30 m x 0.32 mm, I.D., 1.8 μm , P/N: 125-1334, Agilent Technologies). The carrier gas nitrogen was cleaned by a nitrogen purifier (RMSN-2, big universal trap, 1/8" fittings, Agilent Technologies) and controlled by electronic pressure control (EPC). At the column end the constant flow of 2 ml min^{-1} was split 1:1 by a passive Y connector (universal "Y" press-tight ® connector, fused silica tubing, Restek #20405, SeCure "Y" connector kit 0.28/0.32 mm, Restek #20277) and conducted to the PTR-MS and FID by a transfer line (Hydroguard™ fused silica guard transfer line). The transfer line to the FID was placed in the GC oven. The other transfer line to the PTR-MS ran outside the GC and was heated by a tube heater. The PTR-MS needs an inlet sample flow of about 150 ml min^{-1} . As the split flow from the GC column was only 1 ml min^{-1} , zero air was added (produced by a Parker ChromGas Zero Air Generator, model 1000, Parker Balston, Analytical Gas Systems, US) the mixture was then conducted to the PTR-MS inlet.

Air samples were taken in the afternoon (14:00-16:00 LT) of two sunny and hot ($T_{\text{air}} > 25^\circ\text{C}$) midsummer days (26 and 27 July 2005). The plants, separated according to plant functional groups, were cut and placed into the empty 40 L static Teflon walled chamber. Air was collected for 10 minutes with a sample rate of 100 ml min^{-1} , resulting in a total sample

4 Cut induced VOC emissions of agricultural grasslands

volume of 1 L. A pump pulled the sample air through a 15 m long PTFE tube connecting the chambers with the inlet of the GC-PTR-MS. The compounds were then absorbed in the TDS G on a glass tube (1/4'' x 12 cm) filled with Tenax TA at a temperature of 25°C. The sample flow was 100 ml min⁻¹. After the adsorption, the Tenax tube was flushed for 1 minute with nitrogen (60 ml min⁻¹) at a temperature of 25°C in the opposite direction of the adsorption flow, bypassing the GC column, to remove the water. The compounds were then thermally desorbed (temperature program of the TDS G: rate: 60°C min⁻¹, kept at 200°C for 4 min) with a nitrogen flow of 60 ml min⁻¹ and cryo-focussed in the CIS 3 on a glass sleeve filled with Tenax TA at -40°C. The sample was then injected (temperature program of the CIS: rate: 12°C s⁻¹, kept at 200°C for 4 min) on the column (oven program: 35°C held for 5 min, then heated: 10°C min⁻¹ to 200°C and cooled: 70°C min⁻¹ back to 35°C). The nitrogen flow through the column was held constant at 2.0 ml min⁻¹. The total sampling and cryo-focussing time was about 17 min, the GC run time 30 min, which corresponds to a total cycle time of about 50 minutes. The FID at the end of one transfer line had a temperature of 210°C. The PTR-MS on the other end was operating in a single ion monitoring (SIM) mode with a dwell time of 50 ms per compound.

The system was calibrated with a commercially available gas standard (multi-component mix, ApelRiemer Environmental, Inc., US) which was diluted with air generated by a zero air generator (Parker ChromGas Zero Air Generator, model 1000, Parker Balston, Analytical Gas Systems, US). To determine the retention times of the GC column a hot vapour calibrator (HOVACAL, type digital 311, IAS GmbH, Germany) was used to evaporate solutions of liquid standards (Sigma-Aldrich, Fluka Chemie GmbH, Switzerland).

4.2.3 Flux calculation

The EC flux measurement with the PTR-MS was done in combination with a sonic anemometer (Gill Solent, Lymington, UK), the same instrument as used for the routine CO₂ and H₂O flux measurements (see above) placed in the middle of the grassland field. The inlet for the PTR-MS sample air was placed close to the sonic sensor head (distance 15 cm). To calculate the fluxes we used the EC calculation method described by Spirig et al. (2005) and Ammann et al. (2006). The PTR-MS measurement of the methanol ion (for 0.2 s) is regarded to be representative for the whole interval of the measuring cycle (0.7–1.3 s). Technically, this

4.2 Materials and Methods

is implemented by simply repeating the PTR-MS mass concentrations of a particular cycle until the next PTR-MS data point is available. After this procedure, similar equidistant time series (time resolution $\Delta t = 0.05$ s) of sonic wind data and methanol concentration are available for the flux calculations. Following the eddy covariance method the vertical flux of a trace gas F_c (or of another scalar quantity) is calculated as the covariance of the discrete time series of the vertical wind $w(t)$ and the concentration $c(t)$ over an averaging period T_a of typically 30 min.:

$$F_c = \text{cov}_{wc}(\tau_{del}) = \left(\frac{\Delta t}{T_a} \right) \cdot \sum_{t=0}^{T_a} w(t) \cdot c(t - \tau_{del}) \quad (1)$$

The two time series are adjusted to each other by a delay time τ_{del} that accounts for the residence time in the air sampling tube and possible time difference between the data acquisition systems that are different for the PTR-MS and the sonic anemometer. Beside the delay time, the inlet tube also led to a damping of high-frequent turbulent fluctuations of the trace gas concentrations before the detection by the PTR-MS. Additional high-frequency damping effects of the PTR-MS signals stem from the limited time resolution and the corresponding data treatment, as well as from the separation distance between the sampling tube inlet and the anemometer sensor. These damping effects were quantified and corrected for by the empirical ogive method described in detail by Ammann et al. (2006). The high-frequency damping factor mainly depended on the wind speed and ranged between 0.75 (low wind speed) and 0.45 (high wind speed).

The footprints of the flux measurements were routinely calculated (Neftel et al., submitted) using the analytical footprint model of Kormann and Meixner (2001). Cases with significant footprint contributions of the area outside the field were excluded and not considered for the results presented here (see Ammann et al., 2007). Because of the relatively low measurement height of 1.2 m and the orientation of the field along the main wind directions, the flux footprints were mostly dominated by the field of interest (>80% of total footprint) during daytime. During night, the surrounding area contributed 20-50% to the footprint.

4.3 Results

4.3.1 Flux measurements

Figure 1 shows VOC fluxes measured after the cut of the field on 1 June 2005 (11:30 LT): methanol, acetaldehyde, acetone and the fluxes for the PTR-MS ion masses 73, 81, and 83. The highest fluxes for all compounds were observed directly after the cut at 12:30 LT. The maximum values displayed in Figure 1 are $91.5 \text{ nmol m}^{-2} \text{ s}^{-1}$ ($10.5 \text{ mg m}^{-2} \text{ h}^{-1}$) for methanol, $19.4 \text{ nmol m}^{-2} \text{ s}^{-1}$ ($3.1 \text{ mg m}^{-2} \text{ h}^{-1}$) for acetaldehyde, and $12.7 \text{ nmol m}^{-2} \text{ s}^{-1}$ ($2.6 \text{ mg m}^{-2} \text{ h}^{-1}$) for acetone. The daytime average over the entire drying phase corresponding to the three days after the cut (see Table 2) are 21.1, 5.1, and $2.6 \text{ nmol m}^{-2} \text{ s}^{-1}$ (corresponding to 2.43, 0.81, $0.55 \text{ mg m}^{-2} \text{ h}^{-1}$), respectively, for the three compounds. The fluxes of the masses m73, m81, and m83 (Figure 1, Table 2) were calculated using the assumptions described in 2.2.1 but can not be converted directly to weight related units because they may represent several different compounds. More details on species identification are presented below. On the first day, all fluxes decreased steadily until 20:00 LT. During the night, almost no valid flux data could be obtained because of weak turbulence and generally small fluxes. On the first day after the cut, the fluxes showed a maximum in the morning (around 06:30 LT) and one in the early afternoon (around 13:30 LT). Both are associated with hay turning (see Section 2.1) to support the drying process. On 3 June (15:00 LT) the hay was removed from the field. Afterwards the emissions of acetaldehyde, acetone, m81 and m83 declined to very low values. Only methanol and m73 fluxes showed values significantly different from zero. A survey of average daytime fluxes for all detected masses is given in Table 2; corresponding ambient concentrations are also listed. Masses m81 and m83 show a fast decrease after the cut, the other compounds only decreased to low levels after the removal of hay.

4.3 Results

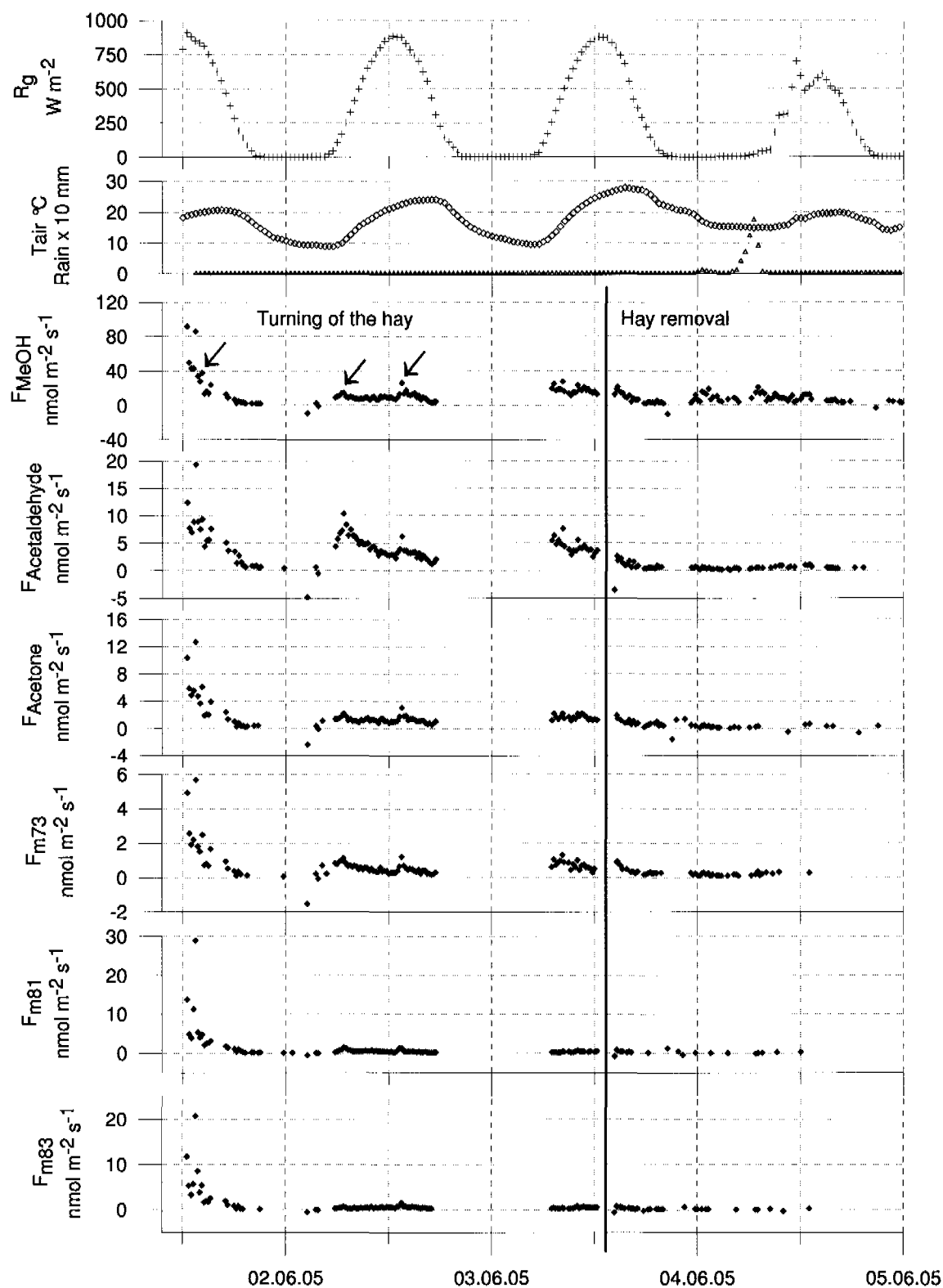


Figure 1: Time series measured above the extensive field after a cutting event (1 June 11.30 LT), from the top to the bottom: Global radiation (R_g), air temperature (T_{air}), rain, fluxes of methanol (F_{MeOH}), acetaldehyde ($F_{Acetaldehyde}$), acetone ($F_{Acetone}$), and of PTR-MS ion masses 73, 81 and 83 (F_{m73} , F_{m81} and F_{m83}).

4 Cut induced VOC emissions of agricultural grasslands

Table 2: Average daytime (07:00-17:00 LT) concentrations and fluxes during and after the cut event (first day: only data after the cut at 11:30 LT).

	1 June	2 June	3 June	4 June
concentrations [ppb]	(cut at 11:30)		(hay removed at 15:00)	
m33 (methanol)	11.66	8.76	14.25	5.68
m45 (acetaldehyde)	1.84	1.55	1.84	0.29
m59 (acetone)	2.03	2.10	2.99	0.88
m73	0.96	0.80	1.28	0.23
m81	0.82	0.16	0.17	0.05
m83	0.92	0.19	0.22	0.05
fluxes [nmol m ⁻² s ⁻¹]				
m33 (methanol)	38.02	9.90	15.47	8.66
m45 (acetaldehyde)	8.37	3.90	3.14	0.64
m59 (acetone)	5.11	1.29	1.46	0.31
m73	2.15	0.49	0.67	0.27
m81	6.82	0.59	0.36	0.21
m83	5.73	0.59	0.44	0.12

Directly after the cut all detected compounds show a similar strong decrease in the emission flux. The temporal variability of the different compounds after the first two hours was compared by means of linear correlation analysis between pairs of fluxes. Table 3 shows the correlation coefficients r^2 for the 15 min fluxes as displayed in Fig. 1. It was observed that methanol has the poorest correlation with the other masses investigated. The correlation between m81 and m83 was the best at 0.89. A strong correlation was also found between m59 and m73 with a coefficient of 0.87. The strong correlation between m81 and m83 reflects their common origin mainly from the hexenal and hexenol family resulting from the LOX pathway. Methanol does not correlate well with these masses indicating a different production mechanism.

4.3 Results

Table 3: Correlation coefficients (r^2) between fluxes of different ion masses measured by PTR-MS (excluding the first two hours after the cut).

mass \\mass	m33	m45	m59	m73	m81
m45	0.34				
m59	0.58	0.65			
m73	0.60	0.71	0.87		
m81	0.19	0.42	0.66	0.54	
m83	0.33	0.31	0.73	0.56	0.89

4.3.2 Compound identification

Tenax tube samples were screened by GC-MS for monoterpenes and a range of hydrocarbons. Grass and clover are not known as major isoprene or monoterpene emitters and in this case none were generally seen in the GC-MS results.

While nonanal and decanal are sometimes associated with contamination from the Tenax sample tubes and/or the cold trap, blank tubes exposed at intervals during sample collection were not found to contain either compound suggesting in this case they were the result of plant emissions. Benzaldehyde has also been associated with contamination from Tenax and while it was observed in some air samples it was also found in some blank tubes and therefore its presence may be the result of contamination. Table 4 shows a list of the compounds identified by GC-MS and GC-FID-PTR-MS. Several of the compounds such as (Z)-3-hexenol and (Z)-3-hexenyl acetate show a close relationship with the hay cut and plant wounding and will be discussed in further detail. Other such as nonanal, decanal and 2-ethyl hexanol are known to be emitted from flowering plants (Chen et al., 2003).

In order to investigate differences in the cut related emission characteristics of the three plant functional groups graminoids, forbs and legumes, we performed measurements with nine individual plant species (three of each group) using GC-FID-PTR-MS. Table 5 shows the VOCs observed after cutting. Methanol and acetaldehyde could not be detected with this gas-chromatographic method. In total 16 compounds could be clearly identified; seven alcohols,

4 Cut induced VOC emissions of agricultural grasslands

three aldehydes, four ketones, and two esters were found in the samples. Six compounds were found in every sample (acetone, 2-butanone, 2-pentanone, (Z)-3-hexenal, hexanal, (Z)-3-hexenol, hexenyl acetate). (E)-2-hexenal was seen only in the sample of *Taraxacum officinale*. Two compounds (methyl acetate and 3-pentanol) were detected only in samples taken from legumes. Propanal and butanal, which are potentially interfering with acetone and 2-butanone on the ion masses m59 and m72, respectively (see Table 1), were not detected in any sample.

Table 4: VOCs detected during the measurement campaign by one or more of the applied analytical techniques: compound names, chemical structure, and molecular weight (mw). For compounds detected by (GC-FID-)PTR-MS, the respective ion masses (parent or fragment ions) are indicated together with their relative occurrence.

compound	structure	mw	PTR-MS ions (% if total signal)
methanol	CH ₃ OH	32	m33 (100)
acetaldehyde	CH ₃ CHO	44	m45 (100)
acetone	CH ₃ COCH ₃	58	m58 (100)
2-butanone (MEK)	C ₂ H ₅ COCH ₃	72	m73 (98)
methyl acetate	CH ₃ COOCH ₃	74	m75 (90), m43 [*] (7)
butanol	C ₄ H ₉ OH	74	m57 [*] (100)
2-pentanone	CH ₃ CO(CH ₂) ₂ CH ₃	86	m87 (91), m45 [*] (7)
1-penten-3-ol	C ₃ H ₆ OHCHCH ₂	86	m69 [*] (85), m45 [*] (11)
3-pentanol	(C ₂ H ₅) ₂ CHOH	88	m71 [*] (80), m59 [*] (10)
1-pentanol	C ₅ H ₁₁ OH	88	m71 [*] (89), m59 [*] (11)
3-methyl-3-penten-2-	CH ₃ CH=C(CH ₃)C(=O)C	98	m99 (99)
(Z)-3-hexenal	C ₂ H ₅ (CH) ₂ CH ₂ CHO	98	m81 [*] (69), m99 (27) ¹
(E)-2-hexenal	C ₃ H ₇ (CH) ₂ CHO	98	m57 [*] (49), m99 (36),
hexanal ²	CH ₃ (CH ₂) ₄ CHO	100	m83 [*] (95), m101 (5) ¹
(E)-3-hexenol	CH ₃ CH ₂ CH=CHCH ₂ CH ₂	100	m83 [*] (73), m55 [*] (20)
(Z)-3-hexenol	CH ₃ CH ₂ CH=CHCH ₂ CH ₂	100	m83 [*] (65), m55 [*] (28)

4.3 Results

(E)-2-hexenol	$\text{CH}_3\text{CH}_2\text{CH}_2\text{CH}=\text{CHCH}_2$	100	m83* (69), m55* (22)
benzaldehyde	$\text{C}_6\text{H}_6\text{CHO}$	106	
heptanal	$\text{CH}_3(\text{CH}_2)_5\text{CHO}$	114	
2-ethyl-hexanal ²	$\text{CH}_3(\text{CH}_2)_3\text{CH}(\text{C}_2\text{H}_5)\text{CHO}$	128	
octanal	$\text{CH}_3(\text{CH}_2)_6\text{CHO}$	128	
2-ethyl-hexanol ²	$\text{CH}_3(\text{CH}_2)_3\text{CH}(\text{C}_2\text{H}_5)\text{CH}_2$	130	
(E,Z)-3-hexenyl-	$\text{CH}_3\text{CH}_2\text{CH}=\text{CH}(\text{CH}_2)_2\text{O}$	142	m83* (57), m55* (42)
nonanal	$\text{CH}_3(\text{CH}_2)_7\text{CHO}$	142	
decanal	$\text{CH}_3(\text{CH}_2)_8\text{CHO}$	156	
tetradecane ²	$\text{CH}_3(\text{CH}_2)_{12}\text{CH}_3$	198	

* fragment ions, ¹ fragmentation fractions taken from Karl et al. (2001b), ² semi-quantitative data as no standards were available. A sensitivity was estimated from the nearest analogous species.

4.4 Discussion

In the present study focussing on emissions after a grass cut several oxygenated VOCs were found, most of them showed a close connection to the cut and hay treatment events, exhibiting their association with the wounding mechanism of plants. Table 4 shows a list of the major compounds and possible ion fragments identified by GC-MS and GC-FID-PTR-MS.

With the PTR-MS mass 33 can be clearly associated with the protonated methanol and mass 45 is generally identified as acetaldehyde. Mass 59 may be from either acetone or propanal. In this instance no propanal was identified in GC-FID-PTR-MS samples (Table 5) and so it is assumed that the protonated ions at mass 59 were mostly from acetone. Only small contributions to the masses 45 and 59 are expected to result from fragments of 2-pentanone or 1-penten-3-ol and 1-pentanol or 3-pentanol, respectively (Table 4).

According to the observations by GC-FID-PTR-MS in this study, the ion mass 73 is uniquely associated with 2-butanone (methyl ethyl ketone, MEK). The other isobaric compound butanal (see Table 1), was never observed here. De Gouw et al. (1999) also observed MEK

4 Cut induced VOC emissions of agricultural grasslands

from cut and drying grass and clover leaves and stems in the laboratory using PTR-MS. The results of our study (Figure 1) show MEK emissions during the entire drying phase with elevated concentrations occurring during the turning events. Static chamber measurements on a clover field (Kirstine et al., 1998) found MEK accounted for nearly 50% of the VOC emissions from the uncut field with significant contributions also of methanol. Upon cutting elevated levels of these VOCs were observed along with those of known wound compounds such as (Z)-3-hexenal, (E)-2-hexenal, (Z)-3-hexenol, and (Z)-3-hexenyl acetate. While MEK was observed to be emitted from all plant types during this study, it was not observed in the high proportions reported by Kirstine et al. (1998).

Protonated ion mass 81 is commonly associated with fragments of monoterpenes and hexenals (see Table 1 and e.g. Ammann et al., 2004b; Karl et al., 2001b). Results from the GC-MS screening found no monoterpene present in the samples taken during this study. Of the potential hexenal species, (E)-2-hexenal was only observed for one of 9 plant species (Table 5), whereas (Z)-3-hexenal was found to be emitted by all investigated species. Therefore we assign the m81 flux by eddy covariance mainly to the latter compound.

For m83 the identification is more complex. Five different compounds fragmenting to this mass were commonly observed by GC-FID-PTR-MS (Table 5). The relative contribution of the different compounds is listed in Table 6. Hexanal, (E)-2-hexenol, and (E)-3-hexenol together account for less than 10% in all cases. Thus (Z)-3-hexenol and (E,Z)-3-hexenyl acetate are the main contributors to the m83 signal with relative shares of about 30% and 65%, respectively. All observed C₆ oxygenated compounds are known to result from plant wounding (Fall, 1999; Hatanaka, 1993; Feussner and Wasternack, 2002; Graus et al., 2004).

4.4 Discussion

Table 5: VOC emission detected by GC-FID-PTR-MS after cut of three individual species of each of the plant functional groups legumes (L), graminoids (G), and forbs (F). 1-*Lotus corniculatus*, 2-*Trifolium pratense*, 3-*Medicago sativa*, 4-*Arrhenatherum elatius* (L.) J. & C. Presl, 5-*Trisetum flavescens* (L.) P. Beauv., 6-*Lolium perenne*, 7-*Plantago lanceolata* L., 8-*Taraxacum officinale* aggr., 9-*Centaurea jacea* (L.)

plant sample:	1	2	3	4	5	6	7	8	9
plant functional group:	L	L	L	G	G	G	F	F	F
compound									
acetone	X	X	X	X	X	X	X	X	X
2-butanone (MEK)	X	X	X	X	X	X	X	X	X
methyl acetate	X	X	X						
butanol	X	X		X		X		X	X
2-pentanone	X	X	X	X	X	X	X	X	X
1-penten-3-ol	X	X	X					X	X
3-pentanol	X	X	X						
1-pentanol	X	X	X	X		X		X	X
3-methyl-3-penten-2-one	X	X	X	X	X	X	X	X	
(Z)-3-hexenal	X	X	X	X	X	X	X	X	X
(E)-2-hexenal								X	
hexanal	X	X	X	X	X	X	X	X	X
(E)-3-hexenol	X	X	X			X	X	X	X
(Z)-3-hexenol	X	X	X	X	X	X	X	X	X
(E)-2-hexenol	X	X	X	X		X	X	X	X
(E,Z)-3-hexenyl acetate	X	X	X	X	X	X	X	X	X

4 Cut induced VOC emissions of agricultural grasslands

Table 6: Relative contribution (%) of compounds detected at protonated mass m83 and m81 by GC-FID-PTR-MS. 1-*Lotus corniculatus*, 2-*Trifolium pratense*, 3-*Medicago sativa*, 4-*Arrhenatherum elatius* (L.) J. & C. Presl, 5-*Trisetum flavescens* (L.) P. Beauv., 6-*Lolium perenne*, 7-*Plantago lanceolata* L., 8-*Taraxacum officinale* aggr., 9-*Centaurea jacea* (L.)

plant sample:		1	2	3	4	5	6	7	8	9
plant functional group:		L	L	L	G	G	G	F	F	F
compound	main									
(Z)-3-hexenal	m81	100	100	100	100	100	100	100	51	100
(E)-2-hexenal	m81	–	–	–	–	–	–	–	49	–
hexanal	m83	< 1	< 1	< 1	< 1	1	2	< 1	< 1	1
(E)-3-hexenol	m83	< 1	< 1	< 1	1	2	1	8	< 1	–
(Z)-3-hexenol	m83	15	38	30	17	36	46	1	25	46
(E)-2-hexenol	m83	1	3	4	1	–	4	< 1	< 1	3
(E,Z)-3-hexenyl acetate	m83	83	58	65	79	61	47	90	74	50

Methanol concentrations were generally the highest and proportionally declined less than the other oxygenated VOC between the harvest period and upon removal of the hay to leave an empty field. This probably reflects their origins from plant processes other than wounding. As with Karl et al. (2001a) the highest fluxes were measured after the cut and dominated by methanol. They obtained fluxes of 1.4-2.0 mg m⁻² h⁻¹ for methanol, 0.5-1.5 mg m⁻² h⁻¹ for acetaldehyde, and 0.1-0.5 mg m⁻² h⁻¹ for acetone using eddy covariance above a cut hayfield in Austria. These are in keeping with the results from this study (Section 3.1, Table 2). Considering the leaf area of the cut grass, the peak emissions of these three compounds were also comparable to the values found by Loreto et al. (2006) for cut phragmite leaves. While the fluxes of m81 ((Z)-3-hexenal) and m83 ((Z)-3-hexenol and (E,Z)-3-hexenyl acetate) were of a very similar magnitude to the fluxes of acetone and acetaldehyde on the day of the cut (Figure 1 and Table 2), they declined much faster on the following days indicating their strong relation to the cutting (plant wounding) process itself. The VOC emissions on 4 June, the day after the hay had been removed, were dominated by methanol accounting for nearly 70%, with minor contributions of acetaldehyde, acetone and MEK (the fluxes of m81 and m83 were negligibly small). These fluxes are comparable to those before cutting (not shown).

4.4 Discussion

Detailed comparisons of cut-related and growth-related (pre-cut) methanol emissions of the same field are presented by Brunner et al. (2007).

The legumes were the functional group which emitted the largest number of different VOC species (14-15 compounds), followed by the forbs (10-14 compounds) and the graminoids (8-12 compounds). The two compounds methyl acetate and 3-pentanol were found to be characteristic for legumes since they were observed in all three legume samples but in none of the other samples. De Gouw et al. (1999) also measured emissions from two individual cut species, namely red fescue grass (*Festuca rubra*) and white clover (*Trifolium repens*). They mainly detected VOCs (methanol, acetaldehyde, butanone, (Z)-3-hexenal, (Z)-3-hexenol, and hexenyl acetate) that were also observed in this study. However, they did not report acetone emission for their graminoid species, while we found acetone emission for all three graminoid species investigated. Further, the two exclusively legume related compounds of our study were not detected in their clover experiment. On the other hand, Karl et al. (2001b) detected 1-penten-3-ol as one of the main VOCs emitted by the graminoid species *Poa pratensis* during drying, while we observed this compound only for non-graminoids. Therefore, the extrapolation of emission rates and patterns from individual species to whole plant groups and larger spatial scales is very problematic. Field scale flux measurements over grassland with typical plant compositions may yield more representative and suitable results for up-scaling purposes.

Using the field scale flux data, we calculated the integral amount of emitted VOC for the entire cutting and drying process in relation to the cut biomass. We found 172 $\mu\text{g gdw}^{-1}$ for methanol, 57 $\mu\text{g gdw}^{-1}$ for acetaldehyde, and 39 $\mu\text{g gdw}^{-1}$ for acetone. Based on the species identification as discussed above, integral emissions of 20 $\mu\text{g gdw}^{-1}$ for MEK, 65 $\mu\text{g gdw}^{-1}$ for (Z)-3-hexenal, and 57 $\mu\text{g gdw}^{-1}$ for (Z)-3-hexenol and (E,Z)-3-hexenyl acetate were obtained. The results for methanol, acetaldehyde, acetone and hexenal are within the (relatively large) range of various studies compiled by Warneke et al. (2002), while the value for MEK is in keeping with the observations by Karl et al. (2001a,b). The total VOC emission of 410 $\mu\text{g gdw}^{-1}$ corresponds to 0.05% of the carbon content of the harvest biomass.

Acknowledgements

The authors would like to acknowledge receipt of a European Science Foundation (ESF) VOCBAS travel grant that helped make this work possible. The work was also financially supported by the Swiss National Science Foundation (Project COGAS, Nr. 200020-101636).

References

- Ammann, C., Flechard, C., Fuhrer, J., and Neftel, A. (2004a). Greenhouse gas budget of intensively and extensively managed grassland. In Lüscher, A. et al. (Eds.). *Land Use Systems in Grassland Dominated Regions, Grassland Science in Europe*, vol. 9, vdf Hochschulverlag, Zürich, Switzerland, pp. 130-132.
- Ammann, C., Spirig, C., Neftel, A., Steinbacher, M., Komenda, M., and Schaub, A. (2004b). Application of PTR-MS for measurements of biogenic VOC in a deciduous forest. *International Journal of Mass Spectrometry*, 239, 87–101.
- Ammann, C., Brunner, A., Spirig, C., and Neftel, A. (2006). Technical note: Water vapour concentration and flux measurements with PTR-MS, *Atmospheric Chemistry and Physics*, 6, 4643-4651.
- Ammann C., Flechard C., Leifeld J., Neftel A., and Fuhrer J. (2007) The carbon budget of newly established temperate grassland depends on management intensity, *Agriculture, Ecosystems and Environment*, doi:10.1016/j.agee.2006.12.002.
- Arey, J., Winer, A.M., Atkinson, R., Aschmann, S. M., Long, W.D., and Morrison, C.L. (1991). The Emission Of (Z)-3-Hexen-1-ol, (Z)-3-Hexenylacetate And Other Oxygenated Hydrocarbons From Agricultural Plant-Species. *Atmospheric Environment Part A-General Topics* 25, 1063-1075.
- Bermejo, V., Gimeno, B. S., Sanz, J., de la Torre, D., and Gil, J. M. (2003). Assessment of the ozone sensitivity of 22 native plant species from Mediterranean annual pastures based on visible injury. *Atmospheric Environment* 37, 4667-4677.
- Brunner, A., Ammann, C., Neftel, A., Spirig, C., and Jocher, M. (2007). Methanol exchange between grassland and the atmosphere. Submitted to *Biogeosciences Discussions*.

4. References

- Chen, F., Tholl, D., D'Auria, J.C., Farooq, A., Pichersky, E., and Gershenzon, J. (2003). Biosynthesis and emission of terpenoid volatiles from *Arabidopsis* flowers. *Plant Cell* 15, 481-494.
- Cojocariu, C., Escher, P., Haberle, K. H., Matyssek, R., Rennenberg, H., and Kreuzwieser, J. (2005). The effect of ozone on the emission of carbonyls from leaves of adult *Fagus sylvatica*. *Plant Cell And Environment* 28, 603-611.
- De Gouw, J.A., Howard, C.J., Custer, T. G., Baker, B.M., and Fall, R. (1999). Emissions of volatile organic compounds from cut grass and clover are enhanced during the drying process. *Geophysical Research Letters* 26, 7, 811-814.
- Ehhalt, D., Prather, M., Dentener, F., Derwent, R., and Dlugokencky, E. (2001). *The Third Assessment Report on Climate Change* (Cambridge, UK: Cambridge University Press).
- Fall, R. (1999). Biogenic Emissions of Volatile Organic Compounds from Higher Plants. In *Reactive Hydrocarbons in the Atmosphere*, C.N. Hewitt, ed (San Diego: Academic Press), pp. 43-91.
- Fall, R. (2003). Abundant oxygenates in the atmosphere: A biochemical perspective. *Chemical Reviews* 103, 4941-4951.
- Feussner, I., and Wasternack, C. (2002). The lipoxygenase pathway. *Annual Review Of Plant Biology* 53, 275-297.
- Flechard, C. R., Neftel, A., Jocher, M., Ammann, C., and Fuhrer, J. (2005). Bi-directional soil/atmosphere N₂O exchange over two mown grassland systems with contrasting management practices, *Global Change Biology* 11, 2114-2127.
- Galbally, I. E. and Kirstine, W. (2002). The production of methanol by flowering plants and the global cycle of methanol. *Journal Of Atmospheric Chemistry* 43, 195-229.
- Graus, M., Schnitzler, J. P., Hansel, A., Cojocariu, C., Rennenberg, H., Wisthaler, A., and Kreuzwieser, J. (2004). Transient release of oxygenated volatile organic compounds during light-dark transitions in grey poplar leaves. *Plant Physiology* 135, 1967-1975.
- Guenther, A., Zimmerman, P., and Wildermuth, M. (1994). Natural Volatile Organic-Compound Emission Rate Estimates For United-States Woodland Landscapes. *Atmospheric Environment* 28, 1197-1210.

4 Cut induced VOC emissions of agricultural grasslands

Guenther, A., Hewitt, C. N., Erickson, D., Fall, R., Geron, C., Graedel, T., Harley, P., Klinger, L., Lerdau, M., McKay, W. A., Pierce, T., Scholes, B., Steinbrecher, R., Tallamraju, R., Taylor, J., and Zimmerman, P. (1995). A Global-Model Of Natural Volatile Organic-Compound Emissions. *Journal Of Geophysical Research-Atmospheres* 100, 8873-8892.

Hatanaka, A. (1993). The Biogenesis Of Green Odor By Green Leaves. *Phytochemistry* 34, 1201-1218.

Karl, T., Guenther, A., Jordan, A., Fall, R., and Lindinger, W. (2001a). Eddy covariance measurements of biogenic oxygenated VOC emissions from hay harvesting. *Atmospheric Environment*, 35, 491-495.

Karl, T., Guenther, A., Lindinger C., Jordan, A., Fall, R., and Lindinger, W. (2001b). Eddy covariance measurements of oxygenated volatile organic compound fluxes from crop harvesting using a redesigned proton-transfer-reaction mass spectrometer. *Journal of Geophysical Research*, 106, 24'157-24'167.

Kesselmeier, J. and Staudt, M. (1999) Biogenic Volatile Organic Compounds (VOC): An Overview on Emission, Physiology and Ecology. *Journal of Atmospheric Chemistry* 22, 23-88.

Kirstine, W., Galbally, I., Ye, Y., and Hooper, M. (1998). Emissions of volatile organic compounds (primarily oxygenated species) from pasture. *Journal of Geophysical Research*, 106, 10'605-10'619.

Kormann, R., and Meixner, F. X. (2001). An analytical footprint model for non-neutral stratification. *Boundary-Layer Meteorology*, 99, 207-224.

Kozłowski, T. T., and Pallardy, S.G. (2002). Acclimation and adaptive responses of woody plants to environmental stresses. *Botanical Review* 68, 270-334.

Kreuzwieser, J., Harren, F. J. M., Laarhoven, L. J. J., Boamfa, I., te Lintel-Hekkert, S., Scheerer, U., Huglin, C., and Rennenberg, H. (2001). Acetaldehyde emission by the leaves of trees - correlation with physiological and environmental parameters. *Physiologia Plantarum* 113, 41-49.

Lindinger W., Hansel, A., and Jordan, A. (1998). On-line monitoring of volatile organic compounds at pptv levels by means of Proton-Transfer-Reaction Mass Spectrometry (PTR-

4. References

MS) Medical applications, food control and environmental research. *International Journal of Mass Spectrometry and Ion Processes* 173, 191-241.

Loreto, F., Barta, C., Brilli, F., and Nogues, I. (2006). On the induction of volatile organic compound emissions by plants as consequence of wounding or fluctuations of light and temperature. *Plant, Cell and Environment*, 29, 1820-1828.

Neftel, A., Spirig, C., and Ammann, C. (submitted). A simple tool for operational footprint evaluations, *Environmental Pollution*.

Noordermeer, M. A., Feussner, I., Kolbe, A., Veldink, G. A., and Vliegthart, J. F. G. (2000). Oxygenation of (3Z)-alkenals to 4-hydroxy-(2E)-alkenals in plant extracts: A nonenzymatic process. *Biochemical And Biophysical Research Communications* 277, 112-116.

Schade, G. W., and Goldstein, A. H. (2001). Fluxes of oxygenated volatile organic compounds from a ponderosa pine plantation. *Journal of Geophysical Research-Atmospheres* 106, 3111-3123.

Singh, H., Chen, Y., Staudt, A., Jacob, D., Blake, D., Heikes, B., and Snow, J. (2001). Evidence from the Pacific troposphere for large global sources of oxygenated organic compounds. *Nature* 410, 1078-1081.

Spirig, C., Neftel, A., Ammann, C., Dommen, J., Grabmer, W., Thielmann, A., Schaub, A., Beauchamp, J., Wisthaler, A., and Hansel A. (2005). Eddy covariances flux measurements of biogenic VOCs during ECHO 2003 using proton transfer reaction mass spectrometry. *Atmospheric Chemistry and Physics* 5, 465-481.

Warneke, C., Luxembourg, S. L., de Gouw, J. A., Rinne, H. J. I., Guenther, A. B., and Fall, R. (2002). Disjunct eddy covariance measurements of oxygenated volatile organic compounds fluxes from an alfalfa field before and after cutting. *Journal of Geophysical Research* 107 (D8), 10.1029/2001JD000594.

5 Methanol exchange between grassland and the atmosphere

A. Brunner, C. Ammann, A. Neftel, and C. Spirig

Agroscope ART, Federal Research Institute, Zurich, Switzerland

Published in Biogeoscience, 4, 395-410, 2007.

Abstract

Concentrations and fluxes of methanol were measured above two differently managed grassland fields (intensive and extensive) in central Switzerland during summer 2004. The measurements were performed with a proton-transfer-reaction mass-spectrometer and fluxes were determined by the eddy covariance method. The observed methanol emission showed a distinct diurnal cycle and was strongly correlated with global radiation and water vapour flux. Mean and maximum daily emissions were found to depend on grassland species composition and, for the intensive field, also on the growing state. The extensive field with a more complex species composition had higher emissions than the graminoid-dominated intensive field, both on an area and on a biomass basis. A simple parameterisation depending on the water vapour flux and the leaf area index allowed a satisfying simulation of the temporal variation of methanol emissions over the growing phase. Accumulated carbon losses due to methanol emissions accounted for 0.024 and 0.048% of net primary productivity for the intensive and extensive field, respectively. The integral methanol emissions over the growing periods were more than one order of magnitude higher than the emissions related to cut and drying events.

5.1 Introduction

Methanol is one of the most abundant oxygenated volatile organic compounds in the atmosphere with typical surface concentrations of 1-10 ppbv over land and marine

5 Methanol exchange between grassland and the atmosphere

concentrations of 0.5-1.5 ppbv (Jacob et al., 2005; Singh et al., 2000). Its role in atmospheric chemistry is significant as it influences the concentrations of various oxidants. Formaldehyde, ozone and peroxy radical concentrations are enhanced while OH radical levels are decreased through the atmospheric reactions of methanol. The effects are most pronounced in the free troposphere, where concentrations of other reactive organic compounds are small while methanol still prevails due to its comparably long atmospheric lifetime of 8-12 days (Tie et al., 2003).

11-20% of the methanol in the atmosphere are of anthropogenic and atmospheric origin, while the major part (80-89%) is of biogenic origin (Heikes et al., 2002; Galbally and Kirstine, 2002; Jacob et al., 2005). Processes leading to biogenic methanol emission are manifold. Several authors reported methanol emission as part of the plant metabolism particularly during growth (e. g. Schulting et al., 1980; Isidorov et al., 1985; MacDonald et al., 1993; Fall and Benson, 1996; Karl et al., 2002). Plant stresses like hypoxia, frost and high ozone concentrations can also cause methanol emissions (Fukui and Doskey, 1998; von Dahl et al., 2006). In addition, senescing, injuring (e. g. herbivore attacks, cutting) and drying of plant leaves as well as biomass burning are known to be sources of methanol (de Gouw et al., 1999; Warneke et al., 2002; Karl et al., 2005; Loreto et al., 2006; Holzinger et al., 1999 and 2004). The major removal processes for methanol are oxidation by OH radicals (in the gas and the aqueous phase; Monod et al., 2000) as well as dry and wet deposition (Heikes et al., 2002; Galbally and Kirstine, 2002; Jacob et al., 2005).

Concerning the metabolism related methanol release, Frenkel et al. (1998) found that methanol within the leaf is mostly produced as a consequence of the demethylation of the pectin matrix, a necessary step in the extension of the cell walls during plant growth. On the basis of the pectin content, Galbally and Kirstine (2002) distinguished between two major cell wall types with a high or low potential for methanol release. In particular graminoids of the family poaceae, to which the main forage crops belong, are low methanol emitters. Most other plants have cell walls with a higher potential of methanol release. To a minor extent, methanol can be the result of an enzymatic cleavage of lignin (see Fall and Benson, 1996, and references therein), demethylation of DNA (see Galbally and Kirstine, 2002, and references therein) and protein repair pathways (Fall and Benson, 1996).

5.1 Introduction

Nemecek-Marshall et al. (1995) described a distinct dependence of methanol emission on stomatal conductance. Niinemets and Reichstein (2003a, b) and Niinemets et al. (2004) relate this behaviour to a temporary storage of methanol in the liquid pools of the leaves due to its high solubility. As a consequence of this buffering effect, the production and release of methanol are not directly coupled. Because the understanding of the mechanisms controlling the methanol emission is still limited, reliable long-term emission datasets with a high temporal resolution are desirable for a variety of different ecosystems.

Until now, field measurements of biogenic methanol emissions have mainly been performed over different types of forest (e. g. Fehsenfeld et al., 1992; Schade and Goldstein, 2001; Spirig et al., 2005; Karl et al., 2005; Schade and Goldstein, 2006). Grasslands cover one quarter of the earth's land surface (Graedel and Crutzen, 1993). Apart from studies concerning the methanol emissions due to harvesting (De Gouw et al., 1999; Karl et al., 2001; Warneke et al., 2002) only few long-term flux studies exist for grassland (Kirstine et al., 1998; Fukui and Doskey, 1998). These are based on chamber measurements characterised by a low time resolution.

In this work we present methanol concentration and flux measurements above two managed grassland fields during summer 2004. The fields are located on the Swiss central plateau and differ in management intensity and species composition. Methanol was detected continuously with high temporal resolution by proton-transfer-reaction mass-spectrometry and the fluxes were determined by the eddy covariance technique at the ecosystem scale. We focus on the temporal variation of fluxes observed throughout a growing phase and attempt to parameterise it in a simple way based on available environmental parameters.

5.2 Materials and methods

5.2.1 Site and measurement description

The experimental site is located near Oensingen on the Swiss Central Plateau (47°17' N, 7°44' E; 450 m a.s.l.). The prevailing climate is temperate continental, with an average annual rainfall of 1100 mm and a mean annual air temperature of 9°C. The experimental field was converted from arable rotation to permanent grassland in 2001 and is part of the projects on

carbon and greenhouse gas budgets CarboEurope and Greengrass (for details see Ammann et al., 2006; Flechard et al., 2005). Since 2006, this grassland is a part of the NitroEurope project. It has a size of 104 m x 146 m and had been split into two parts which differ in management and species composition: (a) an intensively managed part (in the following referred to as intensive or INT) and (b) an extensively managed part (extensive or EXT). The intensive part is cut four times a year and is fertilised after each cut, alternately with slurry and ammonium nitrate. It is mainly composed of three species: two graminoids (*Alopecurus pratensis*, *Lolium perenne*), and one legume (*Trifolium repens*). The extensive part is cut three times a year and is not treated with any fertilizer. It is largely composed of twelve species: six graminoids (*Alopecurus pratensis*, *Arrhenatherum elatius*, *Dactylis glomerata*, *Lolium perenne*, *Poa pratensis*, and *Poa trivialis*), four forbs (*Chrysanthemum leucanthemum*, *Stellaria media*, *Taraxacum officinale*, and *Tragopogon orientalis*), and two legumes (*Lotus corniculatus*, and *Trifolium repens*).

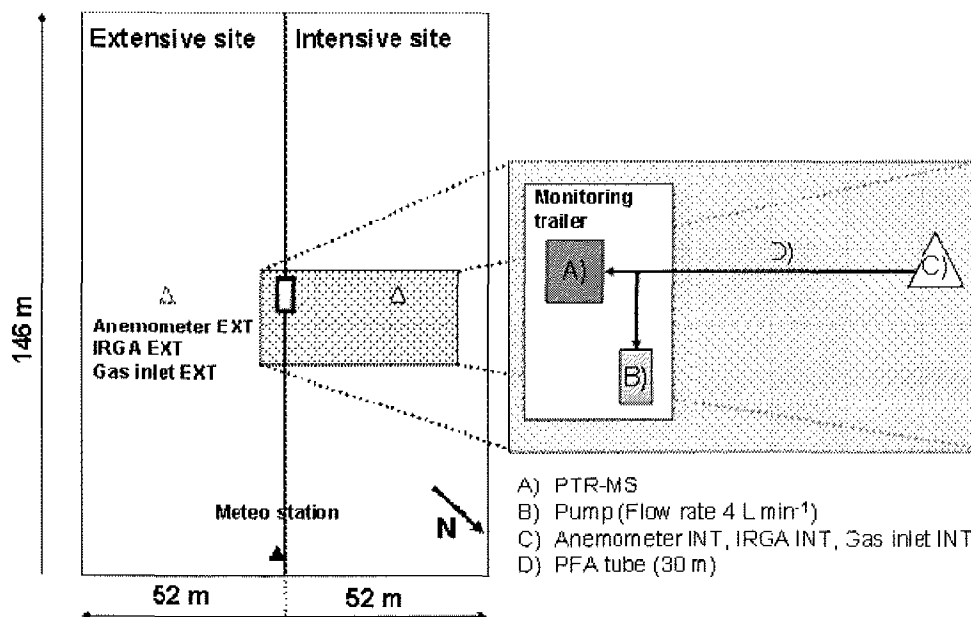


Figure 1. Site sketch: Left: Position of the monitor trailer, the meteo station, the two anemometers, the two open-path infra-red gas analyzer (IRGA) and the gas inlets above the two fields. Right: Measurement arrangement: Gas inlet, pump, and PTR-MS.

Standard monitoring at the site included a weather station continuously measuring global radiation (R_g), air temperature (T_{air}), relative humidity (RH), barometric pressure, rainfall, wind speed and wind direction. The prevailing wind directions are mostly along the field axis

5.2 Materials and methods

(vertical axis in Fig. 1). The single-sided leaf area index (LAI) of both fields was determined every 2-3 weeks by an optical method (LAI-2000, LI-COR, Lincoln NE, USA). Fluxes of CO_2 (F_{CO_2}) and water vapour ($F_{\text{H}_2\text{O}}$) were routinely measured on both fields during the whole summer by eddy covariance using a combination of a sonic anemometer (Gill, Solent, Lymington, UK) and an open-path infra-red gas analyzer (IRGA, LI-7500, LI-COR, Lincoln NE, USA). Figure 1 shows a sketch of the fields and the technical facilities. The CO_2 assimilation rates of each field were calculated from the respective CO_2 fluxes by a specific gap filling and partitioning algorithm (Ammann et al., 2007).

Methanol concentration (c_{MeOH}) and flux (F_{MeOH}) measurements above the intensive field were conducted from 25 June until 1 August 2004, between the second and the third cut of the year. Above the extensive field, methanol measurements were performed from 7 until 24 June 2004 and from 2 August until 7 September 2004, covering periods between the first and the second cut of the year (Fig. 2). In the following, methanol fluxes of the first three days after a cut are referred to as cut-related emissions, the fluxes afterwards until the next cut as growth-related emissions. The corresponding periods are called cut and growing period, respectively (Fig. 2).

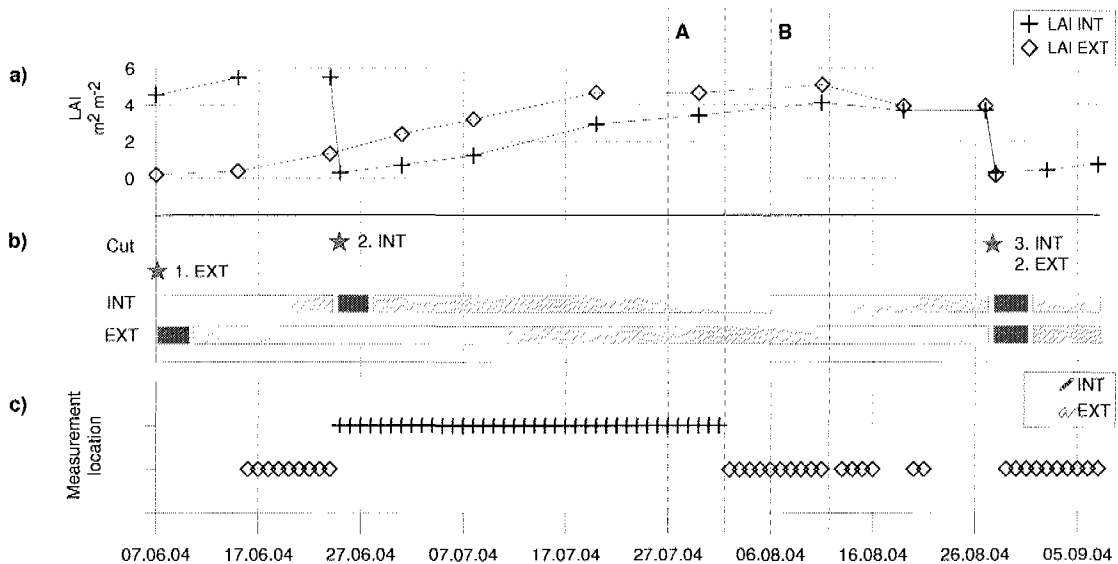


Figure 2. Field experiment summer 2004, overview on the growing state of the fields, the event-related methanol emission, and the measurements between 7 June and 7 Sept: a) LAI of the intensive and the extensive site, b) cuts of the intensive (25.06 and 28.08.04) and the extensive (07.06 and 28.08.04) site, classification into cut-related (dark-grey bar) and growth-related (light-grey bar) emission periods, and c) methanol flux sampling scheme. A: mature phase of the intensive site, B: mature phase of the extensive site.

5.2.2 PTR-MS measurements

Methanol was measured by a commercially available proton-transfer-reaction mass spectrometer (PTR-MS, Ionicon Analytik GmbH, Innsbruck, A). The instrument and its operating mode had been described in detail by Lindinger et al. (1998). Here we describe the experimental setup from the gas inlet to the instrument and go then into specifics of the PTR-MS used in this field study.

Ambient air, collected 1.2 m above ground, was pulled through a 30 m PFA-tube (1/4" O.D., I.D. 3.5 mm) by a vacuum pump with a flow rate of 4 L min⁻¹. The residence time in the tube was about 4.3 s. The tube was connected to the PTR-MS inlet (Fig. 1), where the sampled air was introduced directly into a drift tube. There the reaction between H₃O⁺ ions (generated by electrical discharge of pure water vapour) and methanol molecules produced methanol-H⁺ ions (mass 33) and water molecules. The methanol-H⁺ ions were then detected by a quadrupole mass filter in conjunction with a secondary electron multiplier (SEM, MC-217, Mascom GmbH, Bremen, D).

The PTR-MS used in this field study corresponds to the PTR-MS-HS type, featuring three turbo pumps for increased sensitivity and a drift tube (equipped with Teflon rings) optimized for fast time response and minimal interactions with polar compounds (Spirig et al., 2005). It was running under the following conditions: pressure drift tube of 2.1 mbar and drift tube voltage of 550 V, resulting in an electrical field strength to gas density ratio (E/N) of 122 Td. Five to eight masses were analysed in rotation: m21 (mass of the protonated ion with 21 atomic mass units (amu) which corresponds to a protonated water molecule with an O¹⁸-isotope), m33 (methanol), m37 (water cluster: H₂O • H₃O⁺), m45 (acetaldehyde), m59 (acetone and propanal), m73 (methyl ethyl ketone and butanal), m81 (fragments of hexenals and monoterpenes), and m83 (fragments of C6-alcohols). The integration time for a single compound was 50 (for m21 and m37) to 200 ms (for all other compounds), resulting in a measurement of each compound every 0.7 to 1.3 s (Ammann et al., 2006).

The PTR-MS was calibrated with a gas standard (Apel-Riemer Environmental, Inc., Denver CO, US), that included methanol. It was dynamically diluted with air generated by a zero air generator (ChromGas Zero Air Generator, model 1000, Parker Hannifin Co., Haverhill MA,

5.2 Materials and methods

US). The absolute accuracy of the methanol concentration measurement is estimated to be $\pm 20\%$ due to mass flow controller and gas standard uncertainties.

5.2.3 Eddy covariance method

The EC flux measurement with the PTR-MS was done with the same sonic anemometers as used for the routine CO_2 and H_2O flux measurements (see above) placed in the middle of the grassland fields. The inlet for the PTR-MS sample air was placed close to the sonic sensor head (distance 15 cm). To calculate the fluxes we used the EC calculation method described by Spirig et al. (2005). The PTR-MS measurement of the methanol ion (for 0.2 s) is regarded to be representative for the whole interval of the measuring cycle (0.7–1.3 s). Technically, this is implemented by simply repeating the PTR-MS mass concentrations of a particular cycle until the next PTR-MS data point is available. After this procedure, similar equidistant time series (time resolution $\Delta t = 0.05$ s) of sonic wind data and methanol concentration are available for the flux calculations. Following the eddy covariance method the vertical flux of a trace gas F_c (or of another scalar quantity) is calculated as the covariance of the discrete time series of the vertical wind $w(t)$ and the concentration $c(t)$ over an averaging period T_a of typically 30 min.:

$$F_c = \text{cov}_{wc}(\tau_{\text{del}}) = \left(\frac{\Delta t}{T_a} \right) \cdot \sum_{t=0}^{T_a} [w(t) - \bar{w}] \cdot [c(t - \tau_{\text{del}}) - \bar{c}] \quad (1)$$

The overbars denote the arithmetic mean of the averaging period. The two time series are adjusted to each other by a delay time τ_{del} that accounts for the residence time in the air sampling tube and possible time difference between the data acquisition systems that are different for the PTR-MS and the sonic anemometer. The time delay was calculated for each measuring interval separately by determining the maximum in the covariance function of the flux. In cases where no clear maximum could be found within the physically possible limits of the lag, an interpolated best guess for the lag was used (Ammann et al., 2006).

Beside the effect on the delay time, the inlet tube also led to a damping of high-frequent turbulent fluctuations of the trace gas concentrations before the detection by the PTR-MS. As described in detail by Ammann et al. (2006), the wall sorption effect strongly dominated the high-frequency damping making other factors like the tube flow type, the limited time resolution, the filling of the disjunct time series, and the sensor separation distance less

important. The total damping effect was quantified and corrected for by the empirical ogive method described in detail by Ammann et al. (2006). The high-frequency damping mainly depended on the wind speed and ranged between 25% (low wind speed) and 55% (high wind speed). The detection limit of the EC fluxes was determined empirically from the standard deviation of the covariance function at large delay times according to Wienhold et al. (1995). It was estimated on average to $0.3 \text{ nmol m}^{-2} \text{ s}^{-1}$ and $0.8 \text{ nmol m}^{-2} \text{ s}^{-1}$ for the measurements above the intensive and extensive field, respectively. We performed a footprint analysis for the eddy covariance measurements (following Kormann and Meixner, 2001). Because of the low measurement height (1.2 m above ground) and the main wind directions being mostly along the field axis, there were only few cases (c. 5%) in which the footprint contribution of the study field was less than half. Most of the time, it was even more than 80%. Therefore, the application of a footprint criteria was not considered to be necessary.

5.3 Results

5.3.1 Measurements above the intensively managed field

Weather conditions and vegetation development

During the summer 2004, average temperatures and precipitation at the measurement site were near the long-time seasonal mean. Above the intensive field methanol concentrations and fluxes were measured between 25 June and 1 August. As illustrated in Fig. 3, weather conditions during this time were characterised by two periods of contrasting weather. The first period (till 13 July) showed relatively low temperatures in connection with rain and clouds; it was followed by a mostly clear sky and dry period till the end of July.

The intensive field was cut on 25 June (2nd cut of the year). The hay was removed from the field on 26 June. The average dry matter yield of this growth was 0.32 kg m^{-2} . After the fertilisation with slurry on 1 July, the grassland grew 8 weeks until the next cut on 28 August. On the same day the grass was processed to silage. The average dry matter yield of this growth was 0.19 kg m^{-2} . The leaf area index increased from $0.3 \text{ m}^2 \text{ m}^{-2}$ on 25 June (just after the cut) to $3.7 \text{ m}^2 \text{ m}^{-2}$ on 19 August (last measurement before the 3rd cut) (see Fig. 2).

5.3 Results

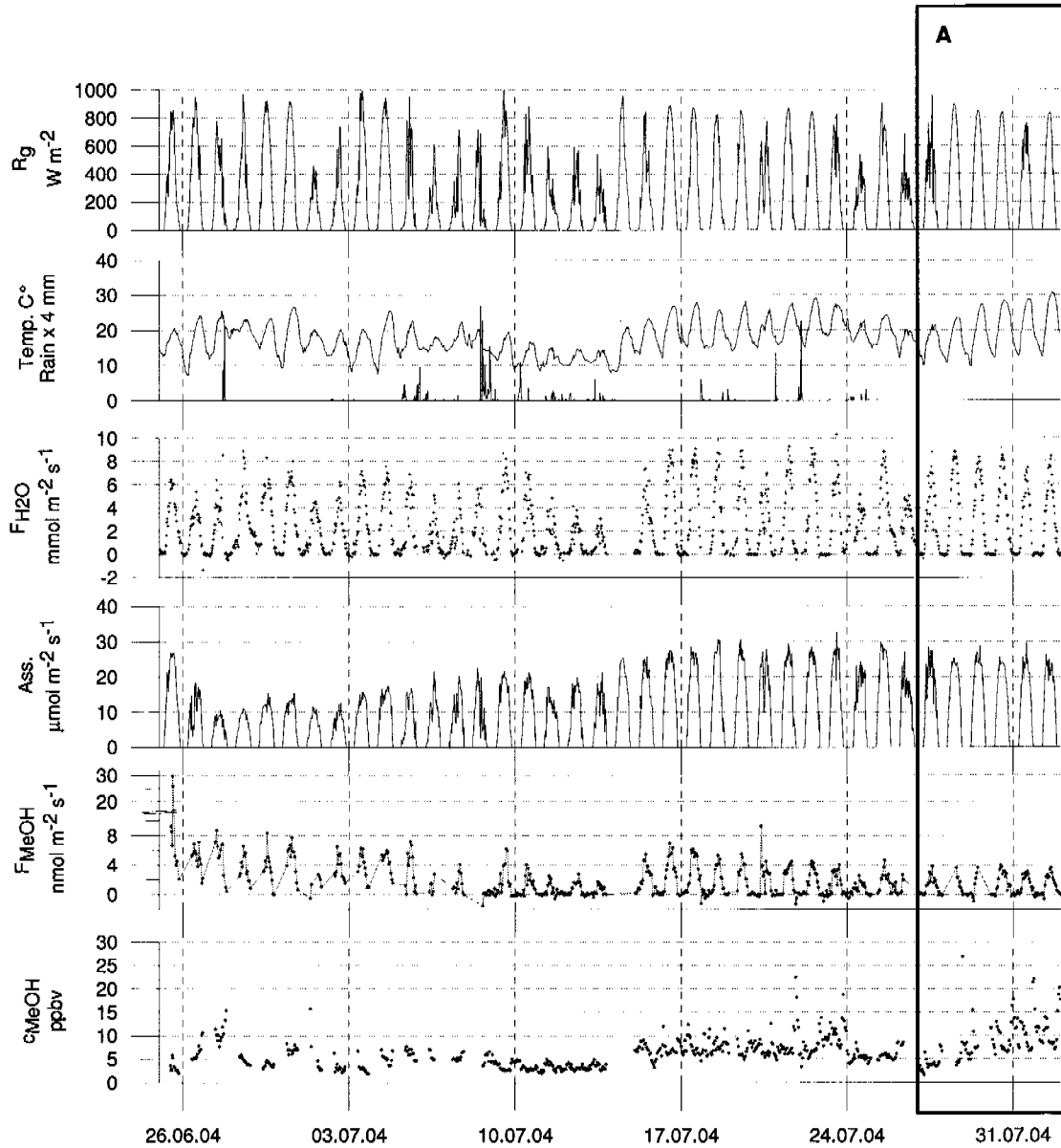


Figure 3. Time series measured above the intensive grassland (25.06-01.08.2004), from the top to the bottom: Global radiation* (R_g), air temperature* (Temp.), rainfall*, water vapour flux (F_{H_2O}), assimilation (Ass.), methanol flux (F_{MeOH}), and methanol concentration (c_{MeOH}). (A: mature phase of the intensive site). * measured at the meteo station, see Fig. 1.

Concentrations

During the measurements on the intensive field, the concentrations were between 1.7 and 26.9 ppbv (Fig. 3), with an overall average concentration of 6.45 ppbv. Low concentrations were mainly detected during or after rainfall (e.g. 5-13 July). High concentrations were found shortly after the cut (28 June) and at the end of July. Figure 4a shows methanol concentrations

5 Methanol exchange between grassland and the atmosphere

plotted against the time of day. The mean concentration shows a characteristic diurnal variation. Highest concentrations were found in the late evening hours. They slowly decreased during the night and increased again around 07:00 LT. During daytime the concentrations dropped continuously to reach lowest levels around 18:00 LT. Figure 4 shows highest methanol concentrations to coincide with lowest wind speeds.

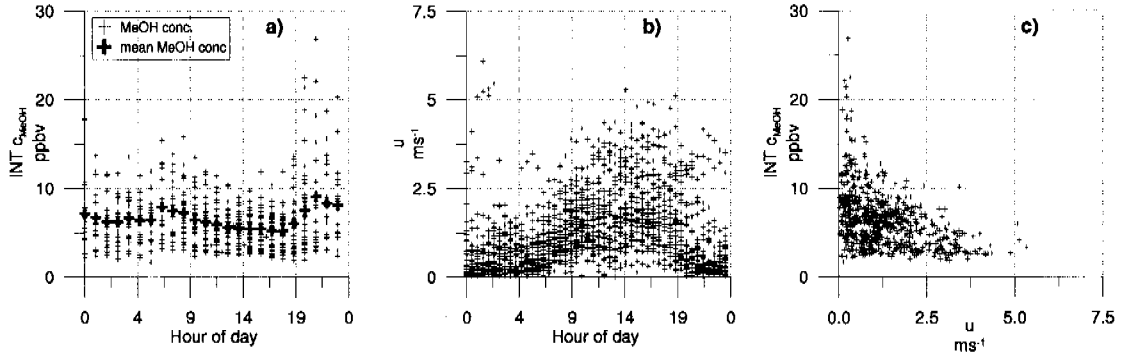


Figure 4. Diurnal cycle of a) methanol concentrations (c_{MeOH}) including hourly mean values above the intensive field, and b) horizontal wind velocities (u). c) shows the scatter plot of methanol concentrations vs horizontal wind velocity. The data cover the period 25.06-01.08.2004.

Fluxes

Methanol fluxes measured on the intensive grassland field are shown in Fig. 3. During the whole period methanol was emitted by the field, and no significant deposition fluxes could be observed. The highest fluxes (up to $30 \text{ nmol m}^{-2} \text{ s}^{-1}$) were measured directly after the cut on 25 June, which can be explained by amplified emissions due to plants wounding (De Gouw et al., 1999). Afterwards the fluxes were generally below $10 \text{ nmol m}^{-2} \text{ s}^{-1}$. They showed a clear diurnal cycle with the maximum around midday and the minimum during night. Nocturnal fluxes were generally small and mostly below the flux detection limit as quantified in Sect. 2.3. Since such fluxes would hardly pass a relative stationarity test as e.g. described by Foken and Wichura (1996), we did not apply such a quality filter. The diurnal cycle of methanol emission followed the global radiation and the water vapour flux in shape and strength. This is most obvious for the period 5-13 July that exhibit a very similar day-to-day variation of all quantities. The liquid manure treatment on 1 July let the emission of methanol rise temporarily with maximum emission of $12.4 \text{ nmol m}^{-2} \text{ s}^{-1}$. Measured methanol fluxes during night were mostly close to zero and/or below the detection limit of the EC method.

5.3 Results

Up to three days after a cut, methanol fluxes seem to be mostly triggered by the injury and the hay drying process. In order to investigate methanol emission during growth we excluded the data of the first three days after the cut. For the growing period 28.06-01.08.04, scatter plots of the methanol flux with various potential controlling parameters are shown in Fig. 5. They suggest a linear correlation between the methanol flux and the global radiation, the water vapour flux, and the sensible heat flux. These three correlations are positive. Further a logarithmic dependence can be seen between the methanol flux and the assimilation rate. Table 1 gives an overview of all calculated correlations coefficients r^2 . Highest correlations exist between methanol flux and global radiation ($r^2 = 0.73$), and water vapour flux ($r^2 = 0.71$). The correlation of methanol flux and air temperature is low. It is likely to be a consequence of the diurnal cycle of the temperature which is similar but delayed in comparison to R_g and F_{H_2O} . The resulting hysteresis becomes evident when looking at individual days as shown in Fig. 5f.

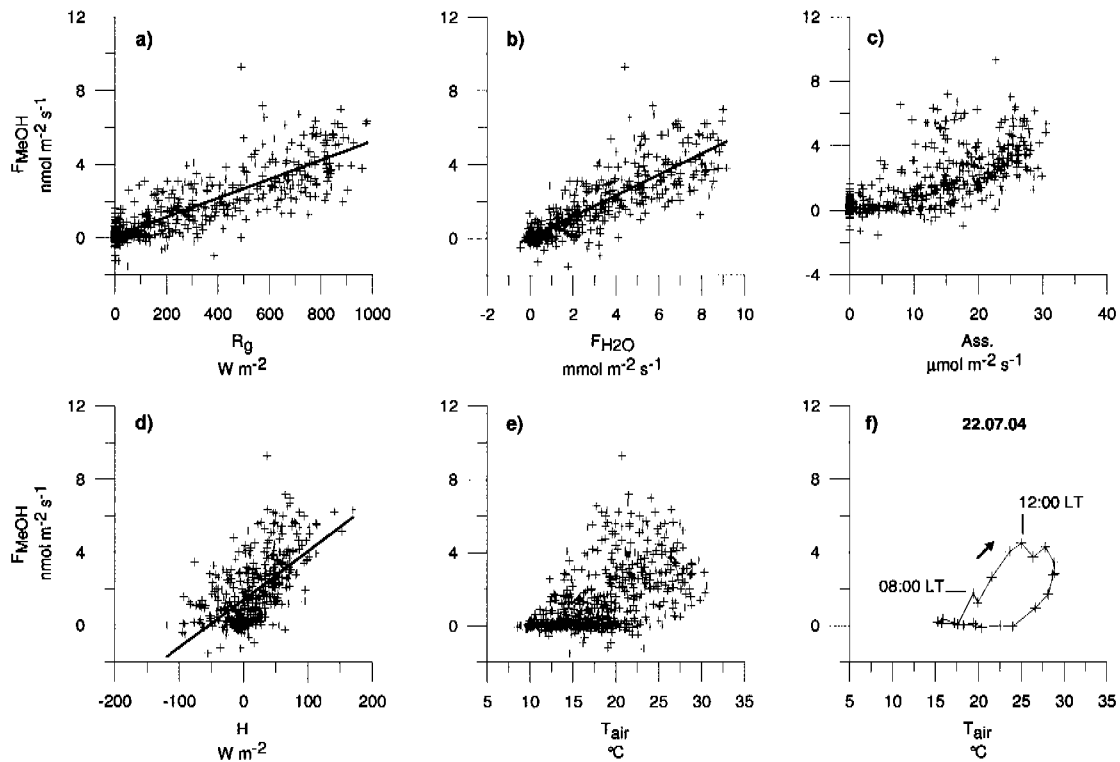


Figure 5. Scatter plots of methanol flux (F_{MeOH}) vs a) global radiation (R_g), b) water vapour flux (F_{H_2O}), c) assimilation (Ass.), d) sensible heat flux (H), and e) air temperature (T_{air}) above the intensive field for the period 28.06-01.08.2004. f) shows the scatter plot of methanol flux and air temperature for one exemplary day (22.7.2004). The arrow indicates the direction of the diurnal course.

5 Methanol exchange between grassland and the atmosphere

Table 1. Correlation coefficients (r^2) of growth related methanol flux (F_{MeOH}) with various environmental parameters: global radiation (R_g), water vapour flux ($F_{\text{H}_2\text{O}}$), sensible heat flux (H), carbon assimilation (Ass.), and air temperature (T_{air}), calculated for the entire growing period and the mature period, respectively.

	R_g	$F_{\text{H}_2\text{O}}$	H	Ass. ¹⁾	T_{air} ¹⁾
INT (2.7.-1.8.)	0.73	0.71	0.36	0.49	0.27
INT mature (27.7. - 1.8.)	0.85	0.86	0.35	0.53	0.44
EXT (16.6.-24.6., 2.8. - 21.8.)	0.70	0.64	0.53	0.54	0.21
EXT mature (6.8. - 11.8.)	0.68	0.64	0.63	0.60	0.14

¹⁾ non-linear dependence

In order to study the longer-term development of methanol emission, the strong short-term variability (diurnal and day-to-day) was sought to be reduced by dividing the observed methanol fluxes by the respective water vapour fluxes:

$$\gamma(t) = \frac{F_{\text{MeOH}}(t)}{F_{\text{H}_2\text{O}}(t)} \quad (2)$$

As shown in Fig. 3, the water vapour flux shows diurnal and weather induced day-to-day variations but no systematic long-term trends. When plotting the ratio $\gamma(t)$ for the intensive grassland (Fig. 6), a systematic decrease with time was found. γ almost linearly declined from an initial value of about 1.1 nmol mmol⁻¹ one week after the cut down to 0.4 nmol mmol⁻¹ within the first four weeks of growth. Afterwards (Fig. 6, Phase A), it stayed more or less constant. Thus normalised by the water vapour flux, methanol emission of the grassland ecosystem (per unit ground area) was three times higher shortly after the cut than four weeks later. If the methanol flux is related to the growing leaf area, the decrease in γ/LAI is even more pronounced with an almost exponential drop from an initial value of about 1.5 to only 0.2 nmol mmol⁻¹ within the first four weeks, indicating that the young grassland vegetation emitted up to 7.5 times more methanol per leaf area than the mature one.

5.3 Results

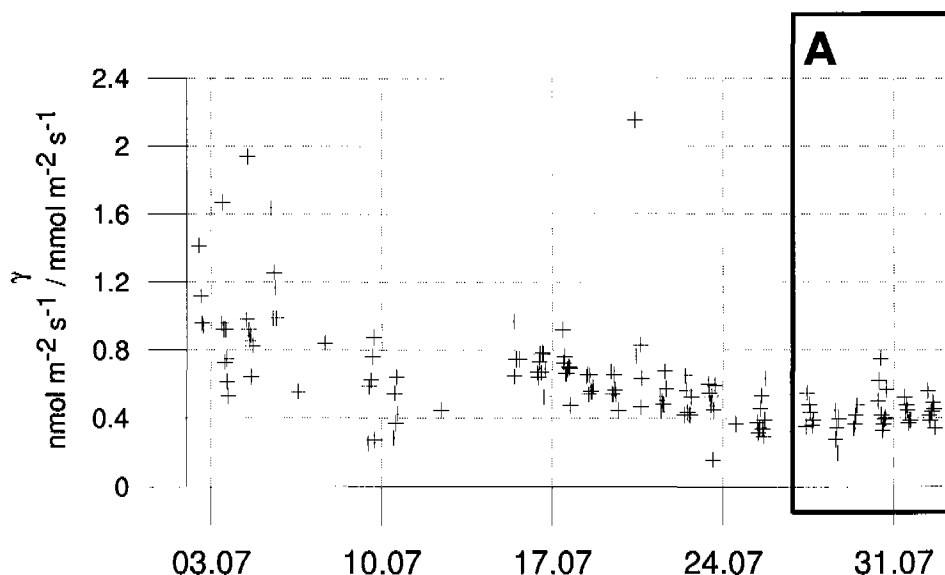


Figure 6. Time series of γ (for $F_{\text{H}_2\text{O}} > 4 \text{ mmol m}^{-2} \text{s}^{-1}$) of the intensive field for the period 02.07-01.08.2004. A: mature phase of the intensive field.

5.3.2 Measurements above the extensively managed field

Weather conditions and vegetation development

Above the extensive field, methanol concentrations were measured between 7 June and 7 September 2004 including the second growing period between the first and second cut. The measurements were not continuous due to an inserted measurement period above the intensive field (25 June – 1 August). The weather conditions during the measurements above the extensive field were characterised by a relatively cold period in the middle of June and a relatively wet period starting in mid-August and lasting for two weeks (see Fig. 7).

The extensive field was cut on 7 June (1st cut of the year). The hay was removed from the field on 9 June. The dry matter yield of this growth was 0.67 kg m^{-2} . Then the grassland grew 11 weeks until the next cut on 28 August (2nd cut of the year). On the same day the grass was processed to silage. The dry matter yield of this growth was 0.31 kg m^{-2} . The leaf area index increased from about $0.2 \text{ m}^2 \text{ m}^{-2}$ on 9 June (just after the 1st cut) to $3.9 \text{ m}^2 \text{ m}^{-2}$ on 19 August (last measurement before the 2nd cut) (see Fig. 2).

Concentrations

Methanol concentrations measured above the extensive field were between 0.38 and 47.8 ppbv, with an overall average of 7.38 ppbv (Fig. 7). Low concentrations were mainly during the relatively cold period in mid June and during the wet period in mid August. High concentrations were found shortly after the first cut (8 June). The mean diurnal cycle was very similar to that found above the intensive field (Fig. 4a) with one maximum in the evening (21:00 LT) and another in the morning (07:00 LT).

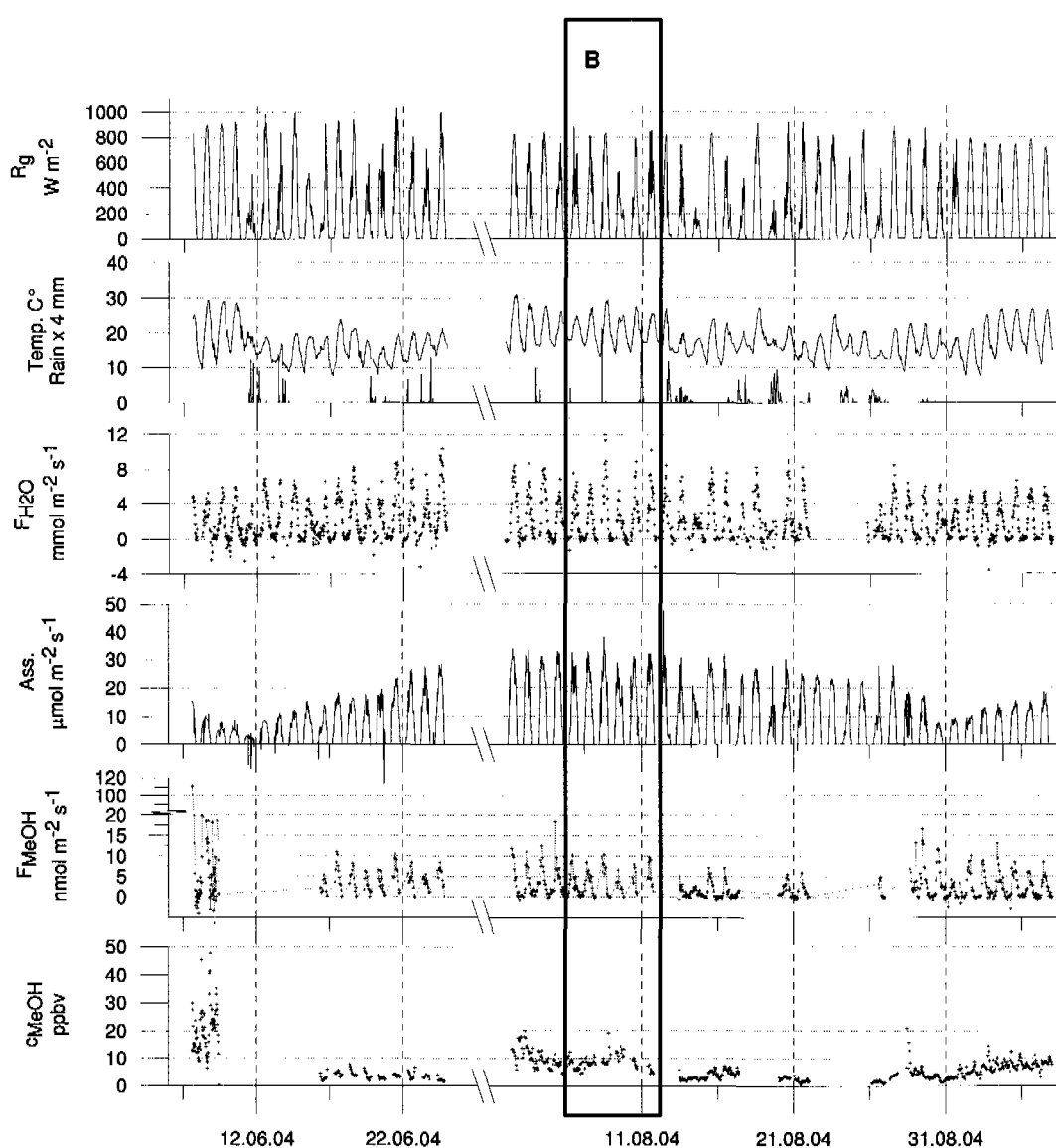


Figure 7. Time series measured above the extensive grassland (07.06-07.09.2004), from the top to the bottom: Global radiation* (R_g), air temperature* (Temp.), rainfall*, water vapour flux (F_{H_2O}), assimilation (Ass.), methanol flux (F_{MeOH}), and methanol concentration (c_{MeOH}). (B: mature phase of the extensive site). * measured at the meteo station, see Fig. 1.

5.3 Results

Fluxes

Figure 7 shows the methanol fluxes measured on the extensive field. Comparable to the intensive field, continuous methanol emission was detected during the whole growing period, and no significant deposition could be observed. The highest flux of $110.9 \text{ nmol m}^{-2} \text{ s}^{-1}$ was observed directly after the cut on 7 June. In general, the methanol emissions above the extensive field showed a similar diurnal cycle as the one seen above the intensive field. For the growing period (excluding the first three days after the cut) the methanol flux correlated best with global radiation and water vapour flux, as also found for the intensive field (see Table 1). The methanol emission normalised by the water vapour flux (γ – see Eq. 2) was very similar at the beginning and at the end of the growing phase with an average value of about 1 nmol mmol^{-1} . However, the LAI related γ (γ / LAI) showed a considerable decrease from 1 to $0.2 \text{ nmol mmol}^{-1}$.

5.3.3 Comparison of both fields

The different plant composition of the two measurement fields could have an effect on the magnitude and the diurnal variation of the methanol emission. A direct comparison of the emission rates of the two fields under identical weather conditions and growing state is not possible because they were cut at different dates and the measurements were performed alternately. Therefore we compared two 6-day periods towards the end of the respective growing phase (Fig. 2, A and B), which are both characterised by a rather steady LAI and assimilation rate (Fig. 3 and 7). These 6-day periods are hereinafter also called “mature” periods.

The accumulated daytime (10:00-16:00 LT) carbon assimilation for these phases were 39.6 mgC m^{-2} and 42.4 mgC m^{-2} for the intensive and the extensive field, respectively. The corresponding LAI was $3.4 \text{ m}^2 \text{ m}^{-2}$ (INT) and $5.1 \text{ m}^2 \text{ m}^{-2}$ (EXT). The mean temperature was similar during these two measurement phases, while the later (EXT) period was characterised by a slightly higher relative humidity and lower solar radiation (Fig. 8, Table 2).

5 Methanol exchange between grassland and the atmosphere

Table 2. Characteristics for the intensive and the extensive field during mature phase: 6-day mean of sum (Σ) of global radiation (ΣR_g), air temperature (T_{air} : 24 h mean), rainfall (ΣRain), relative humidity (RH: 24 h mean), leaf area index (LAI), accumulated daytime (10:00-16:00) carbon assimilation ($\Sigma \text{Ass.}$), and the accumulated methanol emissions (ΣMeOH).

	ΣR_g kW h m^{-2}	T_{air} $^{\circ}\text{C}$	ΣRain mm	RH $\%$	LAI $\text{m}^2 \text{m}^{-2}$	$\Sigma \text{Ass.}$ mgC m^{-2}	ΣMeOH mgC m^{-2}
INT	5910	19.5	0	66.2	3.4	39.5	2.8
EXT	4140	20.6	30.5	82.6	5.1	42.4	6.3

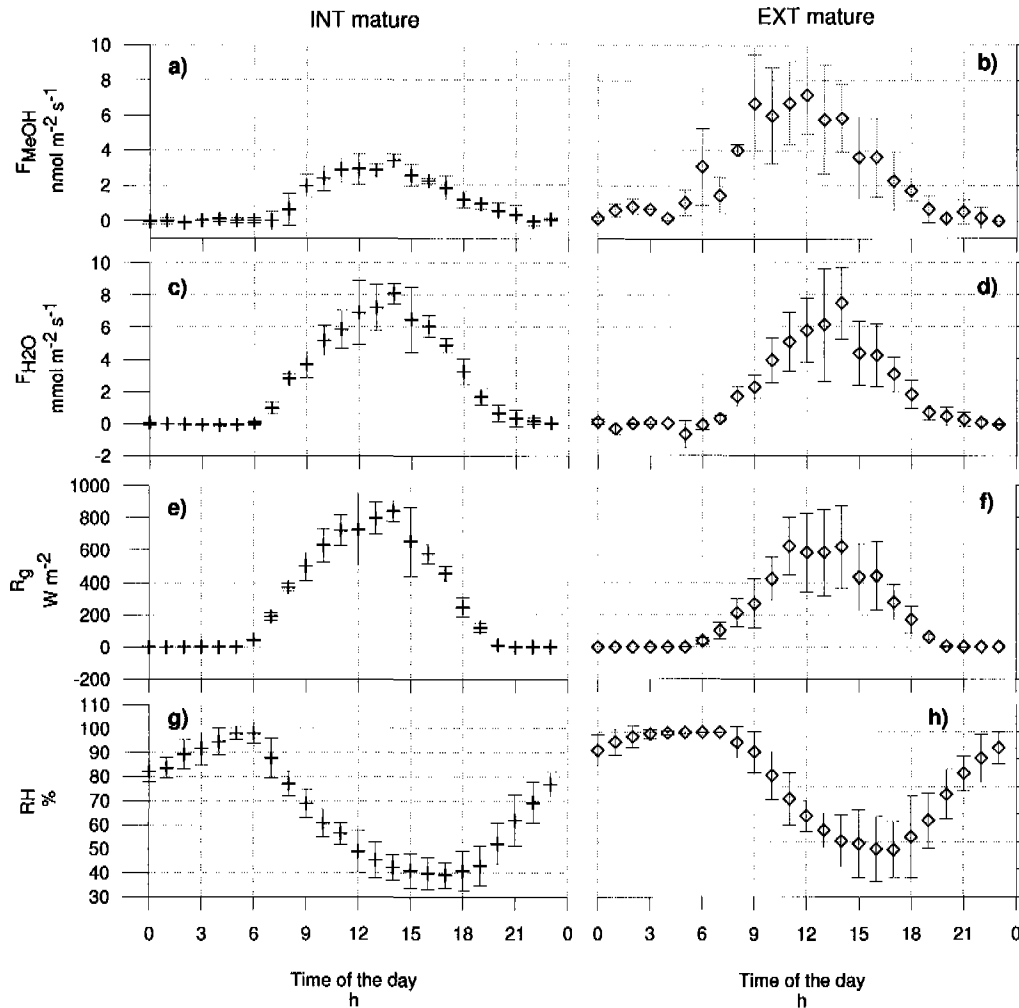


Figure 8. Mean hourly values of the mature phase of the intensive (left, +) and the extensive field (right, ◇): a, b) methanol flux (F_{MeOH}); c, d) water vapour flux ($F_{\text{H}_2\text{O}}$); e, f) global radiation (R_g); g, h) relative humidity (RH). Error bars are the standard deviation.

5.3 Results

Figure 8 shows the mean diurnal cycles of the methanol flux, the water vapour flux, the global radiation, and the relative humidity for the two mature periods. The methanol flux reached a mean maximum emission flux of $3.40 \pm 0.34 \text{ nmol m}^{-2} \text{ s}^{-1}$ (14:00 LT) and $7.17 \pm 2.25 \text{ nmol m}^{-2} \text{ s}^{-1}$ (12:00 LT) above the intensive and the extensive field, respectively (Fig. 8a, b). The accumulated methanol emitted during these six days was 2.8 mgC m^{-2} and 6.3 mgC m^{-2} for the intensive and the extensive field, respectively, i.e. a 2.3 times higher emission above the extensive field. If the emissions are normalised by the respective LAI, this ratio decreases to 1.5. In contrast, the diurnal cycle of the mean hourly water vapour fluxes (Fig. 8c, d) reached quite similar maximum fluxes (INT: $8.1 \text{ mmol m}^{-2} \text{ s}^{-1}$, EXT: $7.5 \text{ mmol m}^{-2} \text{ s}^{-1}$).

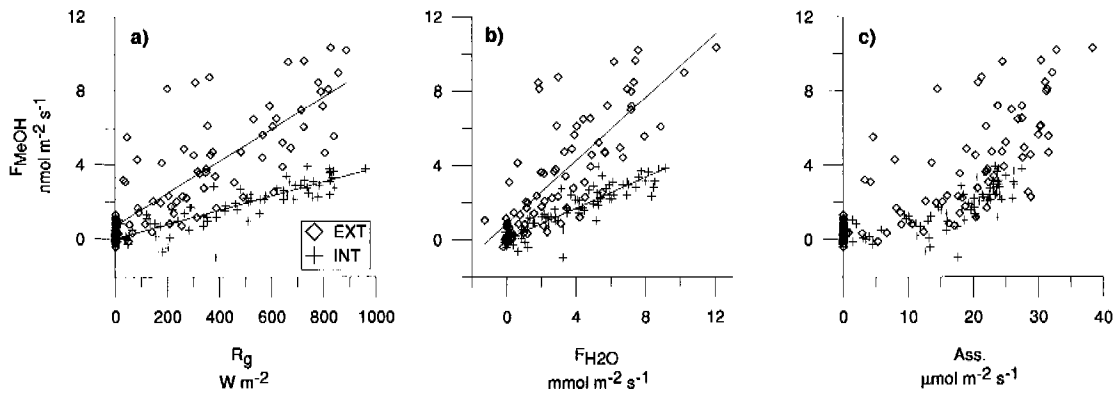


Figure 9. Scatter plots of methanol flux (F_{MeOH}) vs a) global radiation (R_g), b) water vapour (F_{H2O}), and c) assimilation (Ass.) for the mature period of the intensive and the extensive fields (INT: +, EXT: \diamond).

Figure 9 shows the scatter plots of the methanol flux with the global radiation, the water vapour, and the assimilation, respectively, for the intensive and the extensive field during the mature phase. They show positive linear correlations between the methanol flux and the global radiation as well as the water vapour flux. The dependence of the methanol flux and the assimilation seems to be non-linear. In accordance to the γ values mentioned above, the intensive field shows a smaller slope between the methanol and the water vapour flux than the extensive field ($0.40 \text{ nmol mmol}^{-1}$ compared to $0.92 \text{ nmol mmol}^{-1}$). The respective correlation coefficient of the intensive field ($r^2_{INT} = 0.86$) is significantly higher than the one of the extensive field ($r^2_{EXT} = 0.64$). Part of the reduced correlation is due to a systematic difference in the diurnal cycles of methanol and water vapour fluxes; methanol emissions increase more rapidly before noon (Fig. 8). The same is true for the correlation between the methanol flux

and the global radiation ($r^2_{\text{INT}} = 0.85$, $r^2_{\text{EXT}} = 0.64$). The correlation coefficients between the methanol flux and the various environmental parameters for the mature phase are compiled in Table 1. In general, better correlations are found for the mature period alone than for the entire growing phase.

5.4 Discussion

5.4.1 Concentrations

The daily distribution of the methanol concentration above the intensive and the extensive grassland showed a diurnal cycle with two maxima (in the early evening and in the morning) and two minima (during night and in the afternoon). This cycle was observed during the growth and during the mature phase. The trend towards a minimum of methanol in the afternoon can be explained by the growth of the daytime convective boundary layer (CBL) leading to dilution and a relative depletion of methanol near the ground. With the break down of the thermal mixing after sunset a shallow stable nocturnal boundary layer (NBL) of about 50-100 m establishes. A methanol flux in the order of $0.1 \text{ nmol m}^{-2} \text{ s}^{-1}$ (i.e. smaller than our flux detection limit) into this NBL during these evening hours would be high enough to cause an increase of methanol concentrations up to 15 ppbv as observed at the study site (Fig. 4a). The coincidence of the highest concentrations with low wind velocities (Fig. 4c) supports this interpretation, as the wind speeds at this site are generally very low in the NBL. Low methanol concentrations later during the night might be either due to a small loss process near the ground or a dilution by the growth of the NBL height. In the morning, the rising emissions into a yet shallow CBL may cause the increase in methanol concentration. The mean methanol concentrations of 5-10 ppb observed in this study fit in the range of typical rural background concentrations at the surface (e. g. Ammann et al., 2004; Das et al., 2003; Goldan et al., 1995; Warneke et al., 2002). Thus the methanol emissions from the agricultural fields together with reasonable assumptions about the diurnal course of the boundary layer height are sufficient to explain the major fluctuations of the observed methanol concentration. This indicates that advection of nearby anthropogenic sources is unlikely to play a dominant role during the experiment.

5.4 Discussion

5.4.2 Fluxes during growth

Daytime methanol fluxes above the intensive and the extensive field were consistently positive indicating a general emission from the plants into the atmosphere (Fig. 3, 7, 8, Table 3). The maximum fluxes not related to cut events were significantly higher above the extensive field ($18.4 \text{ nmol m}^{-2} \text{ s}^{-1}$ corresponding to $2.21 \text{ mg m}^{-2} \text{ h}^{-1}$) than above the intensive field ($9.3 \text{ nmol m}^{-2} \text{ s}^{-1}$ corresponding to $1.11 \text{ mg m}^{-2} \text{ h}^{-1}$). Compared to other measurements on grassland ecosystems, these values are slightly lower but of the same order of magnitude. Kirstine et al. (1998) detected maximum fluxes of $7.5 \text{ mg m}^{-2} \text{ h}^{-1}$ above a clover field, and Warneke et al. (2002) reported maximum fluxes of $4 \text{ mg m}^{-2} \text{ h}^{-1}$ above an alfalfa field. Nocturnal methanol fluxes in the present study were mostly below the detection limit of $0.3 \text{ nmol m}^{-2} \text{ s}^{-1}$ (INT) and $0.8 \text{ nmol m}^{-2} \text{ s}^{-1}$ (EXT). Similarly, Kirstine et al. (1998) using static chambers did not detect any VOCs emissions during darkness.

Strong correlations of the methanol flux with the water vapour flux as well as with global radiation were found in the present study. In literature, few correlations between methanol fluxes and environmental parameters have been reported for grassland. Kirstine et al. (1998) showed a linear dependence between total VOC emissions from grass or clover and the photosynthetically active radiation (PAR) ($r^2_{\text{grass}} = 0.62$, $r^2_{\text{clover}} = 0.64$). Furthermore, they observed a clear correlation for total VOC fluxes and air temperature ($r^2_{\text{grass}} = 0.54$, $r^2_{\text{clover}} = 0.44$). The good correlation between methanol and water vapour flux, especially for shorter time periods like the mature phase (Table 1, Fig. 9b), indicates a very similar diurnal and day-to-day time variation of the two fluxes. The water vapour flux mainly represents the transpiration of the grassland ecosystem, which is limited by stomatal aperture (stomatal conductance). MacDonald and Fall (1993) found in laboratory measurements that changes in stomatal conductance were closely followed by changes in methanol flux. Niinemets and Reichstein (2003a, b) described the controlling effect of stomatal conductance on methanol emission by its high water solubility. Thus the constraining effect of stomatal conductance (open during day, nearly closed during night), can explain the strong diurnal cycle of methanol emission observed on both fields in this study.

The magnitude of daytime emissions also depends on the rate of methanol production within the plant. As mentioned in the introduction, the production is associated with the growth of plants, and Galbally and Kirstine (2002) distinguished two classes of low and high methanol

emitter species. In particular graminoids of the family poaceae, among them the main forage grass species, are low methanol emitters while most other plants belong to the high emitters (Galbally and Kirstine, 2002 and references therein). In this study, the intensive field was mainly composed of graminoids of the family poaceae (85%), whereas the extensive field was composed of graminoids (35%), legumes (60%), and forbs (5%). This difference in the species composition may explain the generally higher emissions by the extensive field.

The growth rate of plants is not constant but varies with time, and thus may lead to temporal changes in methanol emissions. On a long term, MacDonald and Fall (1993) and Nemecek-Marshall et al. (1995) observed decreasing methanol emissions with plant age in laboratory experiments, and Fukui and Doskey (1998) found similar results in the field. In the present study, we also found that the normalised methanol flux (γ) of the intensive field decreased over the growing period (Fig. 6). In contrast, no significant change in the normalised flux was observed for the extensive field. We attribute this effect to the high number of different species on the extensive field, which may have different individual growth dynamics.

On the short time scale, Körner and Woodward (1987) showed distinct diurnal cycles in growth with maximum rates at midday and minimum rates during night for five poa species (graminoids). Several other plant species, however, are known to grow mostly during night (Walter and Schurr, 2005). In these cases, the methanol produced in the leaf cannot be immediately released to the atmosphere because of the general closure of the stomata during night. Instead it may be temporarily accumulated in liquid pools (Niinemets and Reichstein, 2003a). With the opening of the stomata in the morning the pools are emptied leading to a transient emission peak (Nemecek-Marshall et al., 1995). Niinemets and Reichstein (2003b) simulated such peaks with a complex dynamic model including in-leaf pools for the accumulation of the nocturnally produced methanol. In our study, a short peak at sunrise (06:00 LT) was occasionally detected above the extensive field (Fig. 8b). However, the generally rapid increase of the methanol emission between 07:00 and 09:00 LT may also reflect a slower release of an accumulated pool.

5.4 Discussion

Table 3. Methanol fluxes measured in field experiments.

Reference	Plant species	Time of year	Flux measurement technique	Fluxes (min-max) mg m ⁻² h ⁻¹
Fukui and Doskey (1998)	Grassland	Summer	Static enclosure technique	~0.8 ¹⁾
Kirstine et al. (1998)	Grass	Australian Summer	Static chamber	0.36-0.49
Kirstine et al. (1998)	White clover	Australian Summer	Static chamber	0.03-7.5
Baker et al. (2001)	Subalpine forest	Summer 1999	Relaxed Eddy Accumulation	-0.1-2.5
Schade and Goldstein (2001)	Ponderosa pine	July-September 1999	Relaxed Eddy Accumulation	0.25-1.09
Karl et al. (2002)	Subalpine forest	Summer 2001	Virtual Disjunct Eddy Covariance	0.45-1.05
Warneke et al. (2002)	Alfalfa field	Summer 2000	Disjunct Eddy Covariance	0 - 4
Das et al., (2003)	Maize	May 1995	Vertical gradient	3.45 ²⁾
Karl et al. (2003)	Hardwood forest	Fall 2001-Summer 2002	Disjunct Eddy Covariance	0 - 2
Karl et al. (2004)	Rain forest	2003	Disjunct Eddy Covariance and in-canopy gradient	0.13 ²⁾
Karl et al. (2005)	Loblolly pine forest	July 2003	Eddy Covariance, Relaxed Eddy Covariance and in-canopy gradient	0.32-0.52 ²⁾
Spirig et al. (2005)	Deciduous forest	Summer 2003	Eddy Covariance	0 - 0.31
This study	Intensive grassland	Summer 2004	Eddy Covariance	-0.18-1.11 (0.21 ²⁾)
This study	Extensive grassland	Summer 2004	Eddy Covariance	-0.09-2.21 (0.35 ²⁾)

¹⁾ normalized to 25°C, ²⁾ Average fluxes (24h).

5.4.3 Empirical flux parameterisation

We looked for a simple empirical parameterisation which is able to describe the diurnal and day-to-day variation of the methanol emission as well as its long-term development during the growing phase. One aim of the parameterisation was to calculate missing data that are required for the estimation of the cumulated methanol emission of the entire growing season.

Since the correlation coefficients between F_{MeOH} and R_g or $F_{\text{H}_2\text{O}}$, respectively, are both fairly high and not significantly different from each other, both R_g and $F_{\text{H}_2\text{O}}$ are suitable for a

5 Methanol exchange between grassland and the atmosphere

parameterisation. The global radiation represents a very basic environmental input parameter, which controls important factors such as the temperature and the photosynthesis. The water vapour flux is strongly limited by the stomatal aperture and therefore more evidently linked to plant physiology. We decided to use the water vapour flux as governing parameter. It also allowed to take into account nocturnal emissions that have occasionally been observed during the field experiment. An example for such a case is presented in Fig. 10.

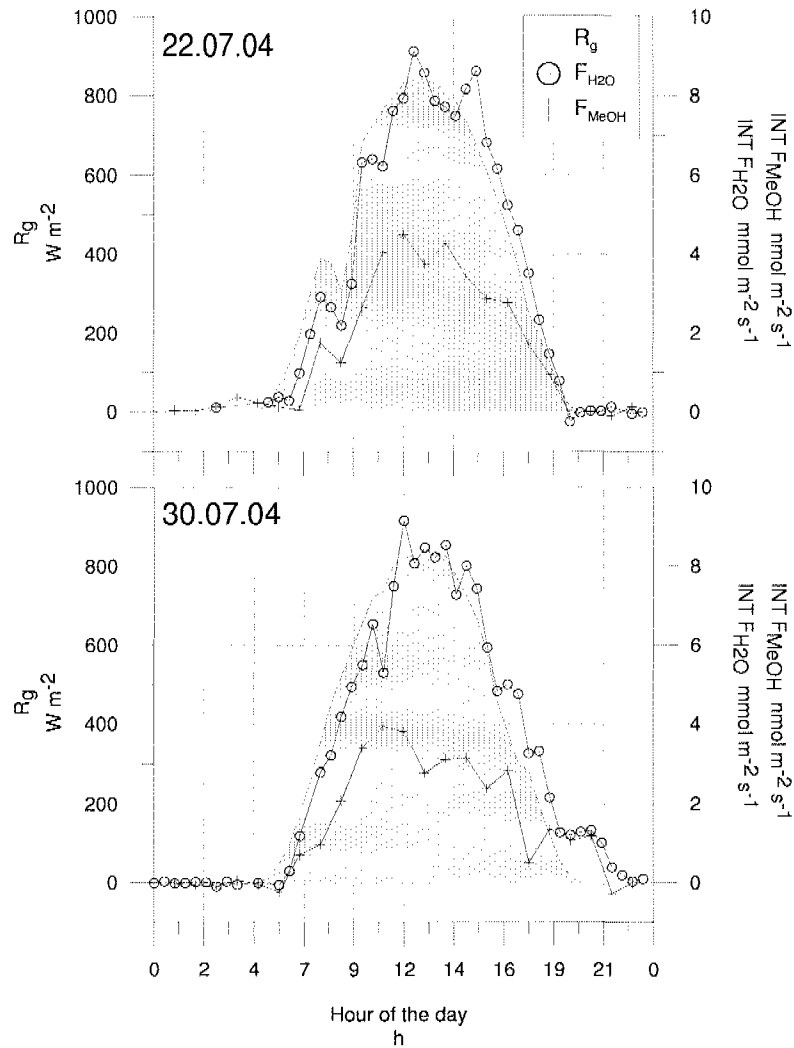


Figure 10. Global radiation (R_g), water vapour flux (F_{H_2O}), methanol flux (F_{MeOH}) measured above the intensive field for the 22.07.04, and the 30.07.04.

In order to combine the diurnal variation and the growth related decrease on the longer time scale, we chose a multiplicative approach. The flux ratio $\gamma(t)$ (Eq. 2) could be linearly related to the $LAI(t)$ describing the plant growth (Fig. 11):

5.4 Discussion

$$\gamma(t) = \gamma_0 - \alpha \cdot \text{LAI}(t) \quad (3)$$

represents the back-extrapolated flux ratio at the beginning of the growing phase and stands for the linear decrease with increasing LAI. A combination of Eqs. (2) and (3) yields the time dependent parameterisation for the methanol flux:

$$F_{\text{MeOH}}(t) = [\gamma_0 - \alpha \cdot \text{LAI}(t)] \cdot F_{\text{H}_2\text{O}}(t), \quad (4)$$

with $\gamma_0 = 0.962$ and $\alpha = 0.15$ for the intensive field,

$\gamma_0 = 1$ and $\alpha \cong 0$ for the extensive field,

$$[F_{\text{MeOH}}(t)] = \text{nmol m}^{-2} \text{s}^{-1},$$

$$\text{and } [F_{\text{H}_2\text{O}}(t)] = \text{mmol m}^{-2} \text{s}^{-1}.$$

The parameters γ_0 and α were determined by a least-squares fit to the measured data. As already described in 3.2.3, no growth related decrease of the flux ratio was observed on the extensive field ($\gamma_0 = 1$), making the LAI term obsolete for this case. The two parameters differ for the two grassland fields most likely due to the different plant composition (see above).

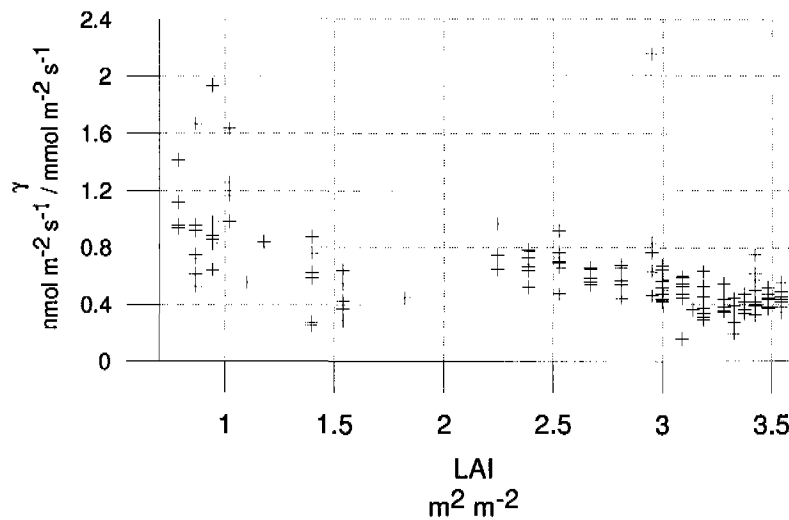


Figure 11. γ versus LAI of the intensive field for the period 02.07-01.08.2004.

5 Methanol exchange between grassland and the atmosphere

Using this parameterisation we calculated continuous time series of methanol flux for both fields. Figure 12 a) shows the results for the intensive field together with the observed data. The overall correlation coefficient of calculated and measured methanol fluxes ($r^2 = 0.79$) is higher than the correlation between methanol and water vapour flux (see Table 1), demonstrating the improvement by considering the growth effect. Figure 12 b) shows the results for the extensive field together with the observed data.

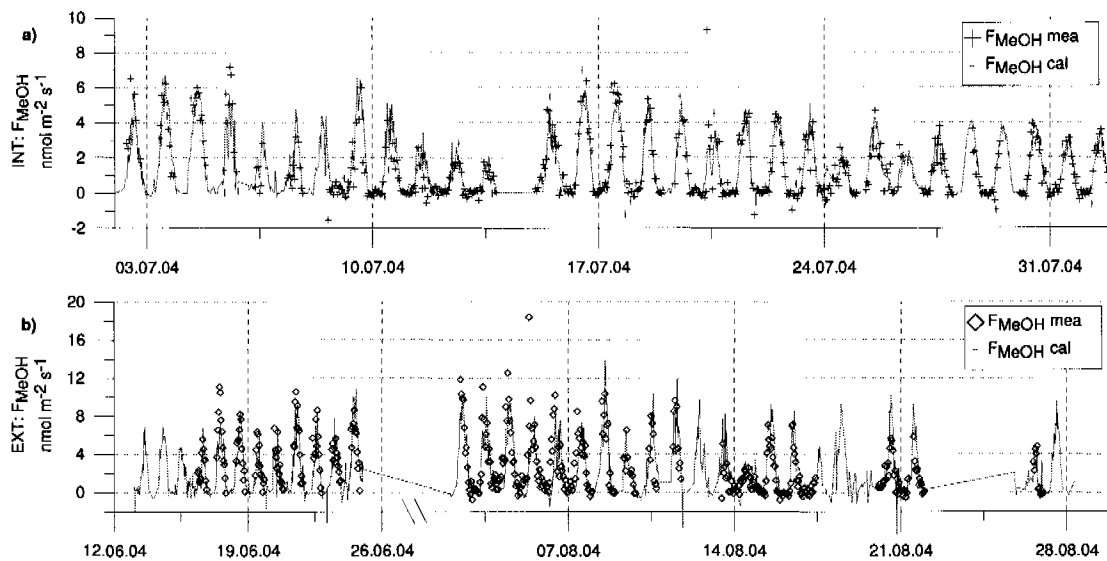


Figure 12. a) Methanol flux (F_{MeOH}) of the intensive field: measured (mea) and calculated (cal) by mean of the multiplicative approach. Correlation between measured and calculated methanol flux of the intensive field ($y=0.80x + 0.28$; $r^2=0.79$). b) Methanol flux (F_{MeOH}) of the extensive field: measured (mea) and calculated (cal) by mean of the multiplicative approach. Correlation between measured and calculated methanol flux of the extensive field ($y=0.79x + 0.79$; $r^2=0.64$).

5.4.4 Time integrated methanol fluxes

Until now, most investigations about VOC of grassland focused on short-term cut-related emissions (Fall et al., 1999 and 2001; de Gouw et al., 1999; Karl et al, 2001a, b, and 2005; Warneke et al., 2002). In this study we measured cut-related as well as growth-related methanol emissions of two different grassland fields. We compare their integral contribution by referring them to the carbon content of the harvest yield ($C_{Harvest}$).

As mentioned in section 2.1, the integral cut-related methanol emission was calculated from the methanol fluxes during the first three days after the cut (Fig. 2). This period is long enough to cover the cutting as well as the whole drying process for all cutting events. The

5.4 Discussion

growth-related methanol emission was taken as the accumulated methanol flux from the fourth day after the cut until the following cut. For this calculation, the time series of measured methanol fluxes was gap-filled using the parameterisation described in section 4.3. The integrated methanol fluxes (expressed as carbon loss C_{MeOH}) and corresponding harvest yield are summarized in Table 4. When normalized by the harvest yield, the growth related methanol emission of the extensive field was about two times higher than that of the intensive field. Thus the higher biomass on the extensive field could only explain a minor part of the emission difference (see also section 3.3 and Fig. 8). The normalised methanol emissions of the cut and hay drying events were more than one order of magnitude lower than the respective growth-related emissions.

For comparison with literature values we referred the accumulated growth-related emissions to the respective net primary productivity (NPP). This information may also be useful for estimates of regional or national methanol emissions for comparison to other biogenic VOCs more commonly measured. Following Ryle (1984), NPP of the two growing periods was estimated as half of the cumulative carbon assimilation. The resulting normalised emissions C_{MeOH}/NPP were 0.024% for the intensive and 0.048% for the extensive field. Kirstine et al. (1998) found for an ungrazed grassland a total VOC emission of 0.25% of the annual NPP, with methanol accounting for 11-15%. Thus their normalised methanol emission compares well with our results. The emission model of Galbally and Kirstine (2002) uses a methanol emission/NPP ratio for grasses of 0.024% and 0.11% for other higher plants. Considering that our intensive field was dominated by grasses whereas the extensive field consisted to more than half of non-graminoid species, the model is able to reasonably predict the emissions observed in this study.

5 Methanol exchange between grassland and the atmosphere

Table 4. Accumulated cut- and growth-related methanol emission (C_{MeOH}), net primary productivity (NPP), and harvest yield ($C_{Harvest}$) of the intensive and the extensive grassland. Growth related emissions are referred to the harvest yield of the following cut.

	Event/ Phase	Date	C_{MeOH} $gC\ m^{-2}$	$C_{Harvest}$ $gC\ m^{-2}$	$C_{MeOH}/$ $C_{Harvest}$	NPP $gC\ m^{-2}$	C_{MeOH}/NPP
INT	Cut 2	25.6.-27.6.04	0.005	138	0.004%		
	Growth 3	28.6.-28.8.04	0.065	81	0.080%	267	0.024%
EXT	Cut 1	7.6.-9.6.04	0.028	288	0.010%		
	Growth 2	10.6-28.8.04	0.199	133	0.150%	415	0.048%
	Cut 2	28.8.-30.8.04	0.007	133	0.005%		

5.5 Conclusions

Continuous flux measurements by an eddy covariance system over two managed grassland fields allowed the quantification of the methanol emissions on the ecosystem scale during the growing phase as well as during cut/hay drying events. The highest fluxes were measured directly after the cuts, which can be explained by amplified emissions due to plants wounding. However, both fields also showed continuous daytime methanol emissions during the growing periods between the cuts. The emission exhibited a distinct diurnal cycle with a maximum around midday. Measured methanol fluxes during night were mostly close to zero and/or below the detection limit of the eddy covariance method. On a day-to-day basis, the diurnal cycle strongly followed the global radiation and the water vapour flux. In the longer term, the emission of the intensive field significantly declined, whereas the one of the extensive field remained relatively constant over the whole growing phase. Accordingly, the observed variations of the methanol emission could be described by a simple empirical parameterisation using the water vapour flux and the leaf area index. The temporal course of the biogenic methanol emission in combination with the typical dynamics of the atmospheric boundary layer could explain at least qualitatively the variations of the local methanol concentration observed in this study.

On both fields, the accumulated carbon loss due to methanol emission was strongly dominated by the metabolism-related emission during the growing phase, which was more

5.5 Conclusions

than ten times higher than the corresponding cut-related emission. The intensive field was dominated by graminoid species, which are known to be low methanol emitters due to their low pectin content in the cell walls (Galbally and Kirstine, 2002). The extensive field, on the other hand, consisted to more than 60% of non-graminoid species that are expected to have a higher pectin content and thus a higher methanol emission potential. This could explain the growing-phase emission found to be two times higher on the extensive than on the intensive field.

Acknowledgements

The work was financially supported by the Swiss National Science Foundation (Project COGAS, Nr. 200020-101636).

References

- Ammann, C., Spirig, C., Neftel, A., Komenda, M., Schaub, A., and Steinbacher, M.: Application of PTR-MS for biogenic VOC measurements in a deciduous forest, *Int. J. Mass Spectrom.*, 239, 87-101, 2004.
- Ammann, C., Brunner, A., Spirig, C., Neftel, A.: Technical note: Water vapour concentration and flux measurements with PTR-MS, *Atmos. Chem. Phys.*, 6, 4643-4651, 2006.
- Ammann, C., Flechard, C., Leifeld, J., Neftel, A., and Fuhrer, J.: The carbon budget of newly established temperate grassland depends on management intensity, *Agriculture, Ecosyst. Environ.*, doi:10.1016/j.agee.2006.12.002, 2007.
- Das, M., Kang, D., Aneja, V. P., Lonneman, W., Cook, D. R., and Wesely, M. L.: Measurements of hydrocarbon air-surface exchange rates over maize, *Atmos. Environ.*, 37, 2269-2277, 2003.
- De Gouw, J. A., Howard, C. J., Custer, T. G., Baker, B. M., and Fall, R.: Emissions of volatile organic compounds from cut grass and clover are enhanced during the drying process, *Geophys. Res. Lett.*, 26(7), 811-814, 1999.

5 Methanol exchange between grassland and the atmosphere

Durand, J. L., Onillon, B., Schnyder, H., and Rademacher I.: Drought effects on cellular and spatial parameters of leaf growth in tall fescue, *J. Exp. Bot.*, 46, 1147-1155, 1995.

Fall, R. and Monson, K.: Isoprene Emission Rate and Intercellular Isoprene Concentration as Influenced by Stomatal Distribution and Conductance, *Plant Physiol.*, 100, 987-992, 1992.

Fall, R. and Benson, A. A.: Leaf methanol - the simplest natural product from plants, *Trends Plant Sci.*, 1(9), 296-301, 1996.

Fehsenfeld, F., Calvert, J., Fall, R., Goldan, P., Guenther, A. B., Hewitt, C. N., Lamb, B., Liu, S., Trainer, M., Westberg, H., and Zimmerman, P.: Emissions of volatile organic compounds from vegetation and the implications for atmospheric chemistry, *Global Biogeochem. Cycles*, 6(4), 389-430, 1992.

Flechard, C. R., Neftel, A., Jocher, M., Ammann, C., and Fuhrer, J.: Bi-directional soil/atmosphere N₂O exchange over two mown grassland systems with contrasting management practices, *Global Change Biol.*, 11, 2114-2127, 2005.

Foken, T. and Wichura, B.: Tools for quality assessment of surface-based flux measurements, *Agric. For. Meteorol.*, 78, 83-105, 1996.

Frenkel, C., Peters, J. S., Tieman, D. M., Tiznado, M. E., and Handa, A. K.: Pectin methylesterase regulates methanol and ethanol accumulation in ripening tomato (*Lycopersicon esculentum*) fruit, *J. Biol. Chem.*, 273(8), 4293-4295, 1998.

Fukui, Y. and Doskey, P. V.: Air-surface exchange of nonmethane organic compounds at a grassland site: Seasonal variations and stressed emissions, *J. Geophys. Res.*, 103(D11), 13153-13168, 1998.

Galbally, I. E. and Kirstine, W.: The Production of Methanol by Flowering Plants and the Global Cycle of Methanol, *J. Atmos. Chem.*, 43, 195-229, 2002.

Goldan, P. D., Kuster, W. C., Fehsenfeld, F., and Montzka, S. A.: Hydrocarbon measurements in the southeastern United States: The Rural Oxidants in the Southern Environment (ROSE) Program 1990, *J. Geophys. Res.*, 100, 25945-25963, 1995.

Graedel, T. E. and Crutzen P. J.: Atmospheric change: An Earth System Perspective, W. H. Freeman, New York, 1993.

5. References

- Guenther, A. B., Zimmermann, P. R., Harley, P. C., Monson, R. K., and Fall, R.: Isoprene and monoterpene emission rate variability: Model Evaluation and sensitivity analyses, *J. Atmos. Chem.*, 45, 195-229, 1993.
- Guenther, A.: Seasonal and spatial variations in natural volatile compound emission, *Ecol. Applications*, 7, 34-45, 1997.
- Heikes, B. G., Chang, W., Pilson, M. E. Q., Swift, E., Singh, H. B., Guenther, A., Jacob, D. J., Field, B. D., Fall, R., Riemer, D., and Brand, L.: Atmospheric methanol budget and ocean implication, *Global Biogeochem. Cycles*, 16(4), doi:10.1029/2002GB001894, 2002.
- Holzinger, R., Warneke, C., Jordan, A., Hansel, A., and Lindinger, W.: Biomass Burning as a Source of Formaldehyde, Acetaldehyde, Methanol, Acetone, Acetonitrile and Hydrogen Cyanide, *Geophys. Res. Lett.*, 26(8), 1161-1164, 1999.
- Holzinger, R., Williams, J., Salisbury, G., Klüpfel, T., de Reus, M., Traub, T., Crutzen, P. J., and Lelieveld, J.: Oxygenated compounds in aged biomass burning plumes over the Eastern Mediterranean: evidence for strong secondary production of methanol and acetone, *Atmos. Chem. Phys.*, 5, 39-46, 2005.
- Isidorov, V. A., Zenkevich, I. G., and Ioffe, B. V.: Volatile organic compounds in the atmosphere of forests, *Atmos. Environ.*, 19(1), 1-8, 1985.
- Jacob, D. J., Field, B. D., Li, Q., Blake, D. R., de Gouw, J., Warneke, C., Hansel, A., Wisthaler, A., Singh, H. B., and Guenther, A.: Global budget of methanol: Constraints from atmospheric observations, *J. Geophys. Res.*, 110, D08303: doi:10.1029/2004jd005172, 2005.
- Karl, T., Guenther, A., Jordan, A., Fall, R., and Lindinger, W.: Eddy covariance measurement of biogenic oxygenated VOC emissions from hay harvesting, *Atmos. Environ.*, 35, 491-495, 2001.
- Karl, T., Spirig, C., Rinne, J., Stroud, C., Prevost, P., Greenberg, J., Fall, R., and Guenther, A.: Virtual disjunct eddy covariance measurements of organic compound fluxes from a subalpine forest using proton transfer reaction mass spectrometry, *Atmos. Chem. Phys.*, 2, 1-13, 2002.

5 Methanol exchange between grassland and the atmosphere

Karl, T., Guenther, A., Spirig, C., Hansel, A., and Fall, R.: Seasonal variation of biogenic VOC emissions above a mixed hardwood forest in northern Michigan, *Geophys. Res. Lett.*, 30(23), 2186, doi:10.1029/2003GL018432, 2003.

Karl, T., Harley, P., Guenther, A., Rasmussen, R., Baker, B., Jardine, K., and Nemitz, E.: The bi-directional exchange of oxygenated VOCs between a loblolly pine (*Pinus taeda*) plantation and the atmosphere, *Atmos. Chem. Phys.*, 5, 3015-3031, 2005.

Karl, T., Harren, F., Warneke, C., de Gouw, J., Grayless, C., and Fall, R.: Senescing grass crops as regional sources of reactive volatile organic compounds, *J. Geophys. Res.*, 110, D15302, doi:10.1029/2005JD005777, 2005.

Kirstine, W., Galbally, I., Ye, Y., and Hooper, M.: Emissions of volatile organic compounds (primarily oxygenated species) from pasture, *J. Geophys. Res.*, 103(D9), 10605-10619, 1998.

Kormann, R. and Meixner, F. X.: An analytical footprint model for non-neutral stratification, *Bound-Lay Meteorol.*, 99, 207-224, 2001.

Körner, Ch. and Woodward, F. I.: The dynamics of leaf extension in plants with diverse altitudinal ranges, *Oecologia (Berlin)*, 72, 279-283, 1987.

Lindinger, W., Hansel, A., and Jordan, A.: On-line monitoring of volatile organic compounds at pptv levels by means of Proton-Transfer-Reaction Mass Spectrometry (PTR-MS) Medical applications, food control and environmental research, *Int. J. of Mass Spectrometry and Ion Processes*, 173, 191-241, 1998.

Loreto, F., Barta, C., Brillì, F., and Nogues, I.: On the induction of volatile organic compounds emissions by plants as consequence of wounding or fluctuations of light and temperature, *Plant Cell Environ.*, 29, 1820-1828, 2006.

MacDonald, R. C., and Fall, R.: Detection of substantial emission of methanol from plants to the atmosphere, *Atmos. Environ.*, 27A(11), 1709-1713, 1993.

Monod, A., Chebbi, A., Durand-Jolibois, R., and Carlier, P.: Oxidation of methanol by hydroxyl radicals in aqueous solution under simulated cloud droplet conditions, *Atmos. Environ.*, 34, 5283-5294, 2000.

Nemecek-Marshall, M., MacDonald, R. C., Franzen, J. J., Wojciechowski, C. L., and Fall, R.: Methanol Emission from Leaves, *Plant Physiol.*, 108, 1359-1368, 1995.

5. References

- Niinemets, Ü. and Reichstein, M.: Controls on the emission of plant volatiles through stomata: Differential sensitivity of emission rates to stomatal closure explained, *J. Geophys. Res.*, 108(D7), 4208, doi:10.1029/2002JD002620, 2003a.
- Niinemets, Ü. and Reichstein, M.: Controls on the emission of plant volatiles through stomata: A sensitivity analysis, *J. Geophys. Res.*, 108(D7), 4211, doi:10.1029/2002JD002620, 2003b.
- Niinemets, Ü., Loreto, F., and Reichstein, M.: Physiological and physicochemical controls on foliar volatile organic compound emissions, *Trends Plant Sci.*, 9(4), 180-186, 2004.
- Obendorf, R. L., Koch, J. L., Gorecki, R. J., Amable, R. A., and Aveni, M. T.: Methanol Accumulation in Maturing Seeds, *J. Exp. Bot.*, 41, 225, 489-495, 1990.
- Ryle, G. J. A.: Respiration and plant growth, in Palmer J. M (Ed.), *Physiology and Biochemistry of Plant Respiration*, Cambridge University Press, Cambridge, UK, 1984.
- Schade, G. W. and Goldstein, A. H.: Fluxes of oxygenated volatile organic compounds from a ponderosa pine plantation, *J. Geophys. Res.*, 106(D3), 3111-3123, 2001.
- Schade, G. W. and Goldstein, A. H.: Seasonal measurements of acetone and methanol: Abundances and implications for atmospheric budgets, *Global Biogeochemical cycles*, 20, GB1011, doi:10.1029/2005GB002566, 2006.
- Schulting, F. L., Meyer, G. M., and v. Aalst, R. M.: Emissie van koolwaterstoffen door vegetatie en de bijdrage aan de luchtverontreiniging in Nederland, *Rapport CMP 80/16 AER* 73, 1980.
- Spirig, C., Neftel, A., Ammann, C., Dommen, J., Grabmer, W., Thielmann, A., Schaub, A., Beauchamp, J., Wisthaler, and A., Hansel, A.: Eddy covariance flux measurements of biogenic VOCs during ECHO 2003 using proton transfer reaction mass spectrometry, *Atmos. Chem. Phys.*, 5, 465-481, 2005.
- Tie, X., Guenther, A., and Holland, E.: Biogenic methanol and its impacts on tropospheric oxidants, *Geophys. Res. Lett.*, 30(17), 1881, doi:10.1029/2003GL017167, 2003.
- von Dahl, C., Hävecker, M., Schlogl, R., and Baldwin, I. T.: Caterpillar-elicited methanol emission: a new signal in plant-herbivore interactions?, *Plant J.*, 46, 948-960, 2006.

5 Methanol exchange between grassland and the atmosphere

Walter, A. and Schurr, U.: Dynamics of Leaf and Root Growth: Endogenous Control versus Environmental Impact, *Annals of Botany*, 95, 891-900, 2005.

Warneke, C., Luxembourg, S. L., de Gouw, J. A., Rinne, H. J. I., Guenther, A. B., and Fall, R.: Disjunct eddy covariance measurements of oxygenated volatile organic compounds fluxes from an alfalfa field before and after cutting, *J. Geophys. Res.*, 107(D8), 6-1 - 6-11, 2002.

Wienhold, F. G., Welling, M., and Harris, G. W.: Micrometeorological Measurement And Source Region Analysis Of Nitrous-Oxide Fluxes From An Agricultural Soil. *Atmos. Environ.*, 29(17), 2219-2227, 1995.

6 Ozone triggered VOC emissions of grassland species

A. Nyfeler-Brunner, C. Ammann, M. Jocher, C. Spirig and A. Neftel

Agroscope Reckenholz-Tänikon Research Station ART, Zurich, Switzerland

To be published in Biogeoscience

Abstract

Four ozone fumigation experiments with two grassland species (*T. repens* and *L. perenne*) were conducted in climate chambers. Air temperature, photosynthetically active radiation and relative humidity in the climate chamber followed a diurnal cycle adapted from summer conditions in Switzerland. The ozone concentrations applied showed a diurnal rhythm with daily maximum concentrations between 70 and 150 ppbv. VOC emissions were measured by proton-transfer-reaction mass-spectrometer and gas-chromatography. We found that ozone triggered the emissions of various VOCs and that the enhancement is related to genotype, plant age and the intensity of ozone exposure. Methanol emissions of *T. repens* showed the strongest reaction on the ozone fumigation.

6.1 Introduction

Volatile organic compounds (VOCs) are present in the atmosphere due to anthropogenic (e.g. incomplete combustion, biomass burning) and biogenic (e.g. growth related emission) activities (Fehsenfeld et al., 1992; Fall, 1999). They reach concentrations between a few pptv and some ppbv (e. g. methanol up to 10 ppbv) (Jacob et al., 2005). One of their most important function in the troposphere is their co-operation in the production of ozone (O_3). Tropospheric ozone is produced by a complex reaction scheme involving VOCs, nitrogen oxides ($NO_x = NO + NO_2$) and solar radiation, as long as NO_x levels exceed about 0.1 ppbv (Seinfeld and Pandis, 1998). This photochemical process is the main source of ozone in the troposphere (the other important source being the intrusion of stratospheric ozone).

6 Ozone triggered VOC emissions of grassland species

Elevated tropospheric ozone is known as an air pollutant which is harmful to human beings (Brook et al., 2002) and plants. The phytotoxic influence of ozone on plants has been studied since the 1950s. Middelton (1950) was one of the first to detect injuries of herbaceous plants due to smog or air pollution, including ozone. Haagen-Smit et al. (1952) described a metallic glaze or silvering on the lower surface of leaves of crops as damage related to air pollution. Further they observed sublethal concentrations of smog to have a depressing effect on the growth of the plants.

Rich (1964) summarised the reasons which can play a role in the susceptibility of plants to ozone such as soil moisture, soil fertility, plant spacing, soil-oxygen diffusion, light, temperature, and sugar/carbohydrate content. Finally he concluded that “ozone damage to crops is now a problem of national importance”. The yield loss due to ozone triggered damage of crops has remained a problem (Fuhrer and Achermann, 1994; Pleijel et al., 1996). Since 1996, the United Nations Economic Commission for Europe (UNECE) International Cooperative Program (ICP) “Vegetation” maintains a bio-monitoring programme of ozone impacts on plants all over Europe with the goal to determine visible leaf injuries (VLI), crop reduction and plant growth rate reduction of two *Trifolium repens* clones of different ozone sensitivities (Heagle et al., 1995) as reaction on ambient ozone concentrations (Nali et al., 2005).

Ozone enters the plant leaf mainly through the stomata (Heck, 1968; Kerstiens and Lenzian, 1989). Within the apoplast of the leaf, it leads to the oxidation of alkenes producing reactive oxygen species (ROS) such as hydrogen peroxide. The accumulation of these ROS precedes the induction of cell death (Langebartels et al., 2002) via the hypersensitive response (HSR), in which cells immediately surrounding the infection site die rapidly. HSR serves a protection mechanism against pathogens, depriving the pathogen of nutrients and preventing its spread. After a completed HSR, a small region of dead tissue is left at the site of the attempted invasion, recognisable as visible leaf injuries (VLI) (Faoro and Iriti, 2005). The reaction of the plants to the air pollutant depends on the ozone dose, the length of the exposure and the sensitivity of the plant. A long-term ozone exposure at low concentration affects plant growth and productivity processes, very often without any VLI (Faoro and Iriti, 2005 and references therein). In case of acute exposure, however, macroscopic ozone symptoms may appear shortly after ozone exposure (Bergmann et al., 1999).

6.1 Introduction

Ozone deposition to ecosystem constitutes a stress for the plants, which can trigger additional VOC emissions as also observed after herbivore attacks or cutting, senescing (Brunner et al., 2007; Davison et al., 2007; Loreto et al., 2006; Dicke, 2001; Karl et al., 2001a). In this respect, several field and laboratory fumigation experiments on woody plants and crops were done until now (Table 1).

During two years, Lluís et al. (2002) studied VOC emissions of Mediterranean woody plants under elevated ozone (+ 40 ppbv to ambient concentration) in open-top chambers. The plants reacted to the ozone fumigation by the emission of additional VOCs, which depended on the plant species as well as on the time of the year. In spite of the resultant variability, when considering overall annual data for all species and seasons, there were increased limonene and total VOC emission rates in ozone-fumigated plants. Cojocariu et al. (2005) measured enhanced acetaldehyde and acetone emissions of ozone exposed (restricted to 150 ppb) adult *fagus sylvatica* leaves. However, a field study on two silver birch clones with different ozone-sensitivities did not show enhanced VOC emissions by neither of the two clones due to the elevated ozone concentration up to 100 ppb (Vuorinen et al., 2005).

Heiden et al. (2003) and Wildt et al. (2003) describe ozone fumigation experiments with pine, sunflower, tomato, corn, canola, and tobacco. Depending on the ozone concentration and the duration of the exposure they found emissions of lipoxygenase activity (LOX) products and C₆-C₁₀ aldehydes. Vuorinen et al. (2004) showed ozone-induced VOC emissions of lima beans (amongst others 2-butanone, 1-penten-3-ol, z-3-hexenol, z-3-hexenyl acetate, nonanal, decanal). They found that the ozone-induced VOC emission pattern resembles the herbivore-induced. Beauchamp et al. (2005) measured emissions of C₆-compounds of an ozone fumigated tobacco clone with a high ozone-sensitivity. In addition he showed a relationship between the emission of C₆-compounds and the uptake of ozone.

In this study we focussed on ozone triggered VOC emissions of white clover (*Trifolium repens* L.) and English ryegrass (*Lolium perenne* L.), two typical grassland species of central Switzerland. We conducted ozone fumigation experiments in climate chambers. The ozone concentrations applied were in a realistic range up to 150 ppbv. VOC emissions of *T. repens* and *L. perenne* were measured by a proton-transfer-reaction mass-spectrometer and put in relation to genotype, plant age and ozone exposure.

6 Ozone triggered VOC emissions of grassland species

Table 1. VOC emissions triggered by ozone in literature.

reference	plant species	O ₃ range	VOC detected
Penuelas et al., 1999	aleppo pines, tomato	10-133 ppb	VOCs and terpenes only by tomatoes
Heiden et al., 1999	tobacco, Scots pine	120-150 ppb	methyl salicylate, sesquiterpenes and C6 compounds
Lluisa et al., 2002	mediterranean woody plants	9-95 ppb	mostly terpenes
Heiden et al., 2003	pine, sunflower, tomato, corn, canola, tobacco	40-200 ppb	hexanal, nonenal, hexenal, nonadienal, hexanol, nonenol, hexenol, hexenyl acetat, nonadienol,
Wildt et al., 2003	pine, sunflower, tomato, corn, canola, tobacco	40-200 ppb	hexanal, heptanal, octanal, nonanal, decanal
Vuorinen et al., 2004	lima bean	150-200 ppb	unidentified alcohols, 2-butanone, methyl-d3 a-dideuterio-2-propenyl ether, 1-penten-3-ol, 2,2-dimethoxybutane, z-3-hexenaol, z-3-hexenyl acetate, nonanal, DMNT, decanal, tetradecane
Beauchamp et al., 2005	tobacco	80-1770 ppb	hexenal, hexanal, hexanal, hexenol, hexenyl acetate
Cojocariu et al., 2005	european beech, norway spruce	Doubling the ambient level, restricted to 150 ppb	acetaldehyde, formaldehyde, acetone
Rinnan et al., 2005	boreal peatland	0-50-100-150 ppb, 9 h a day, 36-38 days	aliphatic hydrocarbons, alcohols, acids and their esters, terpenoids, carbonyl, cyclic, aromatic, N-containing and other compounds
Vuorinen et al., 2005	silver birch	0-100 ppb	O3 had no considerable effect on VOC emissions

6.2 Materials and methods

6.2.1 Plant material

We performed four independent ozone fumigation experiments. In experiment 1 and 2 (exp. 1, 2), we used white clover (*Trifolium repens* L. cv. Regal), which was kindly provided by the ICP-Vegetation Coordination Centre at the Centre for Ecology and Hydrology (Bangor, UK). Exp. 3 and 4 was done with English ryegrass (*Lolium perenne* L. cv. Aligator) from an experimental field of the Agroscope Reckenholz-Tänikon ART research station.

Trifolium repens

Three to four days old *T. repens* stolon-cuttings (25 NC-S (ozone-sensitive clones; also referred to as sensitive) and 25 NC-R (ozone-resistant clones; resistant)) were planted in 1.1 L pots filled with peat soil (Ökohum-Staudenerde, Obi-Ter, Märwil, Switzerland). The soil was composed of peat (41%), humus (36%), expanded clay (20%), clay (3%). The plants were automatically watered each second day. After three weeks of growing in the greenhouse, the plants were repotted in ten 40 L pots, each with five sensitive or five resistant plants. One week later they were cut down to 7 cm above ground level and grown for another 4 weeks in the greenhouse. The greenhouse growing conditions during these 8 weeks were (day/night): 22/18°C air temperature (T_{air}) and 40/70% relative humidity (RH). During 16h of the day (06:00-22:00 LT) lights were on. In case the global radiation outside the greenhouse was higher than 450 W m^{-2} , lamps automatically switched off. After eight weeks, six pots (three of each ozone sensitivity) were moved from the greenhouse to the climate chambers where the ozone fumigation experiment took place. During the experiments each pot was watered every day (one L per day). Two different batches of clones were grown with a temporal distance of two weeks. At the beginning of exp. 1 and 2, all plants were eight weeks old.

Lolium perenne

For the English ryegrass experiments (exp. 3, 4), 13 *L. perenne* monoliths ($30 \times 30 \times 15 \text{ cm}^3$) from an experimental field of the Agroscope Reckenholz-Tänikon ART research station were excavated. Each of these monoliths was put into a 40 L pot filled to about 50% with well watered peat soil (see above) and placed into the greenhouse (T_{air} , RH and PAR conditions as described above). They were watered every second day and fertilised once a week. To

stimulate the growth, the plants were cut down to 6 cm above ground every one to two weeks (week 1, 3 and 4 after the potting). Five days after the third cut plants were moved from the greenhouse to the climate chamber (exp. 3). These plants are also referred to as “young *L. perenne*”. For exp. 4, plants were moved to the climate chamber three weeks after the third cut. These plants are also referred to as “mature *L. perenne*”. During the fumigation experiments the plants were well water each day and fertilised one a week.

After each of the four experiments, the plants were cut down to 5 to 7 cm above ground. The total leaf area was determined by means of a portable area meter (LI-3000C, Li-COR, Lincoln NE, USA) in combination with a transparent belt conveyor accessory (LI-3050C, Li-COR, Lincoln NE, USA) for plants of exp. 1 and 2. The dry matter yield (DM) was determined for all plants in all experiments.

6.2.2 Experimental set-up

Climate chambers (CC)

The fumigation experiments were performed in two identical computer controlled climate chambers (Phytokammer, YORK), one of which was fumigated with ozone. Each chamber has a volume of 27.7 m³ (2.8 x 4.5 x 2.2 m³). Air temperature (T_{air}), relative humidity (RH) and photo synthetically radiation (PAR, up to 1000 $\mu\text{mol m}^{-2} \text{s}^{-1}$) can be defined and adapted every minute. The air pumped into the chambers is non-filtered ambient air.

The climate conditions in the chambers were chosen to resemble summer conditions in central Switzerland. Therefore a mean diurnal cycle of T_{air} , RH and PAR values of a fair weather period of summer 2005 (19.-29.06.2005) of the CarboEurope super site Oensingen was simulated. Figure 1 shows the diurnal cycles of T_{air} , RH, and PAR used in the climate chambers. The parameters in the chambers were adapted every half hour. The maximum value of relative humidity during night was reduced from 100% to 85% to reduce dew formation. The maximum value of the photo synthetically active radiation was kept at 1000 $\mu\text{mol m}^{-2} \text{s}^{-1}$. One day before the start of each fumigation experiment, the plants were moved from the greenhouse to the climate chamber. On this first day in the CC maximum light was restricted to 600 $\mu\text{mol m}^{-2} \text{s}^{-1}$ to help plants to acclimate.

6.2 Materials and methods

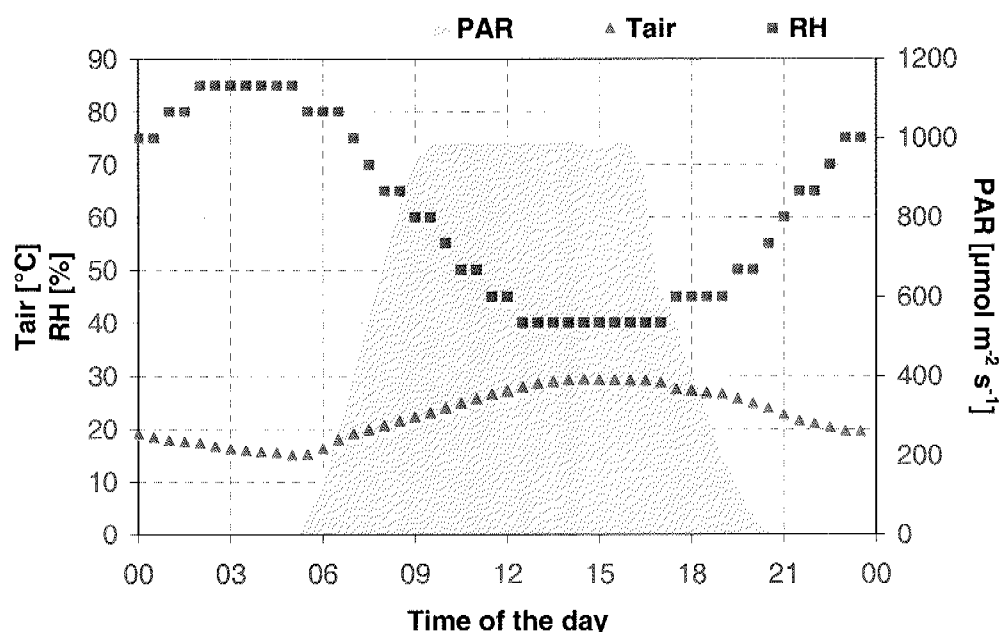


Figure 1: Diurnal cycles of air temperature (Tair), relative humidity (RH), and photosynthetically active radiation (PAR) as applied in the climate chambers.

Ozone exposures

A computer controlled ozone fumigation was installed in one of the two climate chambers. Ozone was generated by an ozone generator (Ozon-Generator 500, Fischer GmbH, Bonn, D) and added to the non filtered ambient air of the climate chambers. The ozone concentration in the chamber was monitored (Dasibi UV ozone monitor) and controlled by a mass flow controller.

The diurnal cycle of the ozone concentration in the climate chamber resembles ozone concentrations during summer ozone episodes in Switzerland (Fig. 2).

Two different ozone exposures were used. Exposure 1 is defined by a slowly increasing daily ozone maximum concentration: day 1 (day 1 of the exp.): ambient ozone concentration (max. 30 ppb), day 2: 70 ppb, day 3 and 4: 100 ppb, day 5 to 7: 120 ppb, day 8 to 10: 150 ppb. This “soft fumigation” was applied only during exp. 1. In exp. 2, 3, and 4 the daily ozone maximum was increased more rapidly from day to day: day 1: ambient ozone concentration (max. 30 ppb), day 2: 70 ppb, day 3: 100 ppb, day 4 to 10: 150 ppb (“strong fumigation”). Table 2 gives an overview on the plants used, the length of each experiment, the number of

6 Ozone triggered VOC emissions of grassland species

days with the corresponding daily ozone maximum and the AOT40 values (accumulated ozone exposure over a threshold of 40 ppb ozone during daylight hours) for the four experiments.

Table 2: Number of experiment (exp.), plant species (TR: *T. repens*, LP: *L. perenne*), daily ozone maximum and number of days of fumigation with these daily ozone maximum and the AOT40 values for each experiment in its full length.

exp.	plants	daily maximum ozone in ppb(# days)	AOT40
1	TR	70(1), 100(2), 120(3), 150(3)	7089 ppbh
2	TR	70(1), 100(1), 150(7)	8523 ppbh
3	LP	70(1), 100(1), 150(6)	6826 ppbh
4	LP	70(1), 100(1), 150(5)	6357 ppbh

The non fumigated climate chamber was used as reference, where ambient air ozone concentration reached values between 0 and 30 ppb. The experiment 1 and 2 were performed in March and April 2005, the experiment 3 and 4 in January and February 2007. The ambient ozone concentrations during all four fumigation experiment didn't exceed 30 ppb.

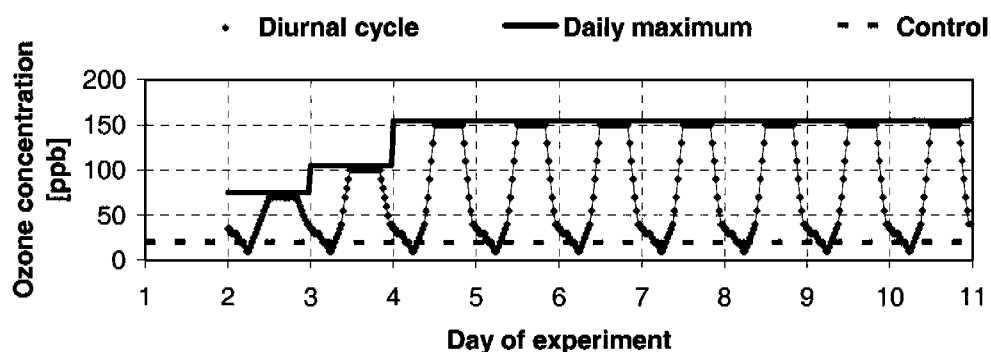


Figure 2: Ozone exposure in the fumigated and the control climate chamber: diurnal cycle of ozone concentrations, daily maximum ozone concentration and the background ozone concentration in the control climate chamber.

6.2 Materials and methods

Dynamic chamber (DC)

An automatic system with five to six dynamic chambers (DC) was used for the VOC flux measurements in the climate chambers. This system was originally developed by the MPI in Mainz, D.

The DC is constructed of an acrylic glass frame (43 cm height, 35 cm inner diameter, volume 41.1 L) covered with a perfluoroalkoxy (PFA) teflon foil. Each cylindrical chamber has a movable lid which is only closed during measurements. Inside the chamber two teflon coated fans are operating continuously. They provide a homogenous air mixture in the chamber when the cover is closed and an efficient air exchange when the cover is open. During closure, an inlet ventilator supplies the chamber with a constant flow of ambient air, providing an air exchange time of less than one minute. Concentration of various trace gases are measured at the inlet (ambient air concentration; m_{am}) and inside of the dynamic chamber (DC air concentration; m_{in}). The sample air (m_{in} and m_{am}) is pulled through PFA tubes (1/4" O. D.) from each chamber to the analysers (see sect. 2.3). Additionally, the air and the soil temperature in the chamber are measured. Each chamber is controlled by its own micro control unit. The assembly of all DC is controlled by a central processing unit which is also responsible for the data acquisition. Figure 3 shows a picture of a DC attached to the edge of the plant pot in a climate chamber.

The air of the individual chambers is measured sequentially for 10 to 12 minutes, depending on the total number of chambers. One minute before the measurement starts, the cover of the dynamic chamber closes and the inlet ventilator starts operating supplying the chamber with ambient air at a rate of 60 L min⁻¹. This is necessary to establish a homogenous mixture in the chamber before the measurement starts.

A 10-minutes-measurement cycle, applied when the system is running with six DC, includes 3 minutes measurement of ambient air, 4 minutes of DC air and another 3 minutes of ambient air. A 12-minutes-measurement cycle, applied when the system is running with five DC, includes 4 minutes of ambient, DC and ambient air measurements, respectively. The ambient air mixing ratio is calculated as the mean of the two ambient air measurements.

The flux (F) is calculated by the following formula (1):

6 Ozone triggered VOC emissions of grassland species

$$F = \frac{Q}{A} * (m_{in} - m_{am}) \quad (1)$$

with Q: air flow rate through the chamber (60 L min⁻¹)

A: surface area covered by the chamber (~0.1 m²)

m_{in}: mixing ratio in the dynamic chamber (in ppbv)

m_{am}: ambient mixing ratio (in ppbv)

During exp. 1 and 2, an assembly of six DC was used, two of them operating in the climate chamber with ambient air and four of them in the ozone fumigated climate chamber. During exp. 3 and 4, five DC were installed, two of them in the climate chamber with ambient air, three of them in the ozone fumigated climate chamber.



Figure 3: Climate chamber: Dynamic chamber on a *T. repens* pot.

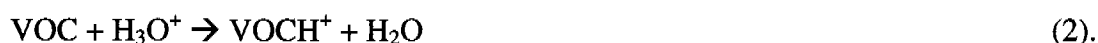
6.2 Materials and methods

6.2.3 Gas exchange measurements

Volatile organic compounds (VOCs)

PTR-MS and GC-PTR-MS

Volatile organic compounds (VOCs) were measured continuously by a proton transfer reaction mass spectrometer (PTR-MS, Ionicon GmbH, Austria). The PTR-MS technique is well described in Lindinger et al. (1998). Here we focus on the general operating mode and the specifications used during the experiments. The air to be analysed coming from the dynamic chamber assembly is aspirated into the drift tube of the PTR-MS where compounds with higher proton affinity than water undergo a proton transfer reaction with H_3O^+ ions (generated by electrical discharge of pure water vapour), following the reaction



The protonated compounds are then selected by a quadrupole mass filter and counted by a selective electron multiplier (SEM, MC-217, Mascom GmbH, Bremen, D). The PTR-MS used in these experiments corresponds to the PTR-MS-HS type, featuring three turbo pumps for increased sensitivity and a drift tube (equipped with Teflon rings) optimised for fast time response and minimal interactions with polar compounds. It was running under the following conditions: pressure drift tube of 2.1 mbar and drift tube voltage of 550 V, resulting in an electrical field strength to gas density ratio (E/N) of 122 Td. 20 to 28 masses were analysed in rotation, with an individual dwell time of 20 ms to 1 s resulting in a measurement cycle length of 16.97 to 20.76 s, respectively. Table 3 shows the protonated masses measured with PTR-MS of the 16 most emitted compounds. The PTR-MS was calibrated with a gas standard (Apel-Riemer Environmental, Inc., Denver CO, US) containing methanol, acetaldehyde, and acetone for defining the instrument response for the corresponding masses m33, m45, and m59. It was dynamically diluted with air generated by a zero air generator (ChromGas Zero Air Generator, model 1000, Parker Hannifin Co., Haverhill MA, US). The absolute accuracy of the concentration measurement is estimated to be $\pm 20\%$ due to mass flow controller and gas standard uncertainties. The concentrations of all other masses were not calibrated with the help of a gas standard but calculated based on physical assumptions described in Ammann et al. (2004).

6 Ozone triggered VOC emissions of grassland species

The PTR-MS detects masses (m/z , respectively), but it is not able to distinguish between compounds having the same mass (isomers). To identify these compounds, we installed a gas chromatograph (GC) in front of the PTR-MS inlet, which allowed the temporal separation of isomeric compounds. A detailed description of the coupled GC-FID-PTR-MS system is given in Davison et al. (2007).

Table 3: Mass identification of the 16 most emitted compounds: molecular weight (mw), measured ion mass, fragments of ion masses, compound, emission (+) or deposition (-) by TR (*T. repens*) or LP (*L. perenne*).

mw	measured ion mass	fragments of ion masses	compounds	TR	LP
32	m33		methanol	+	+
44	m45		acetaldehyde	-a)	+
56	m57		frag. of butanol	+	-
58	m59		acetone	+	+
68	m69	m129, m143	frag. of octanal and nonanal	+	-
70	m71		frag. of pentanol	+	+
72	m73		methyl ethyl ketone	+	+
80	m81	m99	frag. of hexenal	+	-
82	m83	m101, m143	frag. of hexenol, hexanal and hexenyl acetate	+	-a)
86	m87		methyl butenol and methyl butanal	+	+
88	m89		1-pentanol	+	+
98	m99		hexenal	+	+
100	m101		hexenol and hexanal	+	+
114	m115		heptanal	+	+
128	m129		octanal	+	+
142*	m143		hexenyl acetate and nonanal	+	

6.2 Materials and methods

Other trace gases (H₂O, CO₂, O₃)

Water vapour (H₂O) and carbon dioxide (CO₂) were measured continuously by a LI 6262 (Licor environmental, Lincoln NE, USA) with a time resolution of 20 s. The instrument was calibrated for CO₂ with a gas standard (two calibration gases containing 300 and 400 ppmv CO₂, Carbagas, Switzerland,) and for H₂O by a dew point generator system and a dew point mirror (Dewpoint monitor, General Eastern, Hygro-M2). Ozone (O₃) in the dynamic chamber system was measured continuously by UV photometric analysers (exp. 1, 2: Dasibi, Series 1008, Environmental Corp., Glendale CA, USA, exp. 3, 4: 2B tech, Model 205, 2B Technologies, Inc., Boulder, CO, USA).

6.3 Results

6.3.1 Time integrated VOC emissions

To compare the magnitude of fluxes among the different experiments, sums of fluxes were calculated. These sums included fluxes from the first day of fumigation until an AOT40 value of 6000 ppbh ($\pm 5\%$) was achieved. Figure 4 shows the number of days for each experiment until this AOT40 value was reached. A positive overall sum was defined as an emission, a negative overall sum as a deposition. These fluxes were normalised to the dry matter weight (g DW) which was determined at the end of the fumigation of each experiment.

Table 3 gives a general overview of the 16 compounds which were most emitted by *T. repens* or *L. perenne* during the four fumigation experiments. For *T. repens* 17 (18) out of 21 (22) measured compounds were emitted during experiment 1 (exp. 2). For *L. perenne* (exp. 3 and 4), the number of emitted compounds was significantly smaller (12 out of 21 measured). All emissions followed a distinct diurnal cycle, mostly with maximum emission around midday and minimum emission during night. Methanol emissions of *T. repens* showed a maximum in the early morning hours. A detailed description of diurnal cycles and time series of methanol emissions will be given in Sect. 3.2.

6 Ozone triggered VOC emissions of grassland species

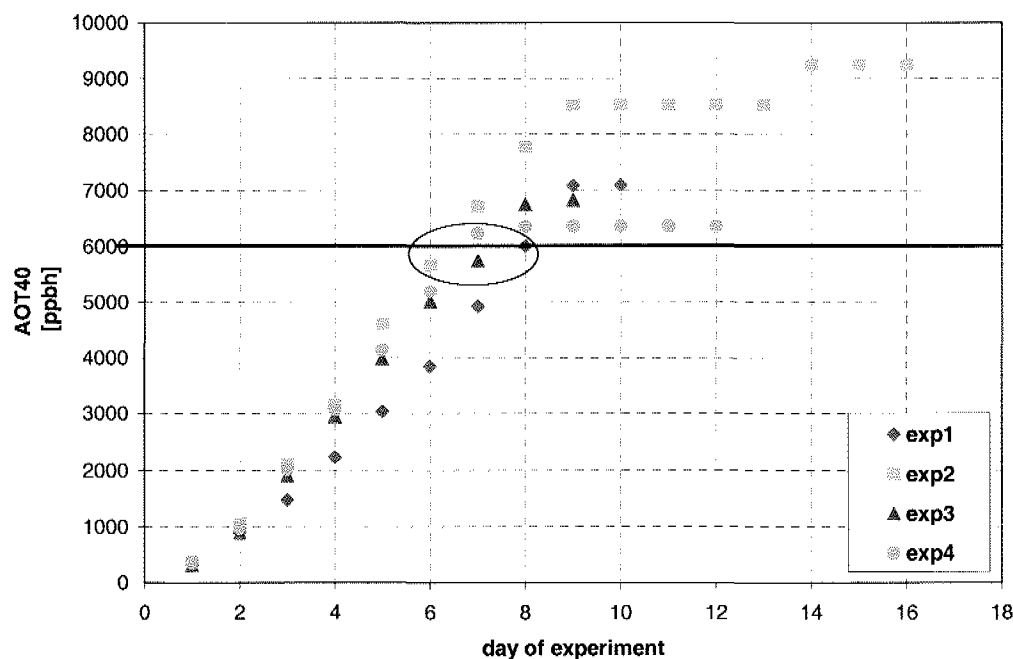


Figure 3: AOT40 of the four fumigation experiments. The circle indicates the AOT40 \approx 6000 ppbh for each experiment.

The identification of the 16 most emitted compounds (as given in Table 3) was conducted by the GC-FID-PTR-MS devices. For this purpose 11 samples were taken during exp. 2 (seven 1 L samples were taken from the ozone fumigated climate chamber: two of the resistant, four of the sensitive *T. repens*, respectively and one sample of the climate chamber background; and four samples were taken from the non-fumigated climate chamber: two of the resistant, two of the sensitive *T. repens*). We assumed the emission composition to remain the same during the other three experiments.

VOC emissions under ozone fumigation

After having selected the compounds which were emitted, we checked the overall sums upon ozone triggered effects. Therefore we calculated the mean and standard deviation of the emissions (as determined above) of the two fumigated pots. If the mean value minus one standard deviation of an emitted compound of the fumigated pots was higher than the emission of this compound of the non-fumigated control pot, it was defined a significant enhanced emission due to ozone exposure. Table 4 gives an overview of the behaviour of the emitted compounds under ozone fumigation.

6.3 Results

VOC emissions of *T. repens* under ozone fumigation

Column 1 and 2 in Table 4 gives the emission behaviour of the sensitive and the resistant *T. repens* during experiment 1 (soft ozone fumigation). The resistant one (column 2) shows an enhanced emission of 7 compounds out of 15 due to ozone exposure. The sensitive plants (column 1) however show an enhancement of all emitted compounds under the soft ozone fumigation. Column 3 and 4 of Table 4 gives the emission behaviour of the sensitive and the resistant *T. repens* during experiment 2 (strong ozone fumigation). Under this exposure regime, the resistant *T. repens* shows more compounds with enhanced emissions (12 out of 15 emitted compounds). The sensitive plants again show always an enhanced emission.

In figure 5 (top) the sums of the ten most emitted compounds of the resistant and the sensitive *T. repens* during exp. 1 and 2 are plotted. In experiment 1 (soft fumigation), the resistant *T. repens* in the control and the fumigated climate chamber show an equal sum of emissions ($0.22 \text{ mmol m}^{-2} / \text{g DM}$). The total emissions of the sensitive *T. repens* in the control climate chamber ($0.44 \text{ mmol m}^{-2} / \text{g DM}$) were higher than those of the resistant one, and they were clearly enhanced in the fumigated chamber (0.6 mmol m^{-2}). In experiment 2 (strong fumigation), both the resistant and the sensitive *T. repens* in the fumigated climate chamber show enhanced emissions compared to their control pots. The emissions of both fumigated *T. repens* are higher than during experiment 1 (soft fumigation). The emissions of the control pots of the resistant *T. repens* are equal in experiment 1 and 2, whereas the emission of the sensitive control pot during experiment 1 is higher than during experiment 2

6 Ozone triggered VOC emissions of grassland species

Table 4: Ozone triggered enhancement of VOC emissions (16 most emitted compounds): If the mean value minus one standard deviation of an emitted compound of the fumigated pots was higher than the emission of this compound of the non-fumigated control pot, it was defined a significant enhanced emission due to ozone exposure. (+) stands for emission, (++) stands for enhanced emission due to ozone fumigation, s means sensitive, r means resistant.

exp. #	1	1	2	2	3	4
plant	TR s	TR r	TR s	TR r	LP	LP
compound						
methanol	++	+	++	++	++	++
acetaldehyde					+	++
frag. of butanol	++	+	++	+		
acetone	++	++	++	++	+	++
frag. of octanal and nonanal	++	+	++	++		
frag. of pentanol	++	+	++	++	++	++
methyl ethyl ketone	++	+	++	+	+	++
frag. of hexenal	++	+	++	+		
frag. of hexenol, hexanal and	++	+	++	++		
hexenyl acetate						
methyl butenol and methyl butanal	++	++	++	++	++	++
1-pentanol	++	++	++	++	+a)	++
hexenal	++	+	++	++	+	++
hexenol and hexanal	++	++	++	++	+	++
heptanal	++	++	++	++	++	++
octanal	++	++	++	++	++	++
hexenyl acetate and nonanal	++	++	++	++	b)	b)

6.3 Results

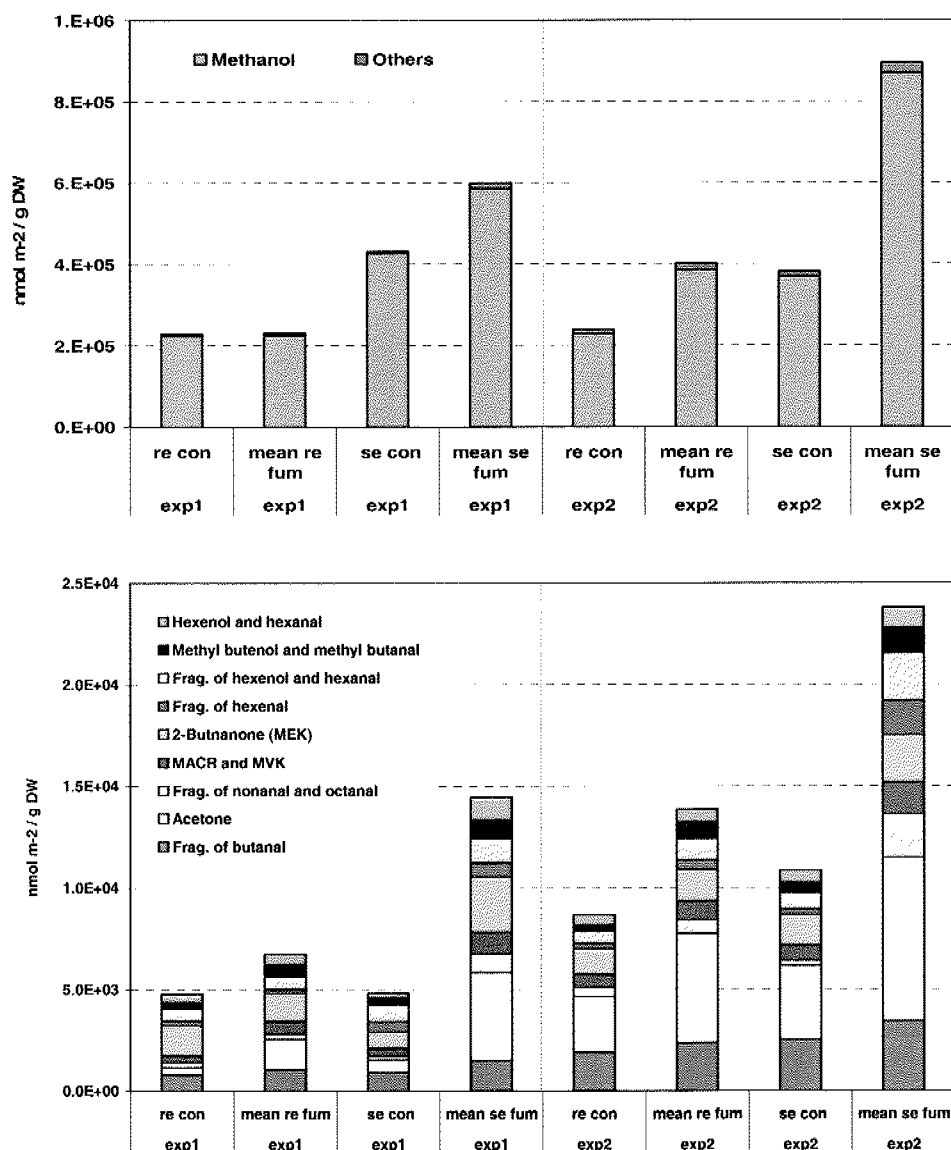


Figure 5: Top: Methanol and the 9 most emitted compounds of *T. repens* during exp. 1 and 2. Bottom: 9 most emitted compounds of *T. repens* during exp. 1 and 2.

Independent of ozone sensitivity and ozone exposure, methanol accounts for more than 95% of the emissions. The remaining 5% are dominated by emissions of fragments of butanol, acetone, fragments of pentanol and fragments of C6 compounds (hexenol and hexanal) (Figure 5 bottom).

VOC emissions of *L. perenne* under ozone fumigation

Column 5 in Table 4 gives the emission behaviour of the young *L. perenne* during experiment 3. Five compounds (out of 11 emitted ones) show enhanced emissions due to ozone exposure.

6 Ozone triggered VOC emissions of grassland species

Column 6 of Table 4 gives the emission behaviour of the mature *L. perenne* during experiment 4. The emissions of all emitted compounds of the fumigated plants are enhanced compared to the control.

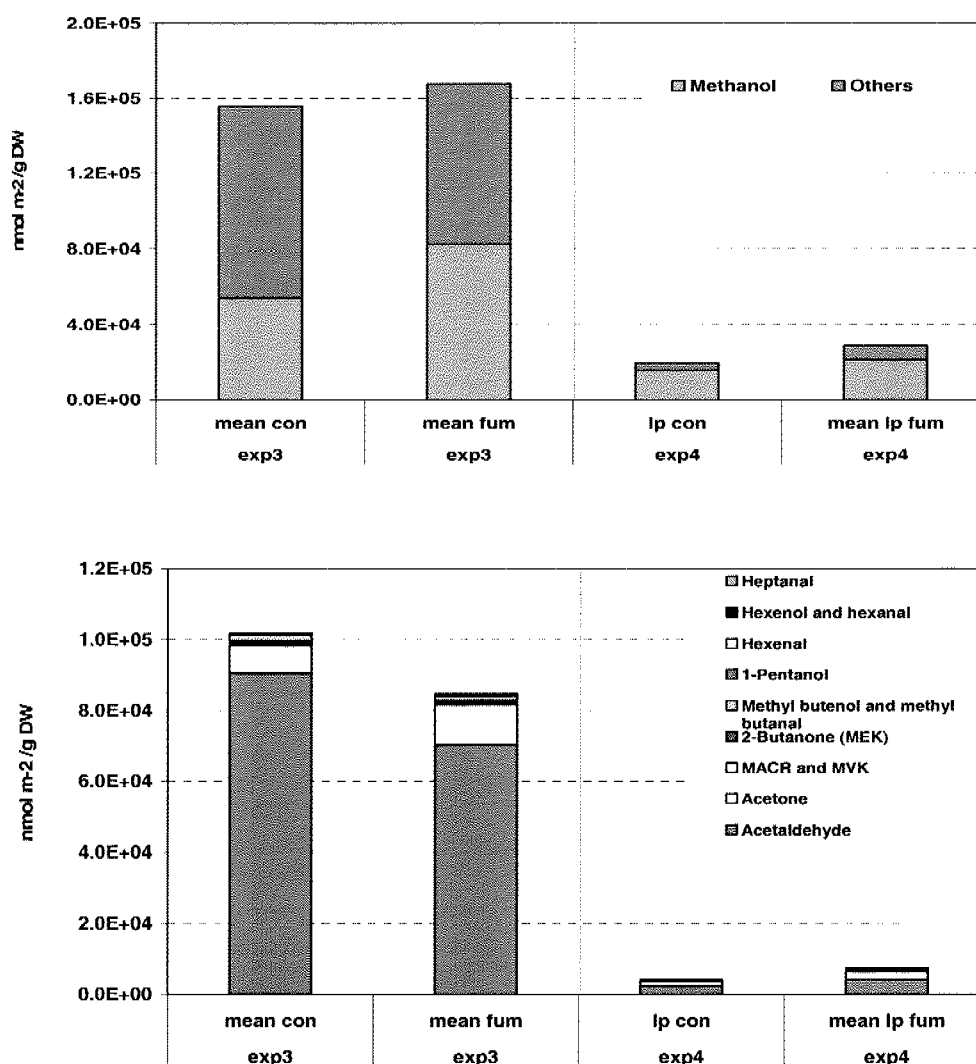


Figure 6: Top: Methanol and the 9 most emitted compounds of *L. perenne* during exp. 3 and 4. Bottom: 9 most emitted compounds of *L. perenne* during exp. 3 and 4.

In figure 6 (top) the sums of the ten most emitted compounds of the young and the mature *L. perenne* during exp. 3 and 4 are plotted. The young *L. perenne* in experiment 3 show emissions in the range of 0.15 to 0.16 mmol m⁻²/ g DW, with slightly enhanced values for the fumigated compared to the control pots. The emission of the control plant mainly consists of methanol (34.8%), acetaldehyde (58.0%) and acetone (5.0%). The emission of the fumigated

6.3 Results

plant is dominated by the same three compounds. However, methanol (49.2%) shows a higher and acetaldehyde (41.8%) a lower relative emission than the control. Acetone (6.7%) is emitted in a comparable range. The mature *L. perenne* in experiment 4 show clearly lower emissions than the young ones, in the range of 0.02 and 0.03 mmol m⁻²/ g DW, with enhanced emissions of the fumigated plants compared to the control. The total emission is composed of more than 95% of methanol (fumigated: 73.2%; control: 78.5%), acetaldehyde (14.8%; 12.6%) and acetone (7.1%; 5.4%). The relative proportion of these compounds remains the same for the fumigated and the control pots.

6.3.2 Methanol time series under ozone fumigation

Methanol represented the major part of the total VOC emissions of *T. repens* (< 95%) and a significant part of the total VOC emissions of *L. perenne* (30-78%). Methanol emissions also showed the fastest and strongest reaction on the ozone fumigation. Therefore time series of methanol will be discussed here in detail.

Methanol time series of T. repens

Figure 7 a) shows the time series of methanol fluxes of *T. repens* during exp. 1. The fluxes of the fumigated *T. repens* are mean values of two pots, those of the control is taken from a single pot. The control of the sensitive *T. repens* is not shown as this pot was the only one during this experiment infected by thrips. The daily emissions of both *T. repens* genotypes is characterised by a distinct diurnal cycle with a sharp emission peak in the early morning and a minimum emission during night. This phenomenon was observed in methanol fluxes above agricultural grassland containing *T. repens* and other legumes, too (Brunner et al., 2007). During the first three days of the experiment, no difference between fumigated and control, neither between resistant and sensitive *T. repens* is visible. The emission of the fumigated sensitive *T. repens* increases significantly on the third day of fumigation. Morning peak, day-time and night-time emissions are affected by this increase, which goes in parallel with the increase of the daily ozone maximum (upper part of Figure 7 a)). In contrast, the resistant *T. repens* shows no clear response to the fumigation.

Methanol emissions of *T. repens* during exp. 2 are shown in Figure 7 b). The sensitive *T. repens* react to the pollutant on day 3 of the experiment, the second day of the fumigation,

with an enhanced morning peak and an increase of day- and night-time emissions. On day 4 of the experiment, a second maximum at 15:00 LT appears. Highest emissions ($4.17 \text{ nmol m}^{-2}\text{s}^{-1} / \text{g DW}$) are observed on day 6. Although the daily maximum ozone concentration of 150 ppb remains for another four days, the methanol emission of sensitive *T. repens* slowly decreases. On day 10 of the experiment, the maximum methanol emission reaches the same value ($3.1 \text{ nmol m}^{-2}\text{s}^{-1} / \text{g DW}$) as on day 4 of the experiment. Other than in exp. 1, the fumigated resistant *T. repens* exhibit changes in the emission on day 6 and 7 of the experiment. This may be a reaction to an ozone fumigation peak of 300 ppb for 7 hours (not shown) that occurred due to a fumigation system error. Methanol emissions of the sensitive control pot are higher throughout the whole experiment than the methanol emissions of the resistant control pot.

Methanol time series of L. perenne

Figure 7 c) shows the time series of methanol fluxes of the young *L. perenne* during exp. 3. Here, the time series of the three fumigated and the two control pots are plotted. The diurnal cycle of *L. perenne* exactly followed the air temperature in the CC. There is no morning peak in methanol emissions. Maximum emissions occurred in the afternoon (~15:00 LT), minimum in the early morning (~06:00 LT), respectively. The fumigated plants increased their methanol emission immediately on the first day of the fumigation (day 3 of exp.). This emission difference between fumigated and control equalised over the 10 days of the experiment. Towards the end of the fumigation period, the emissions of the fumigated and the control *L. perenne* are of the same range.

Time series of methanol fluxes of the mature *L. perenne* during exp. 4 are not shown. The diurnal cycle was still characterised by maximum emissions in the afternoon and minimum emissions in the early morning, however the diurnal cycle was not as pronounced as in exp. 3. Emissions of fumigated and non-fumigated plants did not differ over the whole period of the experiments.

6.3 Results

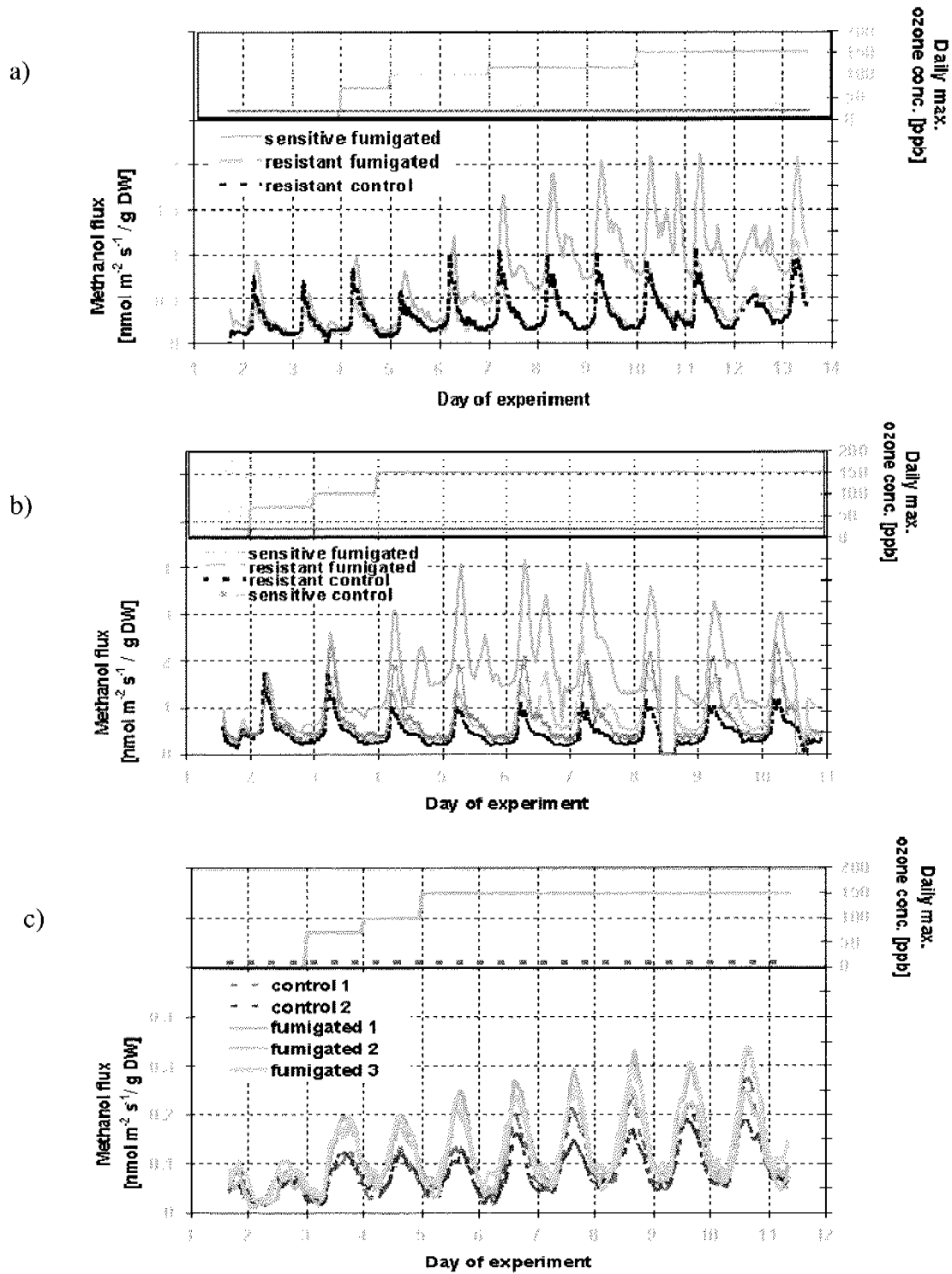


Figure 7: Time series of methanol fluxes: a): *T. repens* in exp.1, b):*T. repens* in exp. 2, c): *L. perenne* in exp. 3.

6.3.3 Ozone deposition fluxes

Figure 8 shows the scatter plot of ozone flux (F_{O_3}) versus ambient ozone concentration (c_{O_3}) for all fumigated plants of all experiments. The diurnal course is indicated by the arrows and the time labels. Highest ozone fluxes of 30 to 35 $\text{nmol m}^{-2} \text{s}^{-1}$ occurred at 14:00 LT at maximum ambient ozone concentrations of about 140 ppb. At the same ozone concentrations at 19:00 LT, ozone fluxes are clearly reduced (less than 10 $\text{nmol m}^{-2} \text{s}^{-1}$). Between 19:00 and 05:00 LT, ozone fluxes slowly decreased to a minimum flux ($\sim 0 \text{ nmol m}^{-2} \text{s}^{-1}$). This decrease went in parallel with the decrease in ozone concentration. The morning hours (05:00-14:00 LT) were characterised by a steep increase of ozone fluxes. This diurnal cycle was observed for both plant species during the four fumigation experiments.

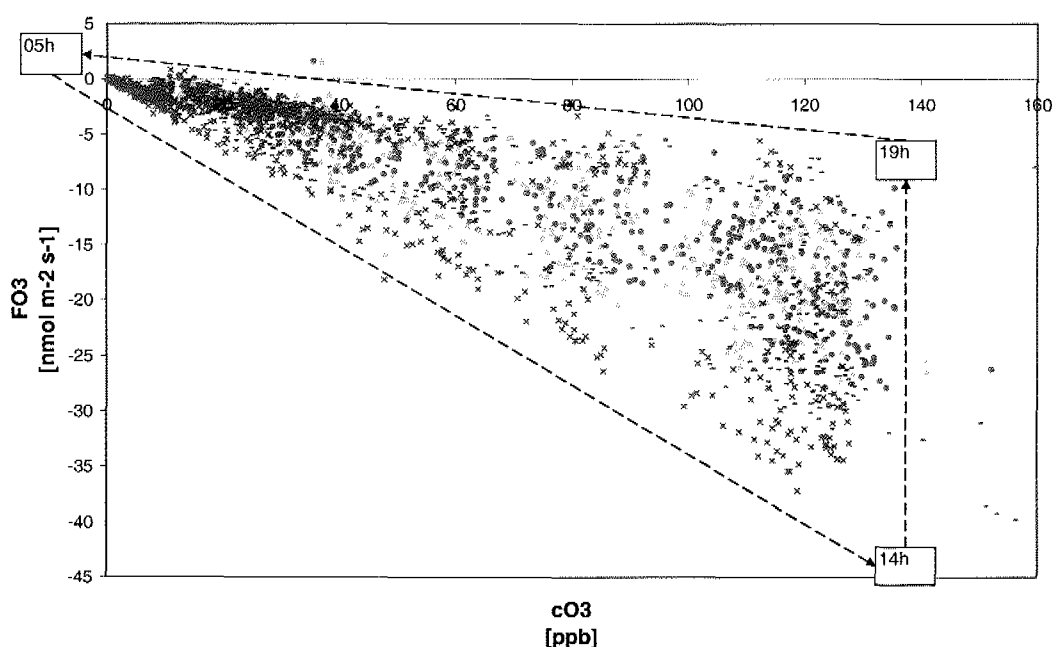


Figure 8: Scatter plot of ozone flux (F_{O_3}) vs ambient ozone concentration (c_{O_3}) for all fumigated plants of all experiments: green circles (o): *T. repens* NC-R clones (resistant), orange triangles (Δ) *T. repens* NC-S clones (sensitive), blue lines (-): *L. perenne* young, blue crosses (x): *L. perenne* mature.

Figure 9 shows a scatter plot of ozone flux into and onto the plant (F_{O_3}) versus water vapour flux out of the plant (F_{H_2O}) for all fumigated plants of exp. 1, 2 and 4. It suggests a negative linear correlation between the F_{O_3} and the F_{H_2O} . As the F_{H_2O} stands for stomatal aperture, the negative correlation predicts an ozone flux into the plant via open stomata. There is no significant difference in ozone fluxes of the sensitive and the resistant *T. repens*. *L. perenne*

6.3 Results

seems to be able of taking up more ozone at a certain stomatal aperture than the *T. repens* genotypes.

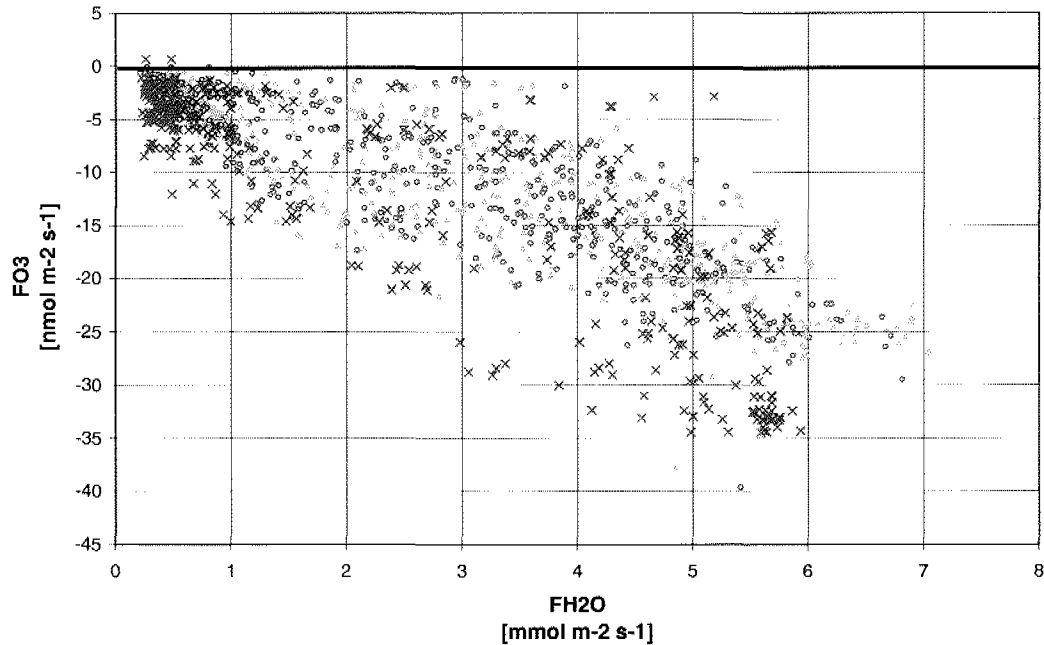


Figure 9: Scatter plot of ozone flux (F_{O_3}) vs water vapour flux (F_{H_2O}), included are data of all fumigated plants of exp.1, 2 and 4: green circles (o): *T. repens* NC-R clones (resistant), orange triangles (Δ) *T. repens* NC-S clones (sensitive), blue crosses (x): *L. perenne* mature.

Figure 10 a) shows the AOT40 value versus the accumulated daily ozone flux for *T. repens* in experiment 2. It suggests a linear relation between AOT40 and accumulated daily ozone flux for the sensitive as well as the resistant *T. repens*. The regression curve for the sensitive *T. repens* shows a steeper slope indicating a higher uptake of ozone by the sensitive *T. repens*.

6 Ozone triggered VOC emissions of grassland species

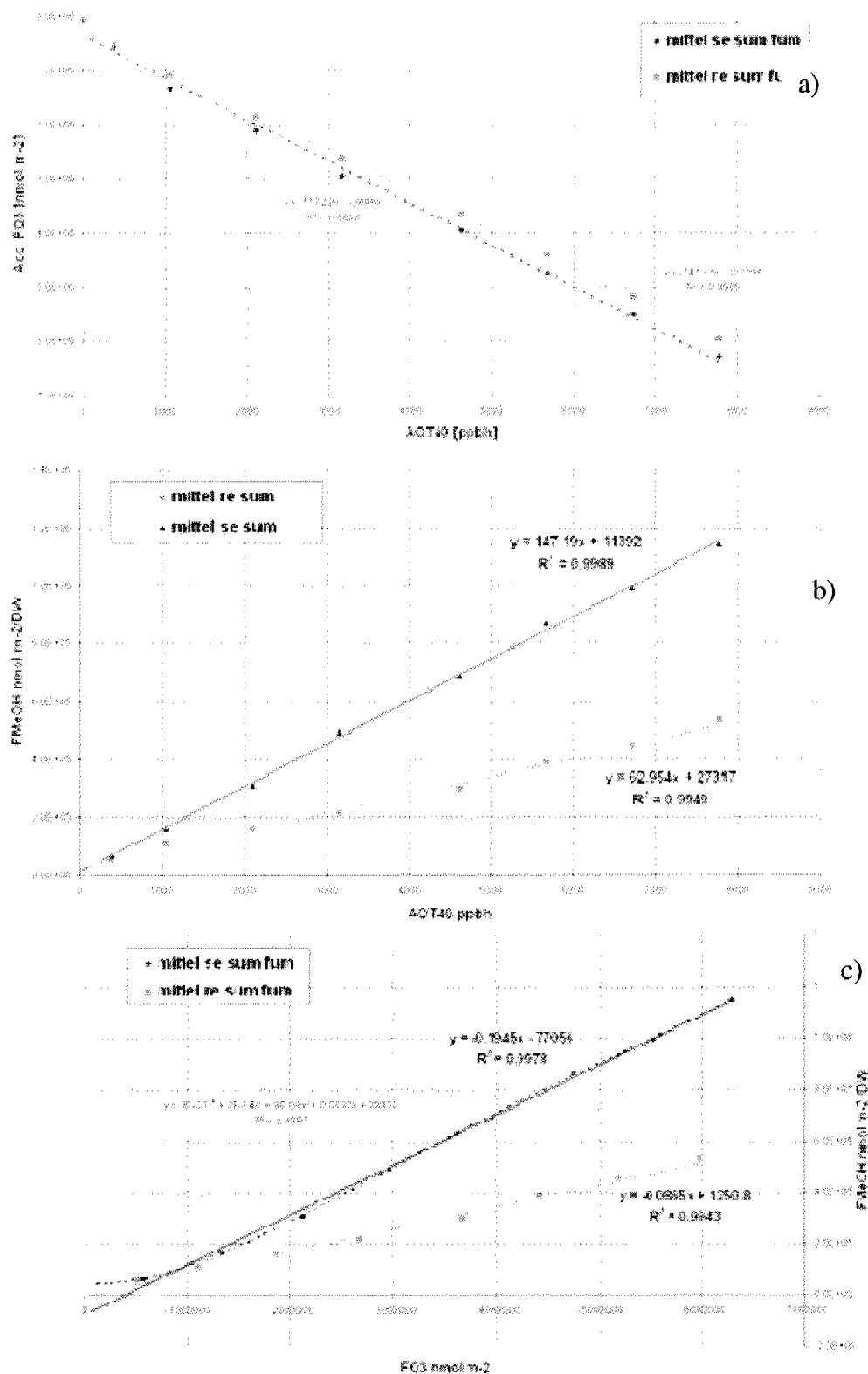


Figure 10 a, b, c: *T. repens*, Exp. 2: Accumulated F_{O_3} and accumulated F_{MeOH} vs AOT40 and F_{MeOH} vs F_{O_3} .

6.4 Discussion

6.4.1 Composition of VOC emission of *T. repens* and *L. perenne*

Table 3 shows a general overview of the compounds which were emitted and deposited by *T. repens* and *L. perenne* during the four fumigation experiments. The two plant species reveal a different emission spectrum. Generally legumes emit more different VOC than graminoids and forbs irrespective whether they are fumigated with ozone or not. Such a plant functional group depending behaviour of emissions was observed during field measurements, too.

Davison et al. (2007) showed that cut legumes (as *T. repens*) emitted significantly more different VOC than cut grasses (as *L. perenne*) and forbs. These findings are based on cut plant material, but there is a notable agreement with the results of this study. De Gouw et al. (1999) also measured emissions from two cut species of different plant functional groups, namely red fescue grass (*Festuca rubra*) and white clover (*Trifolium repens*). They mainly detected VOCs (methanol, acetaldehyde, butanone, (Z)-3-hexenal, (Z)-3-hexenol, and hexenyl acetate) that we observed in this study, too. However, they did not report acetone emissions for their graminoid species, while we found acetone emission for *L. perenne*. Detailed information about the VOC composition of the emissions of a single species can not be made as they even differ within the same functional group.

6.4.2 Temporal variations of methanol fluxes

The control pots showed that the diurnal cycle of methanol emissions of *T. repens* is characterised by a distinct morning peak, whereas the one of *L. perenne* shows a sigmoid course which closely follows the air temperature. Galbally and Kirstine (2002) related methanol production to leaf growth: during cell wall growth methanol is released to the liquid of the apoplasts, transported then through the intracellular space and emitted via open stomata. They distinguished two classes of low and high methanol emitter species. In particular graminoids of the family poaceae, among them *L. perenne*, are low methanol emitters while most other plant belong to the high emitters. These results explain the general difference in the amount of emitted methanol of *T. repens* and *L. perenne*. Körner and Woodward (1987) showed distinct diurnal cycles in growth with maximum rates at midday and minimum rates during night for five poa species (graminoids). Several other plant

6 Ozone triggered VOC emissions of grassland species

species, however, are known to grow mostly during night (Walter and Schurr, 2005). Hüve et al. (2007) measured methanol emissions and leaf growth of three species (cotton, poplar and beech). They observed that methanol emissions of plants which grow during night and store the produced methanol in the apoplast liquid showed a high peak in the morning as soon as stomata opened. From these results we can conclude that *T. repens* grows during night whereas *L. perenne* grows only during daytime.

The increase of methanol emissions of the sensitive *T. repens* during the ozone fumigations is not only growth related but also enhanced due to the reactions of ozone in the leaf. Methanol is part of the cell walls (Galbally and Kirstine, 2002). Peroxides caused by the reaction of ozone and intracellular compounds lead to cell death (Langebartels et al., 2002). We suggest that during this process cell walls are destroyed and decomposed leading to an amount of cell death related emission of methanol. The more sensitive a plant towards ozone is, the more cells were attacked, yielding a release of methanol. The slight increase in methanol emissions of the fumigated resistant *T. repens* over the whole period of the experiment 1 can be explained by increasing emissions due to growth as it resembles the emission of the control pot.

In experiment 3, young *L. perenne* showed an instant reaction of methanol emission on the fumigation with ozone (emission increase goes parallel with start of fumigation). With ongoing fumigation the difference in emission between fumigated and control *L. perenne* disappeared. A possible explanation for this behaviour may be a superposition of methanol fluxes from different sources; on one hand the ozone-triggered methanol flux, on the other hand the growth-related methanol flux. An increasing methanol flux with time due to plant growth (Galbally and Kirstine, 2002) may compensate for a decreasing ozone-triggered methanol flux with ongoing fumigation due to adaptation of the plants to the pollutant.

6.4.3 Ozone triggered VOC emission dependencies

Genotype

In experiment 1 and 2, the sensitive *T. repens* genotype reacted to the ozone fumigation with an emission increase of many more compounds than the resistant one. This reaction occurred earlier than the one of the resistant plant.

6.4 Discussion

The two *T. repens* genotypes were used for several years by the UNECE ICP Vegetation for a bio-monitoring program of ozone-specific injuries. They demonstrate the two extremes in ozone-tolerance and ozone-sensitivity. Thus on a natural grassland field, all possible sensitivities between these extremes will be found. One apparent difference between the two extremes is the occurrence of visible leaf injuries (VLI), small white-yellow flecks. These VLI are caused by cell necrosis triggered by the up take of ozone (Faoro and Iriti, 2005). The ozone-sensitive genotype gets more rapidly VLI than the resistant one. During exp. 2, *T. repens* showed VLI on the 5th (sensitive *T. repens*) and on the 7th (resistant *T. repens*) day of the fumigation, however the increase of the VOC emissions was detected 2 (sen.) and 1 (res.) day before the foliar injury was visible. Most plants react on mechanical injury such as cutting (Fall et al., 1999, and references therein; Loreto et al., 2006) and herbivore attacks (Vuorinen et al., 2004; Dicke et al., 2001) with an increase of VOC emissions. Therefore, an increase of VOC emission due to the ozone triggered leaf injury is plausible. As this increase in VOC emission was detected even before the cell necrosis was visible, we suggest the additional production of VOCs as a defence mechanism. Bungener et al. (1999) showed that across a range of grassland species (legumes, grasses and forbs), leaf injury caused by elevated ozone is most likely to occur in species with high stomatal conductance and that protection from ozone during dry periods is species-specific and depends on a reduction in stomatal conductance. He found *T. repens* in general to have a high stomatal conductance and therefore also a high ozone-sensitivity.

Focussing on methanol, exp. 1 and 2 showed that the sensitive *T. repens* reacts much faster and stronger on the ozone fumigation than the resistant clone. Methanol emissions are known as a by-product during cell wall growth (Galbally and Kirstine, 2002). However, large methanol emissions were also observed after cutting of grassland (De Gouw et al., 1999, Karl et al., 2001, Davison et al., 2007). Combining these two facts, we suggest, that mechanical injury, such as cutting, lead to cell destruction followed by a release of methanol. A similar cell destruction may occur due to ozone uptake and the following intercellular reactions (hypersensitive response).

Ozone exposure

In exp. 1 and 2, *T. repens* of the same age was fumigated with the same amount of ozone (AOT40 \approx 6000 ppbh). The difference between the two fumigation scenarios was the increase of the daily ozone maximum. The sensitive *T. repens* under both fumigations showed an increased emission of almost all emitted VOC. The increased emission of VOCs by the resistant *T. repens* clearly differed under the two different exposures: under the soft fumigation only 8 out of 17 emitted compounds showed an increase, under the strong fumigation however, 14 out of 18 emitted compounds showed a higher emission rate.

Concerning the methanol emission, the sensitive *T. repens* showed an increase due to ozone exposure independent of the strength of fumigation. The decrease of emissions observed during exp. 2 looks like an adaptation of the plant to the pollutant. The resistant *T. repens*, showed an enhanced emission due to the strong fumigation but no reaction on the soft fumigation. This circumstance leads to the assumption that the resistant can deal with slowly increasing ozone concentrations. It may adapt continuously to the pollutant if the increase is not too fast. Similar observations were made by Mehlhorn and Wellburn (1987) concerning visible leaf injuries (VLI). They found plants fumigated regularly with ozone showed no VLI, whereas plants that were grown under ozone free atmosphere, showed VLI after a single fumigation period.

Figure 10 b) and c) show the methanol flux versus the AOT40 value and the ozone flux of *T. repens* during exp. 2. Both, the resistant as well as the sensitive *T. repens* show a clear linear relation between methanol flux and AOT40 /ozone flux ($r^2 \sim 1$). The slope of the sensitive variant is steeper, indicating a stronger reaction on the ozone up take.

Plant age

In experiment 3 and 4, *L. perenne* of different age was identically fumigated (AOT40 \approx 6000 ppbh and same increase of daily ozone maxima over the whole experiment). The young *L. perenne* emitted more total VOCs than mature *L. perenne*. Concerning the ozone sensitivity, it seems, that the mature *L. perenne* is more vulnerable than the young one. The mature *L. perenne* showed more enhanced VOC emissions under ozone fumigation than the young one.

6.4 Discussion

Dugger (1962) investigated the stomatal activity in plants (beans) related to the damage from photochemical oxidants and showed that the physiological age of beans and not the degree of stomatal opening determines the susceptibility to ozone. Rich (1964) summarised that older leaves are most susceptible and younger leaves are most resistant.

6.5 Conclusions

Ozone concentrations as they occur during summer smog episodes induce increased emissions of various oxygenated VOCs in grassland species. The enhancement of VOC emission of grassland species depends on the plant species (and genotype/biotype), the ozone fumigation and the age of the plants. VOC emissions of *T. repens* triggered by ozone were significantly higher and reacted stronger than those of *L. perenne*. A strong ozone fumigation led to an enhancement of the emissions of both *T. repens* genotypes whereas the soft fumigation stressed only the sensitive *T. repens*. The effect of ozone fumigation on emissions decreased with exposure time, indicating an adaptation. Mature *L. perenne* showed a stronger reaction on the enhanced ozone concentrations than the young one. Among the VOCs investigated, methanol emissions were strongest and showed the largest response to ozone fumigation.

Acknowledgements

The authors thanks several research groups for providing plant material and greenhouse and climate chamber know-how: the centre for Ecology and Hydrology, Bangor (UK) (*T. repens*), the greenhouse group ART, Zürich, the grassland system group ART, Zürich (*L. perenne*), and the air quality and climate group ART, Zürich (climate chambers). The work was financially supported by the Swiss National Science Foundation (Project COGAS, Nr. 200020-101636).

References

- Ammann, C., Spirig, C., Neftel, A., Komenda, M., Schaub, A., and Steinbacher, M.: Application of PTR-MS for biogenic VOC measurements in a deciduous forest, *Int. J. Mass Spectrom.*, 239, 87-101, 2004.
- Beauchamp, J., Wisthaler, A., Hansel, A., Kleist, E., Miebach, M., Niinemets, Ü., Schurr, U. and Wildt, J.: Ozone induced emissions of biogenic VOC from tobacco: relationships between ozone uptake and emission of LOX products, *Plant, Cell and Environment*, 28, 1334-1343, 2005.
- Bergmann, E., Bender, J. and Weigel, H. J.: Ozone threshold does and exposure-response relationships for the development of ozone injury symptoms in wild plant species, *New Phytologist*, 144, 3, 423-435, 1999.
- Brook, R. D., Brook, J. R., Urch, B., Vincent, R., Rajagopalan, S. and Silverman, F.: Inhalation of fine particulate air pollution and ozone cause acute arterial vasoconstriction in healthy adults, *Circulation*, 105, 13, 1534-1536, 2002.
- Brunner, A., Ammann, C., Neftel, A. and Spirig, C.: Methanol exchange between grassland and the atmosphere, *Biogeosciences*, 4, 1-16, 2007.
- Cojocariu, C., Escher, P., Haberle, K. H., Matyssek, R., Rennenberg, H. and Kreuzwieser, J.: The effect of ozone on the emission of carbonyls from leaves of adult *Fagus sylvatica*, *Plant Cell and Environment*, 28, 5, 603-611, 2005.
- Davison, B., Brunner, A., Ammann, C., Spirig, C., Jocher, M. and Neftel, A.: Cut-Induced VOC Emissions from Agricultural Grasslands, *Plant Biology*, doi 10.1055/s-2007-965043, 2007.
- De Gouw, J. A., Howard, C. J., Custer, T. G., Baker, B. M. and Fall, R.: Emissions of volatile organic compounds from cut grass and clover are enhanced during the drying process, *Geophys. Res. Lett.*, 26(7), 811-814, 1999.
- Dicke, M. and Bruin, J.: Chemical information transfer between plants: back to the future, *Biochemical Systematics and Ecology*, 29, 981-994, 2001.

6. References

- Fall, R.: Biogenic emissions of volatile organic compounds from higher plants. In C. N. Hewitt (Editor), *Reactive hydrocarbons in the atmosphere*. Academic Press, New York, pp 41-96, 1999.
- Faoro, F. and Iriti, M.: Cell death behind invisible symptoms: early diagnosis of ozone injury, *Biology Plantarum*, 49, 4, 585-592, 2005.
- Fehsenfeld, F., Calvert, J., Fall, R., Goldan, P., Guenther, A. B., Hewitt, C. N., Lamb, B., Liu, S., Trainer, M., Westberg, H. and Zimmerman, P.: Emissions of volatile organic compounds from vegetation and the implications for atmospheric chemistry, *Global Biogeochem. Cycles*, 6(4), 389-430, 1992.
- Fuhrer, J. and Achermann, B.: Critical levels for ozone; a UN-ECE workshop report, FAC Report No16, Swiss Federal Research Station for Agricultural Chemistry and Environmental Hygiene, Liebefeld-Bern, Switzerland, 1994.
- Galbally, I. E. and Kirstine, W.: The Production of Methanol by Flowering Plants and the Global Cycle of Methanol, *J. Atmos. Chem.*, 43, 195-229, 2002.
- Haagen-Smit, A., J., Darley, E. F., Zaitlin, M., Hull, H. and Noble, W.: Investigation on injury to plants from air pollution in the Los Angeles area, *Plant Physiology*, 27, 1, 18-34, 1952.
- Heagle, A., S., Miller, J. E., Chevone, B. I., Dreschel, T. W., Maning, W. J., Mx Cool, P. M., Morrison, C. L., Neely, G. E. and Rebbeck, J.: Response of a white clover indicator system to tropospheric ozone at eight locations in the united states, *Water, Air and Soil Pollution*, 85, 1373-1378, 1995.
- Heck, W. W.: Factors influencing expression of oxidant damage to plants, *Annual Review of Plant pathology*, 6, 165-188, 1968.
- Heiden, A. C., Kobel, K., Langebartels, C., Schuh-Thomas, G., and Wildt, J.: Emissions of Oxygenated Volatile Organic Compounds from Plants, Part I, *J. of Atmospheric Chemistry*, 45, 143-172, 2003.
- Hüve, K., Christ, M. M., Kleist, E., Uerlings, R., Niinements, Ü., Walter, A. and Wildt, J.: Simultaneous growth and emission measurements demonstrate an interactive control of

6 Ozone triggered VOC emissions of grassland species

methanol release by leaf expansion and stomata, *J. of Experimental Botany*, 58, 7, 1783-1793, 2007.

Jacob, D. J., Field, B. D., Li, Q., Blake, D. R., de Gouw, J., Warneke, C., Hansel, A., Wisthaler, A., Singh, H. B. and Guenther, A.: Global budget of methanol: Constraints from atmospheric observations, *J. Geophys. Res.*, 110, D08303: doi:10.1029/2004jd005172, 2005.

Karl, T., Guenther, A., Jordan, A., Fall, R. and Lindinger, W.: Eddy covariance measurement of biogenic oxygenated VOC emissions from hay harvesting, *Atmos. Environ.*, 35, 491-495, 2001.

Kerstiens, G. and Lenzian, K. J.: Interactions between ozone and plant cuticles. I Ozone deposition and permeability, *New Phytologist*, 112, 1, 21-27, 1989.

Körner, Ch. and Woodward, F. I.: The dynamics of leaf extension in plants with diverse altitudinal ranges, *Oecologia (Berlin)*, 72, 279-283, 1987.

Langebartels, C., Wohlgemuth, H., Kschieschan, S., Grun, S. and Sandermann H.: Oxidative burst and cell death in ozone-exposed plants, *Plant physiology and Biochemistry*, 40, 6-8, 567-575, 2002.

Lindinger, W., Hansel, A. and Jordan, A.: On-line monitoring of volatile organic compounds at pptv levels by means of Proton-Transfer-Reaction Mass Spectrometry (PTR-MS) Medical applications, food control and environmental research, *Int. J. of Mass Spectrometry and Ion Processes*, 173, 191-241, 1998.

Lluisà, J., Oenueles, J. and Gimeno, B. S.: Seasonal and species-specific response of VOC emissions by Mediterranean woody plant to elevated ozone concentrations, 2002.

Loreto, F., Barta, C., Brilli, F. and Nogues, I.: On the induction of volatile organic compounds emissions by plants as consequence of wounding or fluctuations of light and temperature, *Plant Cell Environ.*, 29, 1820-1828, 2006.

Middelton, J. T., Kendrick, J. B., Jr. and Schwalm, H. W., Injury to herbaceous plants by smog or air pollution, *Plant Disease Reports*, 34, 245-252, 1950.

Nali, C., Pucciariello, C., Mills, G. and Lorenzini, G.: On the different sensitivity of white clover clones to ozone: physiological and biochemical parameters in a multivariate approach, *Water, Air and Soil Pollution*, 164, 137-153, 2005.

6. References

Pape et al., in preparation

Penuelas, J., Lluisa, J. and Gimeno, B. S.: Effects of ozone concentrations on biogenic volatile organic compounds emission in the Mediterranean region, 1999.

Pleijel, H., Karlsson, G. P., Sild, E., Danielsson, H., Skärby, L. and Seelden G.: Exposure of a grass-clover mixture to ozone in open-top chambers – effects on yield, quality and botanical composition, *Agriculture, Ecosystems and Environment*, 59, 55-62, 1996.

Rich S.: Ozone damage to plants, *Annual reviews of Plant Pathology*, 2, 253-266, 1964.

Rinnan, R., Rinnan, A., Holopainen, T., Holopainen, J. K., and Pasanen, P.: Emission of non-methan volatile organic compounds (VOCs) from boreal peatland microcosms – effect of ozone exposure, *Atmospheric Environment*, 39, 921-930, 2005.

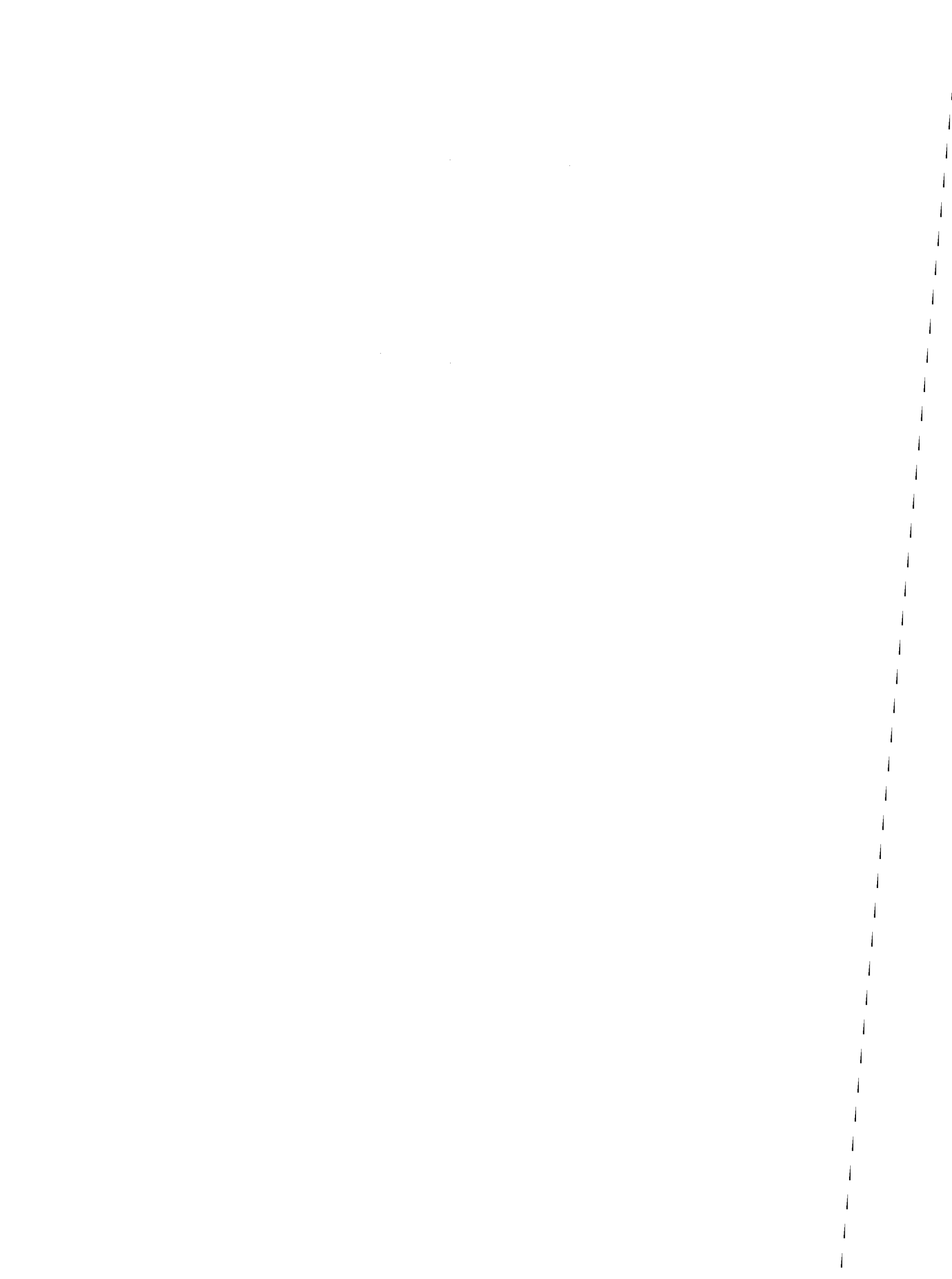
Seinfeld, J. H. and Pandis, S. N.: *Atmospheric chemistry and physics: from air pollution to climate change*, Wiley-Interscience publication, New York, 1326 pp, 1998.

Vuorinen, T., Nerg, A.-M. and Holopainen, J. K.: Ozone exposure triggers the emission of herbivore-induced plant volatiles, but does not disturb tritrophic signalling, *Environmental Pollution*, 131, 2, 305-311, 2004.

Vuorinen, T., Nerg, A.-M. E. Vapaavuori, and Holopainen, J. K.: Emission of volatile organic compounds from two silver birch (*Betula pendula* Roth) clones grown under ambient and elevated CO₂ and different O₃ concentrations, *Atmospheric Environment*, 39, 1185-1197, 2005.

Wildt, J., Kobel, K., Schuh-Thomas, G., and Heiden, A. C.: Emissions of oxygenated Volatile Organic Compounds from Plants Part II, *J. of Atmospheric Chemistry*, 45, 173-196, 2003.

Walter, A. and Schurr, U.: Dynamics of Leaf and Root Growth: Endogenous Control versus Environmental Impact, *Annals of Botany*, 95, 891-900, 2005.



7 Overall conclusions

During the last three years several field and laboratory measurement campaigns have been conducted for studying VOC emissions of grassland in undisturbed conditions as well as with the application of additional ozone related stress. Measurements were performed with a proton-transfer-reaction mass-spectrometer (PTR-MS) that was occasionally coupled to a gas chromatograph with flame ionisation detector (GC-FID) to provide additional information about isobaric compounds.

This work shows that the PTR-MS device is a reliable instrument for field scale flux measurements with the Eddy Covariance (EC) method, which needs a fast-response trace gas detection (> 1 Hz) in combination with a low detection limit. High-frequency damping effects due to the necessary air sampling through a long tube could be well described and corrected for by an empirical function depending mainly on wind speed. The described EC technique enabled the detection of biogenic VOC fluxes with a high temporal resolution of 30 min., which is necessary for deriving process based parameterisations that are essential for improving emission models.

The combination of GC-FID and PTR-MS allowed a clear mass identification of the cut induced VOC emission of grassland species. In addition, we saw that cut related VOC emissions depend on plant functional groups. These investigations focussed on cut induced compounds as after plant wounding highest VOC emissions were detected. However, regular measurements with the coupled GC-FID-PTR-MS system also during the growing phase would give continuous information about the exact composition portion of isobaric compounds.

Ozone fumigation experiments under controlled climatic conditions (climate chamber) with two grassland species typical for intensive grasslands on the Swiss plateau showed stress related VOC emission. The emissions of these ozone triggered VOCs strongly depend on species, genotype, plant age and intensity of ozone exposure. The white clover (especially the ozone-sensitive genotype) emitted more VOC than the English ryegrass. The older (mature) English ryegrass showed a stronger reaction on the enhanced ozone concentrations than the young one. The strong ozone fumigation led to an enhancement of the emissions of both white clover genotypes whereas the soft fumigation stressed only the sensitive white clover.

7 Overall conclusions

Flux measurements during several growing periods above two differently managed grassland fields showed continuous VOC emission strongly dominated by methanol. Depending on the field management and plant composition, different behaviours of methanol emission during the growth phase could be detected. The emissions of the intensive field significantly declined, whereas the one of the extensive field remained relatively constant over the whole growing phase. Differences were also detected in diurnal cycles of methanol emission, reflecting methanol production and release processes of the dominating grassland species of the fields. The methanol emissions of the intensive field showed a sigmoidal course with maximum emission around midday. The diurnal cycle of the extensive field was characterised by a distinct morning peak. The emission of methanol was well correlated with water vapour and global radiation. On both fields, the cumulated methanol emission was strongly dominated by the metabolism-related emission during the growing phase, which was more than ten times higher than the corresponding cut-related emission.

The results of the field studies allow an up-scaling of VOC emissions of grassland systems for Switzerland. The total identified VOCs emitted by grasslands represent up to 0.13% of the total annual harvest biomass (Chapter 4 and 5). In the year 2004, the harvest biomass produced by grassland systems in Switzerland was 21 million tons (Schweizerischer Bauernverband, 2004), resulting in a VOC emission of 27'900 tons. A previous study (Spirig and Nefel, 2002) only considered harvest-related VOC emissions from agricultural areas and estimated these to 5'000 tons/yr, and calculated VOC emissions from forest of 45'000 tons/yr. Using the new results of this work and current data on emissions of anthropogenic origin (102'300 tons/yr; BAFU, 2007), grasslands are responsible for up to 16% of the total annual VOC emissions in Switzerland. As the main VOC compound emitted by grasslands is methanol which has a rather low reactivity with OH radicals, grasslands are less important for the local ozone and aerosol formation than forests, where isoprene and monoterpenes build the major part of the emissions. Still, an accurate representation of methanol in emission inventories is important, as model studies demonstrated that methanol has a non-negligible role in global tropospheric chemistry. It represents a significant source for formaldehyde both in the continental boundary layer and in the free troposphere, and therefore influences global OH concentration (Tie et al., 2003; Jacob et al., 2005).

6. References

References

Bundesamt für Umwelt (BAFU): Anthropogene VOC-Emissionen Schweiz 1998, 2001, 2004, Internetpublikation, 26.02.2007, <http://www.bafu.admin.ch/voc/01265/index.html?lang=de>, 2007.

Jacob, D. J., Field, B. D., Li, Q. B., Blake, D. R., de Gouw, J., Warneke, C., Hansel, A., Wisthaler, A., Singh, H. B., and Guenther, A.: Global budget of methanol: Constraints from atmospheric observations, *Journal of Geophysical Research-Atmospheres*, 110, D08303, doi:10.1029/2004JD005172, 2005.

Schweizerischer Bauernverband, Statistik, Pflanzenbau, pflanzliches Produktion, 2004.

Spirig C. and A. Neftel, Biogene VOC und Aerosole, Schriftenreihe der FAL 42, 2002.

Tie, X., Guenther, A., and Holland, E.: Biogenic methanol and its impacts on tropospheric oxidants, *Geophysical Research Letters*, 30, 1881, doi:10.1029/2003GL017167, 2003.

Acknowledgements

I would like to thank to everyone who contributed in any way to this work:

Albrecht Neftel (ART Zürich) for accepting me as PhD student and his excellent mentoring during my time at the Reckenholz

Christof Ammann (ART Zürich) for all the intensive discussions about plants and devices

Christoph Spirig (ART Zürich) for introducing me into the world of PTR-MS

Markus Jocher (ART Zürich) for all his help in coupling GC and PTR-MS

Thomas Peter (IAC ETH Zürich) for accepting me as his PhD student

Johannes Stähelin (IAC ETH Zürich) for supporting me during the whole study

René Schwarzenbach (ETHZ) and Jürgen Wildt (FZ Jülich) for the review of the manuscript

Patrick Lazzarotto (ART Zürich) for all his tips how to survive a PhD

Daniele Torrioni (ART Zürich) for all the dinners we spent together

David Boliu (ART Zürich) for encouraging me during the last part of my work

Conny Fischer (ART Zürich) for her informative discussions about children

Astrid Gascho for all the discussions about PTR-MS and her tips in Lebanese cooking

Lothar and Marta Brunner, my parents, for their endless support the last 34 years

Sigrid and Roger Seiler, my sister and her husband, for their children which provided me intensive changes during the PhD everyday life

Flavia and Patrick Salzgeber, my other sister and her husband, for visiting me in Zürich, far away from home

Daniel Nyfeler, my husband, for his love and his jokes

Curriculum vitae

Surname	Nyfeler-Brunner
First name	Aurelia
Date of birth	9 August 1973
Citizen of	Eischoll (VS) and Horw (LU), Switzerland

Education

1988-1993	High School graduation (Matura type C), Brig
1993-1999	Conservatoire of Lucerne, Diploma as Piano teacher
1999-2003	Studies in Earth Sciences Swiss Federal Institute of Technology, ETH Zürich Diploma in Natural Sciences
2004-2007	Doctoral thesis at Agroscope Reckenholz-Tänikon, ART, Zürich and Swiss Federal Institute of Technology, ETH, Zürich

Zürich, 20 September 2007